DOTTORATO DI RICERCA IN INGEGNERIA INDUSTRIALE E DELL'INNOVAZIONE
CICLO XXVI

MODELING AND CONTROL OF MULTI-ARM SYSTEMS EQUIPPED WITH ROBOTIC HANDS

ING-INF/04-AUTOMATICA

Coordinatore
Prof. Vinicio Magi

Tutori
Prof. Fabrizio Caccavale
Dott. Francesco Pierri

Tutore ASI
Dott. Raffaele Mugnuolo

Dottorando
Giuseppe Muscio

Il dott. Giuseppe Muscio espone il proprio lavoro concernente la modellazione ed il controllo di sistemi multi-braccio dotati di mani robotiche.

Al termine della presentazione il Collegio si riunisce per decidere sull'ammissione del dottorando all'esame finale. Il tutor, prof. Fabrizio Caccavale, illustra l'attività svolta dal dottorando nel triennio.

Durante tutto lo svolgimento del dottorato di ricerca, il dott. Giuseppe Muscio ha dimostrato acume e dedizione al lavoro di ricerca, predisposizione al confronto costruttivo, rigore metodologico ed una spiccata capacità di elaborare soluzioni originali, qualità che, unitamente ad un'ottima preparazione fisico-matematica di base, delineano i tratti di una personalità di ricercatore tenace e profondo. L'attività di ricerca, inserita in un contesto di collaborazioni nazionali ed internazionali, è stata correttamente impostata grazie ad un assiduo lavoro bibliografico ed è stata sorretta costantemente da un grande impegno, anche in attività di carattere sperimentale. Durante il triennio Giuseppe Muscio ha svolto attività di ricerca all'estero per un periodo di 6 mesi presso il laboratorio *CS Robotics Lab del Department of Computer Science, Rensselaer Polytechnic Institute*, Troy (NY, USA), sotto la supervisione del Prof. Jeff Trinkle.
I risultati ottenuti durante lo svolgimento del dottorato sono caratterizzati da un ottimo grado di originalità e di approfondimento. Nell'esposizione il dottorando dimostra di avere ottima conoscenza delle problematiche trattate e di aver sviluppato un notevole senso critico.
Il Collegio dei Docenti, sentito il parere del tutor, valuta più che positivamente il lavoro svolto e delibera l'ammissione del dottorando Giuseppe Muscio all'esame finale.

OMISSIS

Non essendoci altri punti all'O.d.G. la riunione termina alle ore 17:30.
Il verbale viene redatto, letto ed approvato seduta stante.

Il Segretario
Dott. Fabio Fruggiero

Il Coordinatore del DRIII
Prof. Vinicio Magi

Acknowledgements

At the end of these 3 years, it would be my pleasure to thank all those people who helped me and gave me the strength to get through the days. First of all, I would like to thank Prof. Fabrizio Caccavale for his patience and his academic support during these years. I'm very grateful to Francesco Pierri, he had been teaching me a lot, by providing support to my research activity. A special thank to Dr. Raffaele Mugnuolo.

I'm very grateful to Prof. Jeff Trinkle for allowing me to study in an international environment during my 6-months period at the RPI (Troy, NY); I was part of the CS Robotics Lab's group with Emma, Jed, Yjing, Dan, Michael, Shuai, Cherry and June. They gave me full access to the laboratory hardware set-up and I enjoyed talking about robotics during our weekly meeting, even in the pub every 2nd Friday of each month. Thanks guys.

A great thanks to Alessandro Marino for his precious suggestions, the support and the ideas sheared during our lunch breaks. Thanks to Paolo Renna (the Mechanics) for getting me trough the crazy bureaucracy and, not less important, for the time spent talking about music.

What should I say about my Italian family? They have been simple great people! They have been always able to handle my stress and my anger in the bad days, by giving their love to me *every single moment*, especially my mother, father, sister and girlfriend. Thanks mom, dad, sister and Morena! Love you so much.

I bet someone is asking: "how many families this fool has?". I found a family in Troy. Aunt Jane together with her nephews and nieces took care of me, they always made me feel like I was home, I'll never forget that. I could never forget the way I met Nancy and aunt Jane at Albany International Airport: still laughing about that. Thanks to Elaine for the English lessons, the continuous support and the delicious dinner we had.

During my period in the U.S. I felt very close to my uncle Michel, his wife, aunt Angela (we had phone calls every week-end) and the whole family who live in Canada. I am also very glad to have met uncle Antonio, who lives in Canada too, after 18 years of separation: we had long and very nice conversations.

A great thanks to Nico, Vittorio, Giuseppe (Peppepepe), Antonio, Canio and all my friends for believing in me.

Abstract

This PhD thesis is focused on modeling and control of multi-arm systems equipped with robotic hands. Multi-arm systems have had a huge expansion during the last years in a very wide and heterogeneous range of fields, such as industry, surgery, and space applications.

In industrial environments, robots are currently employed in such a way to improve the productivity and the quality of technological processes. The emergence of more sophisticated perception and control systems allows to confer to the robot higher degrees of flexibility, dexterity and safety. This, in turn, makes possible, not just a robot-human replacement but a more reliable and efficient human-robot interaction. Indeed, it is now possible to design a robotic working cell in which a multi-arm system is capable to execute several tasks that involve a certain grade of interaction with human coworkers.

Multi-arm systems are needed in surgery applications to carry out non-invasive, or minimally invasive, operations by resorting to laparoscopic techniques.

Regarding space applications, robotics has always played a key role in terms of planetary exploration mission as well as service intra/extra vehicular operations. In space applications, the tendency is that of using multi arm systems having a high degree of dexterity: robotic hands are exploited to accomplish manipulation task in a very human-like fashion. The National Aeronautics and Space Administration (NASA) has been using a humanoid

robot called Robotnaut 2 (R2) for a wide number of missions, including human-robot and robot-robot cooperation. R2 is actually a permanent member of the International Space Station's crew (ISS). The Deutsches Zentrum für Luft- und Raumfahrt (DLR), Germany, has designed and realized a humanoid robot, Justin, with high dexterity tendon driven hands, able to move with high autonomy, by means of a suspended wheeled mobile platform.

The thesis is organized as follows:

- Chapter 1 introduces multi-arm system equipped with robotic hands, with a detailed description of modeling and control challenges; the analysis is then focused on multi-arm systems employed for space application.

- Chapter 2 deals with modeling of multi-arm systems equipped with robotic hands, in terms of kineamtics and dynamics.

- Chapter 3 describes a planner able to handle redundancy in such a way to guarantee multiple task fulfilling, by establishing a priority among them, without violating mechanical and environmental constraint; a parallel force/control strategy is presented as control law.

- Chapters 4 presents a control architecture, based on the concepts of direct force control and impedance control at object level. The aim is that of safely handle the object while ensuring compliance in the case of an unexpected collision with the external environment.

- Chapters 5, differently from Chapter 4, considers each arm/hand system, not as a unique mechanical structure but made up of two different, interacting, subsystems in which the hand is force controlled, to achieve a stable grasp, while the arm is controlled via an impedance controller, so as to make the whole system compliant.

Contents

List of Figures

Chapter 1

Introduction

Multi-arm systems consist of two or more robotic arms which are able to cooperate, in a coordinate fashion, to accomplish a given task. The arms could be mounted on different separate platforms or on the same, which, in turn, could be fixed or mobile. Multi-arm cooperative systems are usually employed when complex tasks should be performed with high precision and dexterity, and/or when large or heavy payloads are to be manipulated.

Multifingered robotic hands could be modeled as multi-arm systems: each finger can be treated, from a control point of view, as a manipulator. The main advantage of using a robotic hand as end effector, instead of classical grippers, is due to the possibility of grasping a very large number of objects, with arbitrary shapes, without any reconfiguration or tool changing. A cooperative system made up of multiple manipulators, equipped with robotic hands, allows to achieve a high level of dexterity and flexibility.

1.1 Multi arm/hand systems

Service robotics applications are day by day increasingly relying on multi arm/hand object manipulation with multi-fingered mechanical hands.

The first issue is the complex dynamics of such systems: some mutual effects must be taken into account since the dynamics of one manipulator affects the others through the grasped object and/or the common mobile base.

A multi arm system equipped with robotic hands, is often a kinematically redundant structure. The redundancy is generally a desirable feature for a robotic system, since it allows to execute multiple tasks, arranged in a suitable priority order.

There are two ways to exploit redundancy:

- at the motion planning level, via suitably designed inverse kineamtics algorithms with task priority;
- at the control motion level, via control algorithms designed directly into the cartesian space.

The former solution is easier since redundancy is naturally defined at kinematic level and the planner can be tuned offline.

Execution of grasping and manipulation tasks requires motion synchronization of arms and fingers, so as to guarantee the desired behavior of the manipulation system and control of the interaction forces. More in detail, as concerns force control, two level of interaction forces should be considered:

- Contact forces between the fingers and the grabbed object, which can be further classified in
  - internal contact forces, which do not contribute to object's motion and represent stresses applied to the object (e.g., squeezing of the object);
  - external contact forces, which generate the motion of the object.
- Environmental interaction forces, due to interaction between the object and the external environment.

Internal contact forces need to be controlled in order to make the grasp stable. As concerns environmental interaction forces, they should be always minimized, enforcing a compliant behavior of the manipulation system, unless they are functional to the given task. The control of external contact forces is not needed if the grasped object does not come in contact with the external environment. The kind of systems considered in this thesis are multi-arm systems equipped with robotic hands, mounted on a fixed base, for space applications.

1.2 Space robotics

Space robotics deals with the design of artificial systems that could assist human operators or replace them at all, both for the execution of routine operations or tasks in dangerous scenarios. A way to achieve these objectives is that of developing and implementing space robotic systems capable of accomplishing complex tasks, such as parallel management, supervision and execution of experiments and extra vehicular activities, with a certain degree of autonomy. Those kind of complex scenarios also require high dexterity: multi-arm systems equipped with robotic hands represent the perfect candidate to fulfill those requirements.

1.2.1 Intra-vehicular operation

The International Space Station (ISS) gave an impulse to the design of robotic systems devoted to the execution of tasks inside orbiting structures. The objective of such robotic systems is to guarantee the effective execution of scientific experiments and maintenance tasks.

The reference mechanical structure, adopted by several existing systems, is composed by two or more arms, even mounted on wheeled or legged bases,

often equipped with robotic hands capable of performing manipulation tasks in a human-like fashion. The arms are generally anthropomorphic with at least 6 Degrees of Freedom (DOFs). If more then 6 DOFs are available, the system is redundant and the redundancy can be exploited to improve dexterity and/or other suitable performance indexes.

In order to ensure high flexibility to the whole system, a robotic hand could be installed as grasping tool: a gripper needs to be reconfigured or changed if the object size and/or geometry change, while a humanoid hand can adapt its shape to grab a large number of bodies.

Exteroceptive sensors, i.e. sensors through which a robot gets information about the state of the external world, play a key role in human-robot and robot-robot cooperation. Since the robotic system should cooperate with crew's members, sensing becomes crucial to ensure safe human-robot interaction: a vision system must be able to detect the presence of people in the workspace and avoid them during task execution, while force/torque sensors are needed to make the manipulation system compliant in the case of an unexpected interaction or collision. More in detail, visual systems allow robots to achieve a high degree of flexibility and autonomy. As concerns flexibility, the robotic manipulation system becomes able to work in an unstructured environment, subject to changes of the operating scenario, and/or the state of the surrounding of the environment. As concerns autonomy, the actual orientation is the so called *interactive autonomy*: the robotic system is able to actively interact with a human operator in the sense of a tight cooperation.

A humanoid robot, made up of a dual-arm system, equipped with robotic hands, able to move via a mobile base, becomes the natural candidate for intra-vehicular activities: it has an infinite workspace, a high degree of redundancy, high dexterity, together with the possibility of manipulating object in the same way humans do, which means, in turn, that the robot is able to use tools (like hammers, handles, screws, etc.) designed for human operators,

further enforcing the logic of tight human-robot cooperation.

1.2.2 Extra-vehicular operation

Robotic systems dedicated to service activities for orbiting systems are designed to be installed on mobile platforms. Hence, such systems, called FTS (Flight Telerobotic Systems), are equipped with propulsion devices, like nozzles. FTSs can executes many servicing tasks without being physically constrained to the served orbiting structure.

FTSs can perform operations of external maintenance, exploration to acquire information about the external environment, as well as small satellites retrieving. In general, FTSs should accomplish all those extra-vehicular tasks, which are extremely dangerous or impossible for for a human astronaut.

Due to the nature of the illustrated applications, FTSs must have almost the same dexterity of a human astronaut wearing the heavy suit, high grade of local autonomy, if they are teleoperated, or intelligence, if they are autonomous. Again, a viable choice is the use of a multi-arm system equipped with robotic hands mounted on *free-flying* or *free-floating* platforms. One of the main issue of this kind of robots is that the platform weight is of the same magnitude of the manipulation system weight: when the arms are moving, reaction forces are transmitted to the flying base. In a free-flying solution the vehicle attitude is controlled, both when the system is moving and when it is operating, by using the propulsion system. This solution is fuel consuming. In a free floating configuration, the attitude of the system is controlled only when the system is moving: during the operation the mobile platform could float in the space, the controller of the manipulation system should act in such a way to minimize the forces transmitted to the base. This solution is, as it can be immediately recognized, fuel saving.

1.2.3 Exploration

Exploring missions are aimed at acquiring information, in order to achieve a detailed knowledge of the solar system, by sending fully automated space systems on other planets. The objective of such systems is that of gathering all the elements needed to allow stable human permanence on extraterrestrial locations of the solar system, first of all the Moon and Mars.

The first effort for robotics is that of designing unmanned autonomous vehicles (rovers), capable to travel long distances in unstructured environments and, at the same time, analyze the surrounding environment.

The second effort is that of building highly dextrous manipulation systems, eventually multi-arm, to drill, collect samples and eventually recovery and/or repair the rover in the event of faults.

1.3 Examples of arm/hand manipulation systems for space applications

In the following an overview of some notable arm/hand manipulation systems is carried out.

1.3.1 ROSED

The RObotic SErvicing Demonstrator(ROSED), shown in Figure 1.1, is a robotic cell set up at the Italian Space Agency (ASI), in Matera. ROSED offers a test environment for space robotics. The cell is composed of two COMAU robots: a 6-DOFs SMART S2 anthropomrphic arm, with non-spherical wrist, and a 6-DOFs SMART S4 anthropomrphic arm , with spherical wrist.

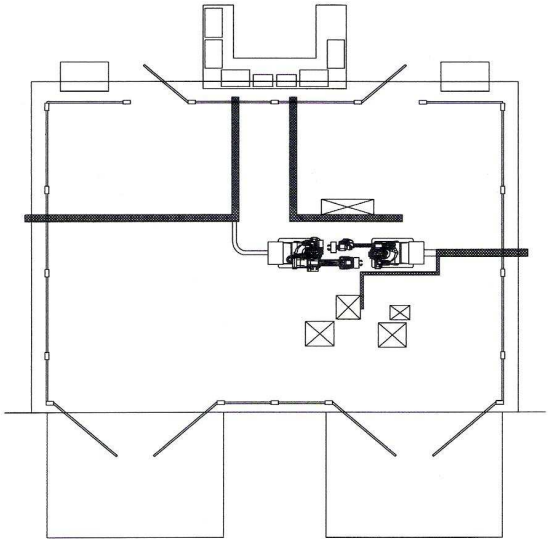

Figure 1.1: The layout of the ROSED cell

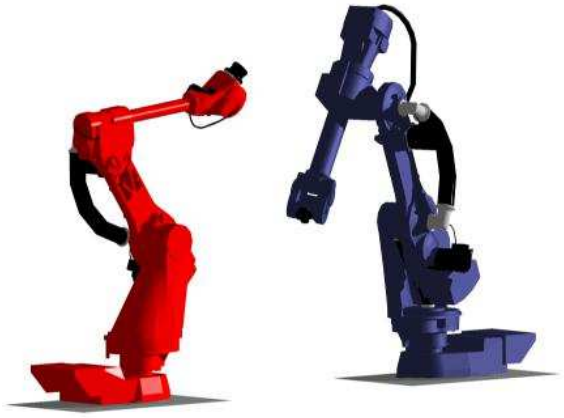

Figure 1.2: The COMAU SMART 2 S, on the left, and SMART 4 S, on the right side

Both the manipulators are equipped with a gripper and a force/torque wrist sensor, in order to allow force control, which becomes crucial in cooperative tasks.

1.3.2 Justin

Justin [6] is a humanoid robot developed by the German Aerospace Center (DLR): it is composed by two light-weight arms and two four-fingered dexterous hands. Photonic Mixer Device (PMD) sensors and cameras allow the 3D reconstruction of the environment and make Justin able to perform tasks autonomously. In order to extend Justin's workspace, a mobile platform carries the humanoid and allows it to lift up. The robot model is a tree-like

Figure 1.3: The DLR humanoid robot Justin

structure with 3 branches - the torso, the right and the left arm. The torso is connected via a flexible element to a mobile base, having 4 wheels attached to extendable legs. The mobile base has 3 DOFs for motion in the plane and 4 active DOFs to extend the legs.

The arms consist of 2 7-DOFs DLR-LWR-III [1] manipulators with integrated torque sensors in each joint.

As concerns the hands, 2 four-fingered DLR-Hand-II [7] are used in a

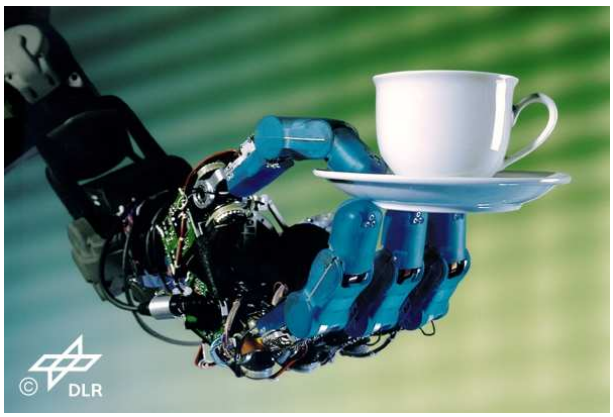

Figure 1.4: The DLR Hand II mounted on Justin

right-handed and a left-handed configuration. The DLRHand-II is equipped with joint torque sensors and a 6-DOFs force/torque sensor at each finger tip. Each hand has 3 DOFs per finger and a reconfigurable palm, offering configurations for power grasp and precision grasp as well.

1.3.3 Robonaut 2

Robonaut 2 or R2 [21], is a dexterous humanoid robot built and designed in collaboration by NASA and General Motors (GM). It has been built to help human workers or replace them in risky missions. R2 can perform dexterous manipulation using tools designed for human workers. R2 robotic system includes: optimized overlapping dual-arm dexterous workspace, elastic joint technology, miniaturized 6-axis load cells, redundant force sensing, ultra-high speed joint controllers, high resolution camera and Infra-Red (IR) systems. The humanoid is composed of two 7-DOFs arms, two 12-DOFs hands, a 3-DOF neck and a single DOF waist, the system includes 50 actuators with low-level joint controllers embedded throughout. The system also integrates built-in computing and power conversion inside its backpack and torso.

As concerns the manipulation system, 5 DOFs of each arm come with

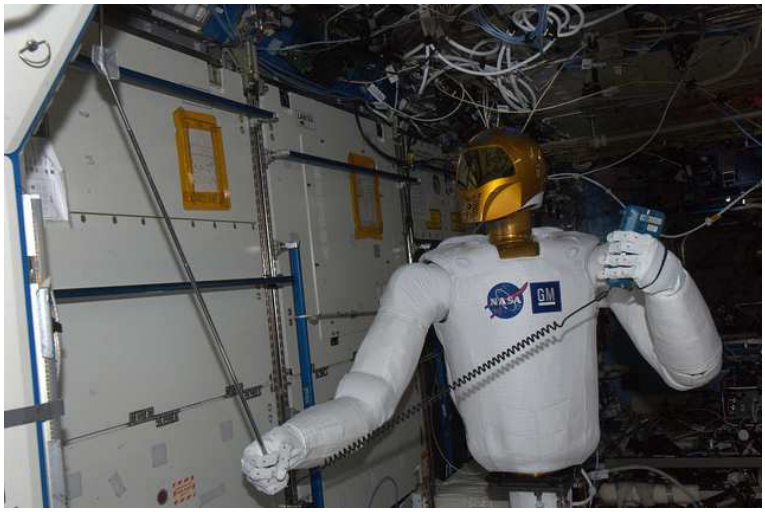

Figure 1.5: The Robonaut 2 built by NASA and GM

the upper arm: brushless DC motors are used to drive the system together with elastic elements. The use of series elastic actuation have been shown to provide improved shock tolerance, beneficial energy storage capacity and a means for accurate and stable force control, via the custom planar torsion springs integrated into each arm actuator.

The five-fingered, 12 DOF hand and the forearm form a completely self-contained unit: the fingers are divided into a dexterous set, used for manipulation, and a grasping set, used to maintain stable grasps while working with large tools. The dexterous set consists of two 3-DOF fingers (the index and middle) and a 4-DOF opposable thumb. The grasping set consists of two 1-DOF fingers (the ring and little fingers).

1.3.4 Dextre

Dextre [19] is made up of a headless torso, fitted with two 3.35 meters, 7 DOFs, robotic arms. The 3.5 meters long body has a grapple fixture at one end that can be grasped by the larger Space Station Arm, called Canadarm2,

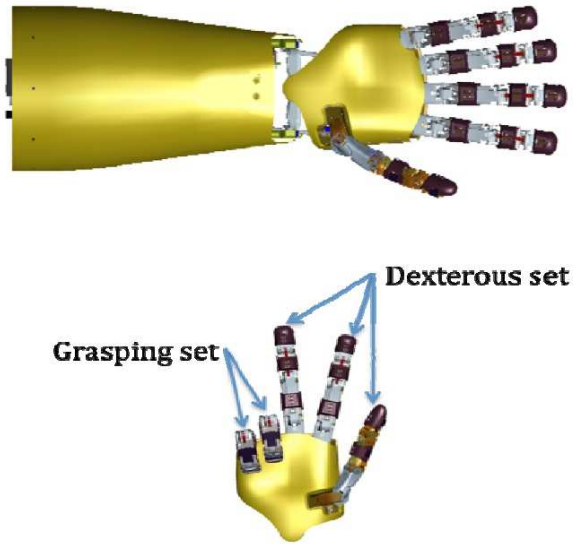

Figure 1.6: Robonaut's hand

(which is is 17.6 meters long 7-DOFs, fully actuated, robotic arm): it allows Dextre to be positioned at the various Orbital Replacement Unit (ORU) worksites around the Space Station. The other end of the body has an end effector identical to that of Canadarm2, allowing Dextre to be stored on Space Station grapple fixtures. At the end of Dextre's arms are ORU/Tool Changeout Mechanisms (OTCMs). The OTCM has built-in grasping jaws, a retractable socket drive, a monochrome TV camera, lights, and an umbilical connector that can provide power, data, and video to/from a payload. The lower body of Dextre has 2 orientable cameras with lights, a platform for stowing ORUs and a tool holder. SARAH (Self-Adaptive Robotic Auxiliary Hand) is a hand attached to the end of Dextre's arm. SARAH [57] is a reconfigurable hand with three self-adapting and orientable fingers. Each of the fingers has three independent phalanges automatically adapting to the shape of the grasped object. An additional DOF is provided to rotate the fingers, to better match the general geometry of the object. SARAH includes

Figure 1.7: The Dextre robotic manipulation system

only passive mechanisms that are actuated by the OTCM.

1.3.5 Ranger 8-DOFs Dextrous Space Manipulator

Ranger [46] is designed for on-orbit servicing of spacecraft and satellites, and, more in general, for task requiring multiple manipulators to grapple a satellite or component, provide video feedback to operators and perform tool-based operations on components being serviced. The robot consists of a central body, which houses the main computers and all the electronics and serves as a base platform for the manipulators. Ranger has two 8-DOFs dexterous manipulators for object manipulation and a 7-DOFs manipulator carrying the vision system. It also has a 6-DOFs positioning leg that anchors

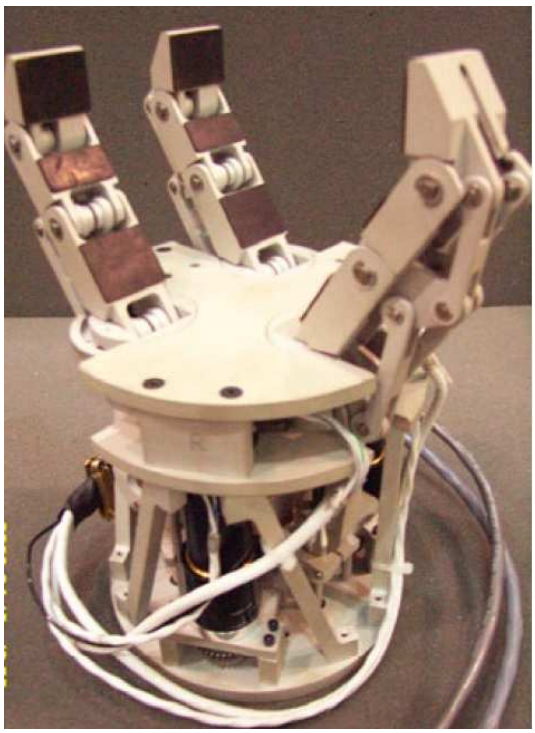

Figure 1.8: The SARAH robotic hand

it to a fixed base, which could be modified to enable grappling or docking to a spacecraft.

1.3.6 ETS-VII

The ETS-VII [32], or Engineering Test Satellite No. 7, is a satellite developed and launched by the National Space Development Agency (NASDA) of Japan. The ETS-VII is equipped with a 2 meters long robotic arm, which can be used to carry out rendezvous and docking tasks, as well as dexterous manipulation, by using the Advanced Robotic Hand of the Japan Ministry of International Trade and Industry (MITI) [47]. It was the world's first satellite to be equipped with a robotic arm, and also the first unmanned spacecraft to conduct autonomous rendezvous and docking operations successfully. The

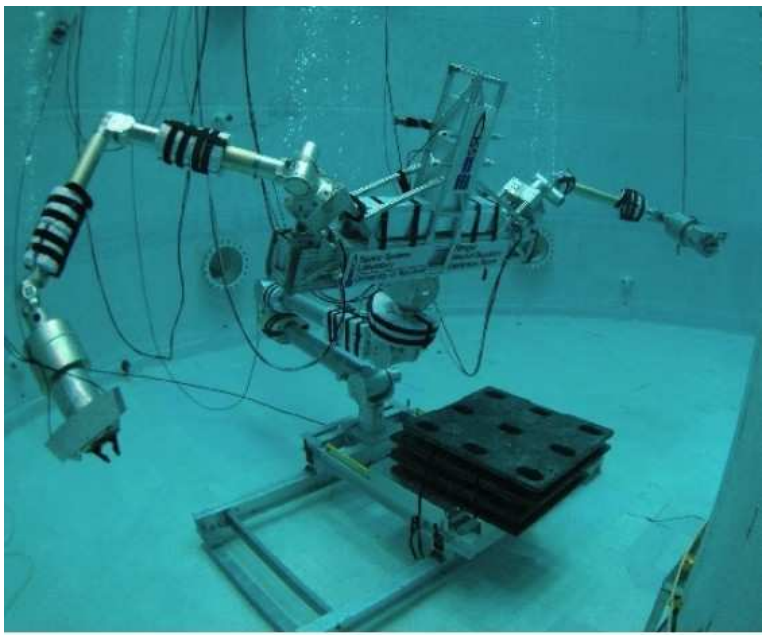

Figure 1.9: The Ranger robotic manipulation system

satellite was controlled remotely by a ground station. Communication between the onboard robot system and the ground control system is achieved by using a data relay satellite (NASA's TDRS) in the geo-stationary Earth orbit.

1.4 Related work

It has been recognized that many tasks are very difficult, or even impossible, to be accomplished by using a single robot, while they become feasible if more than one manipulator are involved in a cooperative way. Such tasks may include manipulation of large or heavy payloads, grasping objects and assembly of multiple parts. The use of cooperative manipulators often requires the adoption of tools and/or grippers designed ad hoc for the specif task they are involved in. This low flexibility can be overcome by using

Figure 1.10: The ETS-7 arm mounted on satellite

robotic hands as grasping tools, for two main reasons: a robotic hand can adjust itself to a wide number of object shapes, without the need of any reconfiguration, and it can handle tools designed for human operators. The latter consideration becomes more important, when space mission should be performed: it is impossible, due to space and/or payload limitation, to carry all the possible specialized tools that could be required.

In the literature there are several works dealing with control of multi-arm systems [8, 10, 4, 5] or robotic hands [31, 36, 52], but none of them is focused on control of multi-arm systems equipped with robotic hands; moreover, only a few works have considered the kinematic redundancy of such systems and the possibility to adopt redundancy resolution approaches with task priority, which has been successfully applied to robotic manipulators [2] and visual servoing [34].

When a cooperative multi-arm system is employed for the manipulation of a common object, it is important to control both the motion of the object and the internal forces not contributing to the object motion, acting as internal stresses. A suitable definition of the parmetrization of forces/moments on the object has been recognized to be helpful in achieving these goals. Force decomposition, studied by Uchiyama and Dauchez [68, 69], Walker et al. [70] as well as Bonitz and Hsia [4], suggests that a geometrically clear parametrization of the internal forces/moments acting on the object is a key issue; Williams and Khatib have given a solution to this [71, 59].

Recent control framework for cooperative systems is the so-called synchronization control [67, 56]; in this class of approaches the control problem is formulated in terms of suitably defined errors, accounting for the motion synchronization between the manipulators involved in the cooperative task. As for the nonlinear control of cooperative manipulation systems, efforts have been spent on intelligent control (see, e.g., [33] and [24], where fuzzy control is exploited to cope with unmodeled dynamics, parametric uncertainties and disturbances) as well as on the investigation of control strategies in the presence of partial state feedback [23]. Other approaches, rely on impedance control in order to keep interaction and contact forces bounded. More in detail, when the held object interacts with the environment, large contact forces may arise if the planned trajectory is not consistent with the geometry of the environment. In order to achieve bounded contact forces, an impedance behavior can be enforced between the object's position/orientation displacements and the contact force/moment (external impedance). On the other hand, even when the object/environment interaction does not take place, the interaction between the manipulators and the object may lead to internal forces and moments, which may cause damage to the system and overloading of the actuators. To counteract building of large values of internal forces, an impedance behavior can be enforced between the position/orientation displacements of

each manipulator and the end-effector force/moment, contributing solely to the internal loading of the object (internal impedance). The two impedance approaches have been applied separately [61],[5] while in [11], by following the guidelines in [9], they have been combined in a unique control framework, aimed at controlling both the contact forces due to the object/environment interaction (external impedance) and the internal forces due to the manipulators/object interaction (internal impedance). Papadopoulos and Moosavian focused on modeling and control of free flying cooperative robots [49, 41] for space operation like satellite chasing and repair. Sabelli at al. [58], designed a control strategy to dynamically select the impedance parameters of multi-arm space manipulators. A key issue in robotic grasping is controlling the forces arising from the contact between the fingertips and the grasped object, in such a way to prevent slippage and/or excessive stresses. At the same time, coordination of arms and fingers motion must be ensured to achieve tracking of the planned trajectory of the object. On the other hand, in the field of object manipulation via multi-fingered hands the focus has been put on manipulability analysis [3] and constrained kinematic control [25, 40].

Impedance control [26, 27] is one of the most adopted control laws for robot manipulators in contact with the external environment. The same approach has been, in turn, employed in object manipulation with multi-fingered hands. An impedance control approach for an arm-hand system is presented in [44]. The passivity property of impedance control is used in [65] to design an Intrinsically Passive Control (IPC), that can be used both in free space (i.e., when the fingers approach the object) and for grasping (the fingers apply forces to the object). In detail, a virtual object is defined, which is connected to each finger via a variable rest length spring, and to a virtual point via another spring; all the springs are 6-dimensional spatial springs [8, 66]. Further developments of IPC control for grasping can be found in [72, 73]. An impedance control scheme is adopted also in [60], combined

with an algorithm for grasp forces optimization, that allows the execution of different phases of a manipulation task, including the re-grasping one.

However the execution of object grasping or manipulation requires controlling also the interaction forces so as to ensure grasp stability [48]. To this end, an alternative to the impedance control could be the adoption of a hybrid force/position control [54, 63], especially if force and position are measured and the corresponding control actions are properly decoupled. The approach proposed in [43] starts from the consideration that the force on the fingers can be seen as the sum of two orthogonal components: the manipulation force, necessary to impose object motion, and the grasping force, necessary to fulfill friction cone constraints. An alternative approach based on feedback linearization is proposed in [20]. A decentralized control law is proposed in [55], where each finger is independently controlled via a hybrid force/position control scheme.

1.5 Objectives of the thesis

The contribution of this thesis rely on the development of a control framework for multi-arm systems equipped with robotic hands. The control framework will ensure kinematic redundancy resolution [12], via task sequencing techiniques and control of internal and external forces, as well as interaction forces limitation, via impedance control.

The first effort to achieve those goals is modeling: kinematic and dynamic models have been devised by considering each arm/hand system as a tree-structured open chained manipulator.

As concerns redundancy, several tasks, not always compatible, have been considered: they are aimed at tracking of the planned trajectory for the object, improving dexterity and ensuring grasp robustness. Those tasks have different priorities and could be dynamically deactivated and/or activated.

Beside tasks, some constraints, either mechanical (e.g., joint limits) or environmental (e.g., arising from workspace sharing with other robots or humans), have been taken into account. Since the constraints must be always satisfied, when a task is responsible to bring the system close to violate one or more constraints, it is deactivated, and reactivated as soon as the system is judged far from any dangerous configuration. Suitable metrics are defined in order to perform such deactivation and reactivation actions.

A fine internal force control is needed in order to achieve a stable grasp: that becomes more challenging when fingers should slide on the object surface in such a way improve grasp stability. A non-model-based parallel force/position controller has been considered, the stability of closed-loop the system has been theoretically proven [13]. A model-based direct force controller has also been used, by assuming knowledge of the dynamic model of the overall system.

In order to optimize the quality of the grasp, a set of virtual forces is introduced. Those fictitious forces act in such a way to reach the desired value when a suitable defined cost function, associated to some performance indexes, is minimum; a theoretical convergence of such algorithm has been also proven.

The impedance controller is in charge of computing the external forces references to impose the desired dynamics to the object (compliance in case of interaction, accurate tracking features otherwise).

A total different approach is that of considering arm and hand separately. The hand is controlled in such a way to achieve the desired internal contact forces, while the arm is made compliant by adopting an impedance controller. The forces to be taken into account in the arm control law are those acting on the wrist, net of the dynamic coupling effects due to the presence of the hand and the grasped object. The model of the coupling effects has been explicitly computed by considering, instead of the whole arm/hand system,

a dynamically equivalent one, made up by the same robotic hand, able to freely move in 3-D space, on which the action exerted on it by the arm is included trough an external wrench acting on the wrist. This wrench is the same exchanged between the arm and the hand which vanishes, by virtue of the second fundamental law of dynamics, in an overall formulation.

Chapter 2

Modeling

This chapter deals with modeling of multi-arm systems equipped with robotic hands: such complex systems are thought as tree-like structures since hands are generally multifingered.

The forward kinematics has been derived in order to relate joint configuration to operational space configuration. Differential kinematics, i.e. the map between joint velocities and contact twists, of the whole system has also been computed. At this point, contacts kinematics has been analyzed to establish a relation between joint velocities and grasped object twist.

Following the Lagrangian approach, the dynamic model of an arm/hand system has been derived, as well as, a specific model of a robotic hand mounted on a floating base: this is useful to understand the dynamic effects and forces exchanged between the arm and the hand at wrist level.

2.1 Kinematics

Let n_a be the number of robotic arms composing the system, and Σ a world frame, i.e. a reference frame common to all robots. Let Σ_{b_i} the base frame of manipulator i and Σ_{a_i} the palm frame attached to the base of the ith

robotic hand. Moreover, it has been assumed that the wrist frame on the arm and the palm frame are coincident. The forward kinematics of the ith manipulator, from the base to the wrist, can be expressed via the following homogeneous transformation matrix

$$\boldsymbol{T}_{a_i}^{b_i}(\boldsymbol{q}_{a_i}) = \begin{bmatrix} \boldsymbol{R}_{a_i}^{b_i} & \boldsymbol{o}_{a_i}^{b_i} \\ \boldsymbol{0}_3^{\mathrm{T}} & 1 \end{bmatrix}, \tag{2.1}$$

where $\boldsymbol{q}_{a_i}$ is the vector of arm's joint positions, $\boldsymbol{R}_{a_i}^{b_i}$ is the rotation matrix representing the orientation of frame Σ_{a_i} with respect to Σ_{b_i}, $\boldsymbol{o}_{a_i}^{b_i}$ is the position of the origin of frame Σ_{a_i} and $\boldsymbol{0}_\alpha$ is a $\alpha \times 1$ null vector. As concerns the hand, a reference frame, $\Sigma_{f_{i,j}}$ attached at the distal phalanx of finger j belonging to hand i, could be defined and, thus, the kinematics of the ith finger, with respect to the palm frame, becomes

$$\boldsymbol{T}_{f_{i,j}}^{a_i}(\boldsymbol{q}_{f_{i,j}}) = \begin{bmatrix} \boldsymbol{R}_{f_{i,j}}^{a_i} & \boldsymbol{o}_{f_{i,j}}^{a_i} \\ \boldsymbol{0}_3^{\mathrm{T}} & 1 \end{bmatrix}, \tag{2.2}$$

where $\boldsymbol{q}_{f_{i,j}}$ is the vector of joint positions of finger j, belonging to hand i, $\boldsymbol{R}_{f_{i,j}}^{a_i}$ is the rotation matrix representing the orientation of the finger frame j with respect to palm frame, $\boldsymbol{o}_{f_{i,j}}^{a_i}$ is the position of the origin of frame $\Sigma_{f_{i,j}}$. The kinematics of the finger with respect to world frame can be computed as

$$\boldsymbol{T}_{f_{i,j}}(\boldsymbol{q}_{i,j}) = \boldsymbol{T}_{b_i}\boldsymbol{T}_{a_i}^{b_i}(\boldsymbol{q}_{a_i})\boldsymbol{T}_{f_{i,j}}^{a_i}(\boldsymbol{q}_{f_{i,j}}), \tag{2.3}$$

where $\boldsymbol{T}_{b_i}$ is the constant homogeneous transformation between Σ_{b_i} and Σ, $\boldsymbol{q}_{i,j}$ is the vector of joint positions of the whole arm/hand system.

In order to derive the differential kinematics, it is useful to represent the velocity of $\Sigma_{f_{i,j}}$ with respect to Σ_{b_i} by the (6×1) twist vector $\boldsymbol{v}_{f_{i,j}}^{b_i} = \begin{bmatrix} \dot{\boldsymbol{o}}_{f_{i,j}}^{b_i\mathrm{T}} & \boldsymbol{\omega}_{f_{i,j}}^{b_i\mathrm{T}} \end{bmatrix}^{\mathrm{T}}$, where $\dot{\boldsymbol{o}}_{f_{i,j}}^{b_i}$ and $\boldsymbol{\omega}_{f_{i,j}}^{b_i}$ denote the linear and angular velocities of the finger frame with respect to the fixed base frame, respectively. It is worth noting that $\dot{\boldsymbol{R}}_{f_{i,j}} = \boldsymbol{S}(\boldsymbol{\omega}_{f_{i,j}})\boldsymbol{R}_{f_{i,j}}$, where $\boldsymbol{S}(\cdot)$ is the skew-symmetric

operator representing the vector product [63]. Hereafter, only for notation compactness, the index i labeling the arm is dropped. The differential kinematics equations relating the joint velocities to the velocity of frame Σ_{f_j} can be thus written as

$$\boldsymbol{v}_{f_j}^b = \begin{bmatrix} \boldsymbol{J}_{P_j}^b(\boldsymbol{q}_j) \\ \boldsymbol{J}_{O_j}^b(\boldsymbol{q}_j) \end{bmatrix} \dot{\boldsymbol{q}}_j = \boldsymbol{J}_{F_j}^b(\boldsymbol{q}_j)\dot{\boldsymbol{q}}_j, \tag{2.4}$$

where $\boldsymbol{q}_j = \begin{bmatrix} \boldsymbol{q}_a^{\mathrm{T}} & \boldsymbol{q}_{f_j}^{\mathrm{T}} \end{bmatrix}^{\mathrm{T}}$, $\boldsymbol{J}_{F_j}^b$ is the Jacobian of the arm, ending with finger j, and $\boldsymbol{J}_{P_j}^b$ and $\boldsymbol{J}_{O_j}^b$ denote the Jacobian linear and rotational part, respectively. The detailed expression of $\boldsymbol{J}_{F_j}^b$ in (2.4) is

$$\boldsymbol{J}_{F_j}^b = \begin{bmatrix} \boldsymbol{G}_a^{\mathrm{T}}(\boldsymbol{o}_{f_j,h})\boldsymbol{J}_a^b(\boldsymbol{q}_a) & \bar{\boldsymbol{R}}_a^b(\boldsymbol{q}_a)\boldsymbol{J}_{f_j}^a(\boldsymbol{q}_{f_j}) \end{bmatrix}, \tag{2.5}$$

where $\boldsymbol{J}_a^b$ is the Jacobian that maps the joint velocity of the arm, $\dot{\boldsymbol{q}}_a$, to the velocity of the frame Σ_a, $\bar{\boldsymbol{R}}_a^b = \mathrm{diag}\{\boldsymbol{R}_a^b, \boldsymbol{R}_a^b\}$, $\boldsymbol{R}_a^b \in SO(3)$ is the rotation matrix denoting the orientation of Σ_a with respect to the fixed base frame, $\boldsymbol{J}_{f_j}^a$ is the Jacobian that maps the joint velocity of the jth finger, $\dot{\boldsymbol{q}}_{f_j}$, to the velocity of Σ_{f_j} expressed with respect to Σ_a, $\boldsymbol{o}_{f_j,a}^b = \boldsymbol{o}_{f_j}^b - \boldsymbol{o}_a^b$ and $\boldsymbol{G}_a^{\mathrm{T}}(\boldsymbol{o}_{f_j,a}^b)$ is given by

$$\boldsymbol{G}_a^{\mathrm{T}}(\boldsymbol{o}_{f_j,a}^b) = \begin{bmatrix} \boldsymbol{I}_3 & -\boldsymbol{S}(\boldsymbol{o}_{f_j,a}^b) \\ \boldsymbol{O}_3 & \boldsymbol{I}_3 \end{bmatrix},$$

where $\boldsymbol{I}_\alpha$ and $\boldsymbol{O}_\alpha$ denote a $(\alpha \times \alpha)$ identity and null matrix, respectively.

Therefore, the differential kinematics equations of the whole arm-hand system can be written in the form

$$\widetilde{\boldsymbol{v}}_f^b = \boldsymbol{J}^b(\boldsymbol{q})\dot{\boldsymbol{q}}, \tag{2.6}$$

where $\widetilde{\boldsymbol{v}}_f^b = \begin{bmatrix} \boldsymbol{v}_{f_1}^{b\mathrm{T}} & \cdots & \boldsymbol{v}_{f_N}^{b\mathrm{T}} \end{bmatrix}^{\mathrm{T}}$, $\boldsymbol{q} = \begin{bmatrix} \boldsymbol{q}_a^{\mathrm{T}} & \boldsymbol{q}_{f_1}^{\mathrm{T}} & \cdots & \boldsymbol{q}_{f_N}^{\mathrm{T}} \end{bmatrix}^{\mathrm{T}}$, and $\boldsymbol{J}$ is the

Jacobian of the overall arm-hand system, whose detailed expression is

$$\boldsymbol{J}^b(\boldsymbol{q}) = \begin{bmatrix} \boldsymbol{G}_a^{\mathrm{T}}(\boldsymbol{o}_{f_1,a}^b)\boldsymbol{J}_a^b(\boldsymbol{q}_a) & \bar{\boldsymbol{R}}_a^b(\boldsymbol{q}_a)\boldsymbol{J}_{f_1}^a(\boldsymbol{q}_1) & \cdots & \boldsymbol{O} \\ \boldsymbol{G}_a^{\mathrm{T}}(\boldsymbol{o}_{f_2,a}^b)\boldsymbol{J}_a^b(\boldsymbol{q}_a) & \boldsymbol{O} & \ddots & \boldsymbol{O} \\ \vdots & \vdots & \ddots & \vdots \\ \boldsymbol{G}_a^{\mathrm{T}}(\boldsymbol{o}_{f_N,a}^b)\boldsymbol{J}_a^b(\boldsymbol{q}_a) & \boldsymbol{O} & \cdots & \bar{\boldsymbol{R}}_a^b(\boldsymbol{q}_a)\boldsymbol{J}_{f_N}^a(\boldsymbol{q}_N) \end{bmatrix},$$

where $\boldsymbol{O}$ denotes a null matrix of appropriate dimensions. The differential kinematics of the ith arm/hand systems, in terms of common world frame coordinate becomes

$$\begin{aligned} \widetilde{\boldsymbol{v}}_{f_i}^{b_i} &= \boldsymbol{J}_i(\boldsymbol{q}_i)\dot{\boldsymbol{q}}_i \\ \boldsymbol{J}_i(\boldsymbol{q}_i) &= \bar{\boldsymbol{R}}_{b_i}\boldsymbol{J}_i^{b_i}(\boldsymbol{q}_{b_i}) \end{aligned}, \tag{2.7}$$

where $\bar{\boldsymbol{R}}_{b_i} = \mathrm{diag}\{\boldsymbol{R}_{b_i}, \boldsymbol{R}_{b_i}\}$, $\boldsymbol{R}_{b_i}$ is the rotation matrix representing the orientation of Σ_b with respect the inertial common reference frame.

2.2 Contact modeling

Contact allows to impose a desired motion to the object or to apply a desired force trough the object. Hence, all possible grasping actions are transmitted trough contacts, whose modeling and control is crucial in grasping. The three models of greatest interest in grasp analysis are known as point contact without friction, hard finger, and soft finger.

The *point contact without friction* (PwoF) model is to be considered when the contact area is very small and the surfaces of the hand and object are slippery; only the component of the translational velocity normal to the object surface on the contact point is transmitted to the object. The two components of tangential velocity and the three components of angular velocity are not transmitted. Analogously, the normal component of the contact force is transmitted, while the frictional forces and moments are assumed to be negligible.

A *hard finger* (HF) model is used when there is significant contact friction and the contact patch is small. When this model is considered, all three translational velocity components of the contact point on the hand and all three components of the contact force are transmitted through the contact. Angular velocity components and moment components are not transmitted through the contacts.

The *soft finger* (SF) model is adopted when contact surface, due to finger deformation, is not negligible: friction moment around the contact normal are significant. The three translational velocity components of the contact on the hand and the angular velocity component about the contact normal are transmitted.

2.3 Contact kinematics

Both the object and the robotic fingers are often smooth surfaces and then, depending on the contact type, manipulation involves rolling and/or sliding of the fingertips on the object's surface. If the fingers and object shapes are completely known, the contact kinematics can be described by introducing contact coordinates defined on the basis of a suitable parametrization of the contact surfaces [39, 42].

2.3.1 Contact kinematics from the object point of view

By assuming that the hand grasps a rigid object, it is, thus, useful to introduce a frame, Σ_o, attached to the object, usually chosen with the origin in the object center of mass. Let $\boldsymbol{R}_o$ and $\boldsymbol{o}_o$ denote, respectively, the rotation matrix and the position vector of the origin of Σ_o with respect to the base frame, and let $\boldsymbol{v}_o$ denote the object velocity twist vector. Let Σ_{c_j} be the contact frame attached to the object with the origin at the contact point,

$\boldsymbol{o}_{c_j}$. Notice that, instantaneously, the object contact point $\boldsymbol{o}_{c_j}$ and the finger contact point $\boldsymbol{o}_{k_j}$ coincide. One of the axes of Σ_{c_j}, e.g., the Z axis, is assumed to be the outward normal to the tangent plane to the object surface at the contact point.

The position of the contact point with respect to the object frame, $\boldsymbol{o}^o_{o,c_j} = \boldsymbol{o}^o_{c_j} - \boldsymbol{o}^o_o$, can be parametrized, at least locally, in terms of a coordinate chart, $\boldsymbol{c}^o_j : U_j \subset \mathbb{R}^2 \mapsto \mathbb{R}^3$, which maps a chart's point $\boldsymbol{\xi}_j = \begin{bmatrix} u_j & v_j \end{bmatrix}^{\mathrm{T}} \in U_j$ to the point $\boldsymbol{o}^o_{o,c_j}(\boldsymbol{\xi}_j)$ on the surface of the object [39].

By assuming that $\boldsymbol{c}^o_j$ is a diffeomorphism and that the coordinate chart is orthogonal and right-handed, the contact frame Σ_{c_j} can be thus chosen as a Gauss frame [39], where the relative orientation, expressed by the rotation matrix $\boldsymbol{R}^o_{c_j}$, has the following expression

$$\boldsymbol{R}^o_{c_j}(\boldsymbol{\xi}) = \begin{bmatrix} \dfrac{\boldsymbol{c}^o_{u_j}}{\|\boldsymbol{c}^o_{u_j}\|} & \dfrac{\boldsymbol{c}^o_{v_j}}{\|\boldsymbol{c}^o_{v_j}\|} & \dfrac{\boldsymbol{c}^o_{u_j} \times \boldsymbol{c}^o_{v_j}}{\|\boldsymbol{c}^o_{u_j} \times \boldsymbol{c}^o_{v_j}\|} \end{bmatrix}, \tag{2.8}$$

and hence it is computed as function of the orthogonal tangent vectors $\boldsymbol{c}^o_{u_j} = \partial \boldsymbol{c}^o_j / \partial u_j$ and $\boldsymbol{c}^o_{v_j} = \partial \boldsymbol{c}^o_j / \partial v_j$. Function $\boldsymbol{c}^o_j(\boldsymbol{\xi}_j(t))$ denotes a curve on the object's surface parametrized by the time variable t. Hence, the corresponding motion of Σ_{c_j} with respect to the base frame can be determined as a function of the object motion, the geometric parameters of the object and the curve geometric features. Namely, computing the time derivative of equation $\boldsymbol{o}_{c_j} = \boldsymbol{o}_o + \boldsymbol{R}_o \boldsymbol{c}^o_j(\boldsymbol{\xi}_j)$, which provides the position of the object contact point in the base frame, yields

$$\dot{\boldsymbol{o}}_{c_j} = \dot{\boldsymbol{o}}_o - \boldsymbol{S}(\boldsymbol{R}_o \boldsymbol{c}^o_j(\boldsymbol{\xi}_j))\boldsymbol{\omega}_o + \boldsymbol{R}_o \frac{\partial \boldsymbol{c}^o_j}{\partial \boldsymbol{\xi}_j} \dot{\boldsymbol{\xi}}_j, \tag{2.9}$$

where the first two terms on the right-hand side specify the velocity contribution due to the object motion, while the last term represents the finger velocity relative to the object surface. On the other hand, for the angular velocity, the following equality holds

$$\boldsymbol{\omega}_{c_j} = \boldsymbol{\omega}_o + \boldsymbol{R}_o \boldsymbol{\omega}^o_{o,c_j}, \tag{2.10}$$

where $\boldsymbol{\omega}^o_{o,c_j}$ is the angular velocity of Σ_{c_j} with respect to Σ_o, that can be expressed as

$$\boldsymbol{\omega}^o_{o,c_j} = \boldsymbol{C}(\boldsymbol{\xi}_j)\dot{\boldsymbol{\xi}}_j, \tag{2.11}$$

where $\boldsymbol{C}(\boldsymbol{\xi}_j)$ is a (3×2) matrix depending on geometric parameters of the surface [42]. Matrix $\boldsymbol{C}$ is not necessarily full rank (e.g., is null in the case of planar surfaces). In view of (2.9), (2.10) and (2.11), the velocity of the contact frame can be expressed as

$$\boldsymbol{v}_{c_j} = \begin{bmatrix} \dot{\boldsymbol{o}}_{c_j} \\ \boldsymbol{\omega}_{c_j} \end{bmatrix} = \boldsymbol{G}^{\mathrm{T}}_{\xi_j}(\boldsymbol{\xi}_j)\boldsymbol{v}_{o_j} + \boldsymbol{J}_{\xi_j}(\boldsymbol{\xi}_j)\dot{\boldsymbol{\xi}}_j, \tag{2.12}$$

where $\boldsymbol{G}_{\xi_j}(\boldsymbol{\xi}_j)$ and $\boldsymbol{J}_{\xi_j}(\boldsymbol{\xi}_j)$ are (6×6) and (6×2) full rank matrices, respectively, having the following expressions

$$\boldsymbol{G}^{\mathrm{T}}_{\xi_j}(\boldsymbol{\xi}_j) = \begin{bmatrix} \boldsymbol{I}_3 & -\boldsymbol{S}(\boldsymbol{R}_o\boldsymbol{c}^o_j(\boldsymbol{\xi}_j)) \\ \boldsymbol{O}_3 & \boldsymbol{I}_3 \end{bmatrix}, \qquad \boldsymbol{J}_{\xi_j}(\boldsymbol{\xi}_j) = \begin{bmatrix} \boldsymbol{R}_o \dfrac{\partial \boldsymbol{c}^o_j}{\partial \boldsymbol{\xi}_j} \\ \boldsymbol{R}_o\boldsymbol{C}(\boldsymbol{\xi}_j) \end{bmatrix}.$$

2.3.2 Contact kinematics from the finger point of view

It is assumed that the fingertips are sharp (i.e., they end with a point, denoted as tip point) and covered by an elastic pad. The elastic contact is hence modelled by introducing a finger contact frame Σ_{k_j}, attached to the soft pad and with the origin in the tip point $\boldsymbol{o}_{k_j}$, and a spring-damper system connecting $\boldsymbol{o}_{k_j}$ with the origin of Σ_{f_j}. This last frame is attached to the rigid part of the finger (w.r.t. Fig. 2.1) and has the same orientation of Σ_{k_j}. The displacement between Σ_{f_j} and Σ_{k_j}, due to the elastic contact force, can be computed as

$$\boldsymbol{o}_{f_j} - \boldsymbol{o}_{k_j} = (l_j - \Delta l_j)\boldsymbol{R}_o\hat{\boldsymbol{n}}^o(\boldsymbol{\xi}), \tag{2.13}$$

where l_j and $0 \leq \Delta l_j \leq l_j$ are the rest position and the compression of the spring, respectively, and $\hat{\boldsymbol{n}}^o$ is the unit vector representing the outward

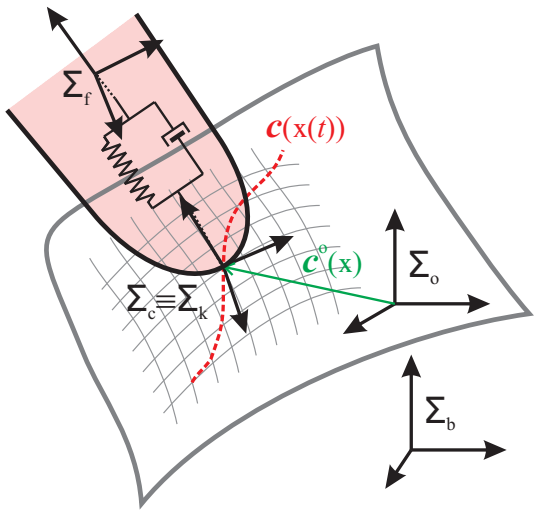

Figure 2.1: Local parametrization of the object surface with respect to Σ_o

normal to the object's surface at the contact point, expressed with respect to Σ_o.

The contact can be modeled with an unactuated 3-DOFs ball and socket kinematic pair centered at the origin $\boldsymbol{o}_{k_j}$ of Σ_{k_j}. This origin is, in general, fixed to the soft pad of the finger, but it may also move on the surface if sliding is allowed. Therefore, the relative orientation of Σ_{c_j} with respect to Σ_{k_j}, $\boldsymbol{R}_{c_j}^{k_j}$, can be computed in terms of a suitable parametrization of the ball and socked joint, e.g., Euler angles or angle-axis representations. If the parametrization in terms of XYZ Euler angles is adopted, a vector $\boldsymbol{\theta}_j = \begin{bmatrix}\theta_{1_j} & \theta_{2_j} & \theta_{3_j}\end{bmatrix}^{\mathrm{T}}$ can be considered; thus, $\boldsymbol{R}_{c_j}^{k_j} = \boldsymbol{R}_{c_j}^{k_j}(\boldsymbol{\theta}_j)$. In detail, θ_{1_j} and θ_{2_j} parametrize the so-called "swing" motion, aligning axis Z of a moving frame to axis Z of the contact frame, while θ_{3_j} corresponds to the "twist" motion about axis Z of the contact frame. Singularities occurs for $\theta_{2_j} = \pm\pi/2$, but they do not correspond to physical kinematic singularities.

Notice that, in the presence of a contact force, tip elasticity allows mutual translation of Σ_{k_j} with respect to Σ_{f_j}, according to (2.13), while the mutual orientation does not change. Therefore, $\boldsymbol{R}_{c_j}^{k_j} = \boldsymbol{R}_{c_j}^{f_j}$. Moreover, the angular

velocity of Σ_{c_j} relative to Σ_{f_j} can be expressed as $\boldsymbol{\omega}_{f_j,c_j}^{f_j} = \boldsymbol{D}(\boldsymbol{\theta}_j)\dot{\boldsymbol{\theta}}_j$, where $\boldsymbol{D}$ is a transformation matrix depending on the chosen parametrization [63]. In view of the decomposition $\boldsymbol{\omega}_{c_j} = \boldsymbol{\omega}_{f_j} + \boldsymbol{R}_{f_j}(\boldsymbol{q}_j)\boldsymbol{\omega}_{f_j,c_j}^{f_j}$ and equation (2.4), the angular velocity of Σ_{c_j} can be computed also as a function of joint and contact variables in the form

$$\boldsymbol{\omega}_{c_j} = \boldsymbol{J}_{O_j}(\boldsymbol{q}_j)\dot{\boldsymbol{q}}_j + \boldsymbol{R}_{f_j}(\boldsymbol{q}_j)\boldsymbol{D}(\boldsymbol{\theta}_j)\dot{\boldsymbol{\theta}}_j, \tag{2.14}$$

with $\boldsymbol{J}_{O_j}$ defined in (2.4). Moreover, since the origins of Σ_{c_j} and Σ_{k_j} coincide, the following equality holds

$$\boldsymbol{o}_{c_j} = \boldsymbol{o}_{k_j} = \boldsymbol{o}_{f_j} - (l_j - \Delta l_j)\boldsymbol{R}_o\hat{\boldsymbol{n}}_j^o(\boldsymbol{\xi}_j), \tag{2.15}$$

while the time derivative of (2.15) yields

$$\begin{aligned} \dot{\boldsymbol{o}}_{c_j} &= \boldsymbol{J}_{P_j}(\boldsymbol{q}_j)\dot{\boldsymbol{q}}_j + \dot{\Delta l}_j\boldsymbol{R}_o\hat{\boldsymbol{n}}_j^o(\boldsymbol{\xi}_j) + \\ &+ (l_j - \Delta l_j)\left[\boldsymbol{S}(\boldsymbol{R}_o\hat{\boldsymbol{n}}_j^o(\boldsymbol{\xi}_j))\boldsymbol{\omega}_o - \boldsymbol{R}_o\frac{\partial\hat{\boldsymbol{n}}_j^o(\boldsymbol{\xi}_j)}{\partial\boldsymbol{\xi}_j}\dot{\boldsymbol{\xi}}_j\right], \end{aligned} \tag{2.16}$$

with $\boldsymbol{J}_{P_j}$ defined in (2.4).

By considering (2.14) and (2.16), the velocity of the contact frame can be expressed as

$$\begin{aligned} \boldsymbol{v}_{c_j} &= \boldsymbol{J}_{F_j}(\boldsymbol{q})\dot{\boldsymbol{q}} + \boldsymbol{J}_{\theta_j}(\boldsymbol{\theta}_j, \boldsymbol{q}_j)\dot{\boldsymbol{\theta}}_j + \boldsymbol{J}_{\Delta l_j}(\boldsymbol{\xi}_j)\dot{\Delta l}_j - \\ &- \boldsymbol{J}'_{\xi_j}(\boldsymbol{\xi}_j, \Delta l_j)\dot{\boldsymbol{\xi}}_j - \boldsymbol{G}_{\Delta l_j}^{\mathrm{T}}(\boldsymbol{\xi}_j, \Delta l_j)\boldsymbol{v}_o, \end{aligned} \tag{2.17}$$

where $\boldsymbol{J}_{F_j}$ is defined in (2.5), $\boldsymbol{J}_{\theta_j}$ is a (6×3) full column rank matrix

$$\boldsymbol{J}_{\theta_j} = \begin{bmatrix} \boldsymbol{O}_3 \\ \boldsymbol{R}_{f_j}(\boldsymbol{q}_j)\boldsymbol{D}(\boldsymbol{\theta}_j) \end{bmatrix},$$

$\boldsymbol{J}_{\Delta l_j}$ is a (6×1) vector

$$\boldsymbol{J}_{\Delta l_j} = \begin{bmatrix} \boldsymbol{R}_o\hat{\boldsymbol{n}}_j^o(\boldsymbol{\xi}_j) \\ \boldsymbol{0_3} \end{bmatrix},$$

$\boldsymbol{J}'_{\xi_j}$ is a (6×2) full column rank matrix

$$\boldsymbol{J}'_{\xi_j} = \begin{bmatrix} (l - \Delta l_j)\boldsymbol{R}_o \dfrac{\partial \hat{\boldsymbol{n}}_j^o(\boldsymbol{\xi}_j)}{\partial \boldsymbol{\xi}_j} \\ \boldsymbol{O}_{3\times 2} \end{bmatrix},$$

where $\boldsymbol{O}_{3\times 2}$ is the (3×2) null matrix, and $\boldsymbol{G}^{\mathrm{T}}_{\Delta l_j}$ is the (6×6) matrix

$$\boldsymbol{G}^{\mathrm{T}}_{\Delta l_j} = \begin{bmatrix} \boldsymbol{O}_3 & (\Delta l_j - l_j)\boldsymbol{S}(\boldsymbol{R}_o \hat{\boldsymbol{n}}_j^o(\boldsymbol{\xi}_j)) \\ \boldsymbol{O}_3 & \boldsymbol{O}_3 \end{bmatrix}.$$

Therefore, from (2.12) and (2.17), the contact kinematics of finger i can be expressed as

$$\boldsymbol{J}_{F_j}(\boldsymbol{q}_j)\dot{\boldsymbol{q}}_j + \boldsymbol{J}_{\eta_j}(\boldsymbol{\eta}_j, \boldsymbol{q}_j, \Delta l_j)\dot{\boldsymbol{\eta}}_j + \boldsymbol{J}_{\Delta l_j}(\boldsymbol{\xi})\dot{\Delta} l_j = \boldsymbol{G}_j^{\mathrm{T}}(\boldsymbol{\eta}_j, \Delta l_j)\boldsymbol{\upsilon}_o, \qquad (2.18)$$

where $\boldsymbol{\eta}_j = \begin{bmatrix} \boldsymbol{\xi}_j^{\mathrm{T}} & \boldsymbol{\theta}_j^{\mathrm{T}} \end{bmatrix}^{\mathrm{T}}$ is the vector of contact variables,

$$\boldsymbol{J}_{\eta_j} = \begin{bmatrix} -(\boldsymbol{J}_{\xi_j} + \boldsymbol{J}'_{\xi_j}) & \boldsymbol{J}_{\theta_j} \end{bmatrix},$$

is a (6×5) full rank matrix, and $\boldsymbol{G}_j = \boldsymbol{G}_{\xi_j} + \boldsymbol{G}_{\Delta l_j}$ is a (6×6) full rank grasp matrix.

Equation (2.18) can be interpreted as the differential kinematics equation of an "extended" finger corresponding to the kinematic chain which includes the arm, the finger joint variables (*active joints*) and the contact variables (*passive joints*). Moreover, notice that (2.18) involves all the 6 components of the velocity, while grasping constraints adopted in the literature usually consider only those transmitted by the contact [40, 42].

Depending on the considered contact type, some of the parameters $\boldsymbol{\xi}_j$ and $\boldsymbol{\theta}_j$ are constant. Hence, by assuming that such contact type remains unchanged during the task, the variable parameters at each contact point are grouped in a $(n_{c_j} \times 1)$ vector, $\boldsymbol{\eta}_j$, of contact variables, with $n_{c_j} \leq 5$.

Differently form the classical grasp analysis, in this thesis the elasticity of the soft pad has been explicitly modelled, although using a simplified model. This means that the force along the normal to the contact surface is always of elastic type. The quantity Δl_j, at steady state, is related to the normal contact force f_{n_j} by the equation $\Delta l_j = f_{n_j}/k_j$, being k_j the elastic constant of the soft pad of finger j.

2.4 Dynamics of the arm/hand system

In the following the analysis will be focused on a single arm manipulator equipped with a multifinger robotic hand; here, different from the previous sections, the index i no longer indicate a particular arm/hand system.

The lagrangian formulation, according to [63], is chosen to have a compact and not recursive description of the system dynamics. As first step, the computation of the total energy, given by the sum of the kinetic and potential energy, of the system needs to be performed. It is worth pointing out that all the vectors and the matrices are expressed in terms of the manipulator base frame coordinates.

2.4.1 Kinetic energy

The kinetic energy, associated to the arm, can be computed as

$$\mathcal{K}_a = \frac{1}{2} \sum_{i=1}^{h} m_i \dot{\boldsymbol{p}}_i^T \dot{\boldsymbol{p}}_i + \boldsymbol{\omega}_i^T \boldsymbol{M}_i \boldsymbol{\omega}_i, \tag{2.19}$$

where m_i and $\boldsymbol{M}_i$ are, respectively, the mass and inertia tensor of link i of the arm, $\dot{\boldsymbol{p}}_i \in \Re^3$, $\boldsymbol{\omega}_i \in \Re^3$ are the linear and angular velocity of the frame attached on the center of gravity (CoG) of the link i.
The generalized CoG velocity of the ith link belonging to the arm can be

further expressed as

$$\boldsymbol{v}_i = \begin{bmatrix} \dot{\boldsymbol{p}}_i \\ \boldsymbol{\omega}_i \end{bmatrix} = \begin{bmatrix} \boldsymbol{J}_p^i(\boldsymbol{q}_i) \\ \boldsymbol{J}_o^i(\boldsymbol{q}_i) \end{bmatrix} \dot{\boldsymbol{q}}_i, \tag{2.20}$$

where $\boldsymbol{p}_i$ is the CoG position of the ith link, $\boldsymbol{J}_p^i(\boldsymbol{q}_i)$, $\boldsymbol{J}_o^i(\boldsymbol{q}_i)$ are computed according to [63]

$$\boldsymbol{J}_p^i(\boldsymbol{q}_i) = \begin{bmatrix} \boldsymbol{J}_{p1}^i(q_1) & \boldsymbol{J}_{p2}^i(q_2) & \dots & \boldsymbol{J}_{pi}^i(q_i) & \boldsymbol{0}_{a-i} \end{bmatrix}, \tag{2.21}$$

$$\boldsymbol{J}_o^i(\boldsymbol{q}_i) = \begin{bmatrix} \boldsymbol{J}_{o1}^i(q_1) & \boldsymbol{J}_{o2}^i(q_2) & \dots & \boldsymbol{J}_{oi}^i(q_i) & \boldsymbol{0}_{a-i} \end{bmatrix}, \tag{2.22}$$

where $\boldsymbol{q}_i = [q_1 \ q_2 \ \dots \ q_i]^T$, $\boldsymbol{J}_{pi}^i(q_j)$ $\left(\boldsymbol{J}_{oi}^i(q_j)\right)$ is the contribution of joint j to the linear (angular) velocity of link i. Equations (2.21), (2.22) represent the contribution of all joints, up to the ith, to the linear and angular velocity of the CoG of link i.

The kinetic energy associated to the fingers can be expressed as

$$\mathcal{K}_f = \frac{1}{2} \sum_{j=1}^{N} \sum_{i=1}^{f_j} m_i^j \dot{\boldsymbol{p}}_i^{j\mathrm{T}} \dot{\boldsymbol{p}}_i^{j\mathrm{T}} + \boldsymbol{\omega}_i^{j\mathrm{T}} \boldsymbol{M}_i^j \boldsymbol{\omega}_i^j, \tag{2.23}$$

where m_i^j, $\boldsymbol{M}_i^j$ are, respectively, the mass and inertia tensor of link i belonging to finger j, $\dot{\boldsymbol{p}}_i^j \in \Re^3$, $\boldsymbol{\omega}_i^j \in \Re^3$ are the linear and angular velocity of the frame attached on the center of gravity (CoG) of the link i belonging to finger j, f_j is the number of links composing finger j.

The velocity of the CoG of each link of the jth finger can be computed as

$$\boldsymbol{v}_i^j = \boldsymbol{G}_{i,a}^{j\mathrm{T}} \boldsymbol{v}_a + \boldsymbol{v}_{i,a}^j, \tag{2.24}$$

where $i = 1, 2, \dots, n_j$,

$$\boldsymbol{G}_{i,a}^{j\mathrm{T}}\left(\boldsymbol{p}_{i,a}^j\right) = \begin{bmatrix} \boldsymbol{I}_3 & -\boldsymbol{S}(\boldsymbol{p}_{i,a}^j) \\ \boldsymbol{O}_3 & \boldsymbol{I}_3 \end{bmatrix}, \tag{2.25}$$

$\boldsymbol{v}_a = \left[\dot{\boldsymbol{p}}_a^{\mathrm{T}} \ \boldsymbol{\omega}_a^{\mathrm{T}}\right]^{\mathrm{T}} \in \Re^6$ is the generalized velocity of the palm frame Σ_a (which coincides with the arm end-effector frame), $\boldsymbol{v}_{i,a}^j = \left[\dot{\boldsymbol{p}}_{i,a}^{j\mathrm{T}} \ \boldsymbol{\omega}_{i,a}^{j\mathrm{T}}\right]^T$, $\boldsymbol{p}_{i,a}^j \in \Re^3$ is

the relative position of the CoG of link i, belonging to finger j, with respect to the palm frame, $\boldsymbol{\omega}_{i,a}^{j} \in \Re^3$ is the relative angular velocity of the CoG of the link i, belonging to finger j, with respect to the palm frame. Linear and angular relative velocities $\dot{\boldsymbol{p}}_{i,a}^{j}$, $\boldsymbol{\omega}_{i,a}^{j}$ could be further expressed as

$$\boldsymbol{v}_{i,a}^{j} = \begin{bmatrix} \dot{\boldsymbol{p}}_{i,a}^{j} \\ \boldsymbol{\omega}_{i,a}^{j} \end{bmatrix} = \begin{bmatrix} \boldsymbol{J}_{p}^{i,j}(\boldsymbol{q}_{i}^{j}) \\ \boldsymbol{J}_{o}^{i,j}(\boldsymbol{q}_{i}^{j}) \end{bmatrix} \dot{\boldsymbol{q}}_{i}^{j} = \boldsymbol{J}_{f}^{i,j} \dot{\boldsymbol{q}}_{i}^{j}, \tag{2.26}$$

where $\boldsymbol{q}_{i}^{j} = \left[q_{1}^{j}, q_{2}^{j}, \ldots, q_{i}^{j}\right]$, q_{i}^{j} is the position of the ith joint belonging to the jth finger, while $\boldsymbol{J}_{p}^{i,j}$, $\boldsymbol{J}_{o}^{i,j}$ can be formally obtained via (2.21), (2.22) by replacing $\boldsymbol{q}_{i}$ with $\boldsymbol{q}_{i}^{j}$, q_{k} with q_{k}^{j} and h with f_{j}. The kinetic energy of the system is given by

$$\mathcal{K} = \mathcal{K}_{a} + \mathcal{K}_{f},$$

which, in turn, could be rewritten in a more compact form, by considering equations (2.23)-(2.45), as

$$\mathcal{K} = \frac{1}{2} \dot{\boldsymbol{q}}^{\mathrm{T}} \boldsymbol{B}(\boldsymbol{q}) \dot{\boldsymbol{q}}, \tag{2.27}$$

where $\boldsymbol{q} = \left[\boldsymbol{q}_{a}^{\mathrm{T}},\ \boldsymbol{q}_{f}^{\mathrm{T}}\right]^{\mathrm{T}}$, $\boldsymbol{q}_{a} \in \Re^{h}$, $\boldsymbol{q}_{f} \in \Re^{n-h}$ are the vectors of arm and fingers' joints, respectively, $\boldsymbol{B}(\boldsymbol{q})$ is the block matrix

$$\boldsymbol{B}(\boldsymbol{q}) = \begin{bmatrix} \boldsymbol{B}_{aa}(\boldsymbol{q}) & \boldsymbol{B}_{af}(\boldsymbol{q}) \\ \boldsymbol{B}_{fa}(\boldsymbol{q}) & \boldsymbol{B}_{ff}(\boldsymbol{q}) \end{bmatrix}, \tag{2.28}$$

whose elements have the following expressions

$$\begin{aligned} \boldsymbol{B}_{aa}(\boldsymbol{q}) &= \sum_{i=1}^{h} \left(m_{i} \boldsymbol{J}_{p}^{i\,T}(\boldsymbol{q}_{i}) \boldsymbol{J}_{p}^{i}(\boldsymbol{q}_{i}) + \boldsymbol{J}_{o}^{i\,T}(\boldsymbol{q}_{i}) \boldsymbol{M}_{i} \boldsymbol{J}_{o}^{i}(\boldsymbol{q}_{i}) \right) + \\ &\quad + \sum_{j=1}^{N} \sum_{i=1}^{f_{j}} \left(\boldsymbol{J}_{a}^{T}(\boldsymbol{q}_{a}) \boldsymbol{G}_{i,a}^{j}(\boldsymbol{p}_{i,a}^{j}) \bar{\boldsymbol{M}}_{i}^{j} \boldsymbol{G}_{i,a}^{j\mathrm{T}}(\boldsymbol{p}_{i,a}) \boldsymbol{J}_{a}(\boldsymbol{q}_{a}) \right), \\ \boldsymbol{B}_{af}(\boldsymbol{q}) &= \sum_{j=1}^{N} \sum_{i=1}^{f_{j}} \boldsymbol{J}_{a}^{\mathrm{T}}(\boldsymbol{q}_{a}) \boldsymbol{G}_{i,a}^{j}(\boldsymbol{p}_{i,a}^{j}) \bar{\boldsymbol{M}}_{i}^{j} \boldsymbol{J}_{f}^{i,j}(\boldsymbol{q}_{f}), \end{aligned}$$

$$\boldsymbol{B}_{fa}(\boldsymbol{q}) = \sum_{j=1}^{N}\sum_{i=1}^{f_j}\left(\boldsymbol{J}_a^{\mathrm{T}}(\boldsymbol{q}_a)\boldsymbol{G}_{i,a}^{j}(\boldsymbol{p}_{i,a}^{j})\bar{\boldsymbol{M}}_i^j\boldsymbol{J}_f^{i,j}(\boldsymbol{q}_a)\right)^{\mathrm{T}}, \tag{2.29}$$

$$\boldsymbol{B}_{ff}(\boldsymbol{q}) = \sum_{j=1}^{N}\sum_{i=1}^{n_j}\left(m_i{\boldsymbol{J}_p^i}^T(\boldsymbol{q}_i^j)\boldsymbol{J}_p^i(\boldsymbol{q}_i^j)+{\boldsymbol{J}_o^i}^T(\boldsymbol{q}_i^j)\boldsymbol{M}_i^j\boldsymbol{J}_o^i(\boldsymbol{q}_i^j)\right),$$

where $\boldsymbol{J}_a \in \Re^{m\times h}$ is the geometric Jacobian of the arm and $\bar{\boldsymbol{M}}_i^j = \mathrm{diag}\{m_i^j\boldsymbol{I}_3, \boldsymbol{M}_i^j\}$. The block matrices $\boldsymbol{B}_{af}$ and $\boldsymbol{B}_{fa}$ in (2.29) are coupling terms which take into account the dynamic effect of the hand on the arm and viceversa. The following properties hold:

1. mutual symmetry of $\boldsymbol{B}_{af}$ and $\boldsymbol{B}_{fa}^{\mathrm{T}}$, i.e. $\boldsymbol{B}_{af} = \boldsymbol{B}_{fa}^{\mathrm{T}}$;
2. $\boldsymbol{B}$ is symmetric and positive definite.

2.4.2 Potential energy

The potential energy of the arm can be written as

$$\mathcal{T}_a = -\sum_{i=1}^{h} m_i\boldsymbol{g}_a^{\mathrm{T}}\boldsymbol{p}_i, \tag{2.30}$$

where $\boldsymbol{g}_a = [0,\, 0,\, -g]^{\mathrm{T}}$ is gravity acceleration, while for the hand the potential energy is given by

$$\mathcal{T}_f = -\sum_{j=1}^{N}\sum_{i=1}^{f_j} m_i^j\boldsymbol{g}_a^{\mathrm{T}}\boldsymbol{p}_i^j, \tag{2.31}$$

where $\boldsymbol{p}_i^j$ can be further expressed as

$$\boldsymbol{p}_i^j = \boldsymbol{p}_a + \boldsymbol{p}_{i,a}^j, \tag{2.32}$$

and thus, the potential energy of the overall system is

$$\mathcal{T} = -\sum_{i=1}^{h} m_i\boldsymbol{g}_a^{\mathrm{T}}\boldsymbol{p}_i - \sum_{j=1}^{N}\sum_{i=1}^{f_j} m_i^j\boldsymbol{g}_a^{\mathrm{T}}\boldsymbol{p}_a - \sum_{j=1}^{N}\sum_{i=1}^{f_j} m_i^j\boldsymbol{g}_a^{\mathrm{T}}\boldsymbol{p}_{i,j}^j. \tag{2.33}$$

2.4.3 Lagrangian equation

The Langrangian of the mechanical system is given by the difference between the kinetic and the potential energy

$$\mathcal{L} = \mathcal{K} - \mathcal{T}, \tag{2.34}$$

while the Lagrangian equation could be expressed as

$$\frac{\mathrm{d}}{\mathrm{d}t}\left(\frac{\partial \mathcal{L}}{\partial \dot{\boldsymbol{q}}}\right)^{\mathrm{T}} - \left(\frac{\partial \mathcal{L}}{\partial \boldsymbol{q}}\right)^{\mathrm{T}} = \boldsymbol{\xi}, \tag{2.35}$$

where $\boldsymbol{\xi}$ is the vector of the generalized forces acting along the generalized coordinates $\boldsymbol{q}$. By substituting (2.27), (2.28) and (2.33) in (2.35), after some computation, the ith component of (2.35) becomes

$$\sum_{j=1}^{n} b_{ij}(\boldsymbol{q})\ddot{q}_j + \sum_{j=1}^{n} c_{ij}(\boldsymbol{q}, \dot{\boldsymbol{q}})\dot{q}_j + g_i(\boldsymbol{q}) = \xi_i, \tag{2.36}$$

where n is the total number of DOFs

$$n = h + \sum_{j=1}^{N} f_j,$$

b_{ij} is the element i, j of the inertia matrix $\boldsymbol{B}$, while a possible choice for the element $c_{i,j}(\boldsymbol{q}, \dot{\boldsymbol{q}})$ of $\boldsymbol{C}(\boldsymbol{q}, \dot{\boldsymbol{q}})$, according to [63], could be the following

$$c_{i,j} = \sum_{k=1}^{n} \frac{1}{2}\left(\frac{\partial b_{i,j}}{\partial q_k} + \frac{\partial b_{ik}}{\partial q_j} - \frac{\partial b_{j,k}}{\partial q_i}\right)\dot{q}_k, \tag{2.37}$$

$g_i(\boldsymbol{q})$ is the ith element of

$$\boldsymbol{g}(\boldsymbol{q}) = \left(\frac{\partial \mathcal{T}}{\partial \boldsymbol{q}}\right)^{\mathrm{T}} = -\sum_{i=1}^{n} m_i \boldsymbol{J}_p^{i\mathrm{T}} \boldsymbol{g}_a - \sum_{j=1}^{N}\sum_{i=1}^{f_j} m_i^j \bar{\boldsymbol{J}}_f^{i,j\mathrm{T}} \boldsymbol{g}_a, \tag{2.38}$$

where $\bar{\boldsymbol{J}}_f^{i,j} = \left[\boldsymbol{Z}\boldsymbol{G}_{i,a}^j(\boldsymbol{p}_{i,a}^j) \;\; \boldsymbol{J}_f^{i,j}\right]$ and $\boldsymbol{Z} = [\boldsymbol{I}_3 \; \boldsymbol{O}_3]$. The generalized force $\boldsymbol{\xi}$ is the resultant of the actuation torques, $\boldsymbol{\tau}$, and the torques due to external generalized contact forces (wrenches), $\boldsymbol{h}_c$, acting on the fingers

$$\boldsymbol{\xi} = \boldsymbol{\tau} - \boldsymbol{J}_c^{\mathrm{T}} \boldsymbol{h}_c,$$

where $\boldsymbol{J}_c$ the geometric jacobian mapping joint velocities into contact point twists; if the grasp involves only fingertips, then $\boldsymbol{J}_c = \boldsymbol{J}^b$. Finally the dynamic model of the overall system can be written as

$$\boldsymbol{B}(\boldsymbol{q})\ddot{\boldsymbol{q}} + \boldsymbol{C}(\boldsymbol{q}, \dot{\boldsymbol{q}})\dot{\boldsymbol{q}} + \boldsymbol{g}(\boldsymbol{q}) = \boldsymbol{\tau} - \boldsymbol{J}_c^{\mathrm{T}}\boldsymbol{h}. \tag{2.39}$$

2.5 Dynamic model of the floating base hand

The model of the coupling effects between the hand and the arm, could be computed by considering, instead of the whole system, a dynamically equivalent one, made up by the same robotic hand, able to freely move in 3-D space, on which the arm's action has been considered by means of an external wrench acting on the floating wrist.

Let us define the state of the wrist as

$$\boldsymbol{x}_a = \begin{bmatrix} \boldsymbol{p}_a^{\mathrm{T}} & \mathcal{Q}_a^{\mathrm{T}} \end{bmatrix}^{\mathrm{T}}, \tag{2.40}$$

where $\boldsymbol{p}_a$ is the vector pointing at the origin of the wrist frame Σ_a, $\mathcal{Q}_a$ is is the unit quaternion

$$\mathcal{Q}_a = \{\eta_a, \boldsymbol{\epsilon}_a\},$$

representing the orientation of Σ_a with respect to the base frame Σ_b. In order to determine the dynamics of the floating base hand, a set of lagrangian generalized coordinates is chosen as

$$\boldsymbol{x} = \begin{bmatrix} \boldsymbol{x}_a^{\mathrm{T}} & \boldsymbol{q}_f^{\mathrm{T}} \end{bmatrix}^{\mathrm{T}}, \tag{2.41}$$

where $\boldsymbol{q}_f$ is the vector of finger joint positions. Following the Lagrangian formulation the total energy of the system needs to be computed.

2.5.1 Kinetic Energy

The kinetic energy of the system can be computed as follows

$$\mathcal{K} = \frac{1}{2}\boldsymbol{v}_a^{\mathrm{T}}\bar{\boldsymbol{M}}_a\boldsymbol{v}_a + \frac{1}{2}\sum_{j=1}^{N}\sum_{i=1}^{f_j}\boldsymbol{v}_i^{j\mathrm{T}}\bar{\boldsymbol{M}}_i^j\boldsymbol{v}_i^j, \tag{2.42}$$

where $\boldsymbol{v}_a = \left[\dot{\boldsymbol{p}}_a^{\mathrm{T}}\ \boldsymbol{\omega}_a^{\mathrm{T}}\right]^{\mathrm{T}} \in \Re^6$ is the generalized velocity of the palm frame Σ_a (which coincides with the arm end-effector frame), $\bar{\boldsymbol{M}}_a = \mathrm{diag}\{m_a\boldsymbol{I}_3,\ \boldsymbol{M}_a\}$, m_a and $\boldsymbol{M}_a$ are the mass and the inertia tensor of the wrist, respectively, $\boldsymbol{v}_i^j$ is the generalized velocity (twist) of the frame attached to the CoG of link i belonging to finger j, $\bar{\boldsymbol{M}}_i^j = \mathrm{diag}\{m_i^j\boldsymbol{I}_3,\ \boldsymbol{M}_i^j\}$. The twist of the CoG frame of each link belonging to the jth finger can be computed as

$$\boldsymbol{v}_i^j \ = \ \boldsymbol{G}_{i,a}^{j\mathrm{T}}\boldsymbol{v}_a + \boldsymbol{v}_{i,a}^j, \tag{2.43}$$

where

$$\boldsymbol{G}_{i,a}^{j\mathrm{T}}\left(\boldsymbol{p}_{i,a}^j\right) = \begin{bmatrix} \boldsymbol{I}_3 & -\boldsymbol{S}(\boldsymbol{p}_{i,a}^j) \\ \boldsymbol{O}_3 & \boldsymbol{I}_3 \end{bmatrix}, \tag{2.44}$$

$\boldsymbol{v}_{i,a}^j = \left[\dot{\boldsymbol{p}}_{i,a}^{j\mathrm{T}}\ \boldsymbol{\omega}_{i,a}^{j\mathrm{T}}\right]^T$, $\boldsymbol{p}_{i,a}^j \in \Re^3$ is the relative position of the CoG of link i, belonging to finger j, with respect to the palm frame, $\boldsymbol{\omega}_{i,a}^j \in \Re^3$ is the relative angular velocity of the CoG of the link i, belonging to finger j, with respect to the palm frame. Linear and angular relative velocities $\dot{\boldsymbol{p}}_{i,a}^j$, $\boldsymbol{\omega}_{i,a}^j$ could be further expressed as

$$\boldsymbol{v}_{i,a}^j = \begin{bmatrix} \dot{\boldsymbol{p}}_{i,a}^j \\ \boldsymbol{\omega}_{i,a}^j \end{bmatrix} = \begin{bmatrix} \boldsymbol{J}_p^{i,j}(\boldsymbol{q}_i^j) \\ \boldsymbol{J}_o^{i,j}(\boldsymbol{q}_i^j) \end{bmatrix}\dot{\boldsymbol{q}}_i^j = \boldsymbol{J}_f^{i,j}\dot{\boldsymbol{q}}_i^j, \tag{2.45}$$

where $\boldsymbol{q}_i^j = \left[q_1^j, q_2^j, \ldots, q_i^j\right]$, q_i^j is the position of the ith joint belonging to the jth finger, where

$$\boldsymbol{J}_p^{i,j}(\boldsymbol{q}_f^j) = \left[\boldsymbol{J}_{o1}^{i,j}(q_1^j)\ \ \boldsymbol{J}_{p2}^{i,j}(q_2^j)\ \ \ldots\ \ \boldsymbol{J}_{pi}^{i,j}(q_i^j)\ \boldsymbol{0}_{f_j-i}\right],$$

$$\boldsymbol{J}_o^{i,j}(\boldsymbol{q}_f^j) = \left[\boldsymbol{J}_{o1}^{i,j}(q_1^j)\ \ \boldsymbol{J}_{o2}^{i,j}(q_2^j)\ \ \ldots\ \ \boldsymbol{J}_{oi}^{i,j}(q_i^j)\ \mathbf{0}_{f_j-i}\right],$$

and $\boldsymbol{J}_{pk}^{i,j}$ ($\boldsymbol{J}_{pk}^{i,j}$) is the Jacobian representing the contribution of joint k to the linear (angular) velocity of the CoG of link i belonging finger j.

The wrist velocity could be written in terms of $\dot{\boldsymbol{x}}_a$

$$\begin{aligned}
&\boldsymbol{v}_a = \boldsymbol{L}_a\dot{\boldsymbol{x}}_a,\\
&\boldsymbol{L}_a = \begin{bmatrix} \boldsymbol{I}_3 & \boldsymbol{O}_{3,4}, \\ \boldsymbol{O}_3 & \bar{\boldsymbol{L}}_a \end{bmatrix},\\
&\bar{\boldsymbol{L}}_a = 2\begin{bmatrix} \boldsymbol{\epsilon}_a & \eta_a\boldsymbol{I}_3 - \boldsymbol{S}(\boldsymbol{\epsilon}_a) \end{bmatrix}.
\end{aligned} \tag{2.46}$$

In view of (2.46), the kinetic energy can be rewritten in a compact form

$$\mathcal{K} = \frac{1}{2}\boldsymbol{x}^{\mathrm{T}}\boldsymbol{\mathcal{B}}(\boldsymbol{x})\boldsymbol{x}, \tag{2.47}$$

where

$$\boldsymbol{\mathcal{B}}(\boldsymbol{x}) = \begin{bmatrix} \boldsymbol{\mathcal{B}}_{aa}(\boldsymbol{x}) & \boldsymbol{\mathcal{B}}_{af}(\boldsymbol{x}) \\ \boldsymbol{\mathcal{B}}_{fa}(\boldsymbol{x}) & \boldsymbol{\mathcal{B}}_{ff}(\boldsymbol{x}) \end{bmatrix}$$

is the inertia matrix of the floating base hand and

$$\begin{aligned}
\boldsymbol{\mathcal{B}}_{aa}(\boldsymbol{x}) &= \boldsymbol{L}_a^{\mathrm{T}}\left(\bar{\boldsymbol{M}}_a + \sum_{j=1}^{N}\sum_{i=1}^{f_j}\boldsymbol{G}_{i,a}^j\bar{\boldsymbol{M}}_i^j\boldsymbol{G}_{i,a}^{j\mathrm{T}}\right)\boldsymbol{L}_a,\\
\boldsymbol{\mathcal{B}}_{af}(\boldsymbol{x}) &= \sum_{j=1}^{N}\sum_{i=1}^{f_j}\boldsymbol{L}_a^{\mathrm{T}}\boldsymbol{G}_{i,a}^j\bar{\boldsymbol{M}}_i^j\boldsymbol{J}_f^{i,j}\boldsymbol{L}_a,\\
\boldsymbol{\mathcal{B}}_{fa}(\boldsymbol{x}) &= \sum_{j=1}^{N}\sum_{i=1}^{f_j}\left(\boldsymbol{L}_a^{\mathrm{T}}\boldsymbol{G}_{i,a}^j\bar{\boldsymbol{M}}_i^j\boldsymbol{J}_f^{i,j}\right)^{\mathrm{T}},\\
\boldsymbol{\mathcal{B}}_{ff}(\boldsymbol{x}) &= \sum_{j=1}^{N}\sum_{i=1}^{n_j}\boldsymbol{J}_f^{i,j\mathrm{T}}\bar{\boldsymbol{M}}_i^j\boldsymbol{J}_f^{i,j}.
\end{aligned} \tag{2.48}$$

It is worth remarking that $\boldsymbol{\mathcal{B}}$ is symmetric and positive definite.The following properties hold:

1. mutual symmetry of $\boldsymbol{\mathcal{B}}_{af}$ and $\boldsymbol{\mathcal{B}}_{fa}^{\mathrm{T}}$, i.e. $\boldsymbol{\mathcal{B}}_{af} = \boldsymbol{\mathcal{B}}_{fa}^{\mathrm{T}}$;
2. $\boldsymbol{\mathcal{B}}$ is symmetric and positive definite.

2.5.2 Potential energy

The potential energy of the floating base hand is computed according to

$$\mathcal{T} = m_a \boldsymbol{g}_a^{\mathrm{T}} \boldsymbol{p}_a + \sum_{j=1}^{N} \sum_{i=1}^{f_j} m_i^j \boldsymbol{g}_a^{\mathrm{T}} \boldsymbol{p}_i^j, \tag{2.49}$$

It is worth noting that

$$\boldsymbol{p}_i^j = \boldsymbol{p}_a + \boldsymbol{R}_a \boldsymbol{p}_{i,a}^{jh},$$

where $\boldsymbol{p}_{i,a}^{jh}$ is the relative position of the link i CoG, belonging to finger j, with respect to Σ_a, with respect to the wrist frame coordinate, while $\boldsymbol{R}_a$ is a function of $\mathcal{Q}_a$

$$\boldsymbol{R}_a\left(\mathcal{Q}_a\right) = \eta_a^2 \boldsymbol{I}_3 + 2\boldsymbol{\epsilon}_a \boldsymbol{\epsilon}_a^{\mathrm{T}} - 2\eta_a \boldsymbol{S}(\boldsymbol{\epsilon}_a).$$

2.5.3 Lagrangian equation

Since a non-minimal representation has been chosen for the orientation of the wrist frame, the so-called lagrangian variables, i.e. the component of the vector $\boldsymbol{x}$, are not independent: 4 of them are constrained. Thus, the Lagrangian of the system must take into account this constraint, which, in turn, can be expressed as

$$\phi(\boldsymbol{x}) = \frac{1}{2}\left(1 - \boldsymbol{x}^{\mathrm{T}} \boldsymbol{Q}^{\mathrm{T}} \boldsymbol{Q} \boldsymbol{x}\right) = 0, \tag{2.50}$$

where $\boldsymbol{Q} = [\boldsymbol{O}_3 \;\; \boldsymbol{I}_4 \;\; \boldsymbol{O}_f]$ and f is the number of the hand's joint. The constraint expressed via (2.50) establishes that $\mathcal{Q}_a$ must be a unit quaternion. Finally, according to [42], the Lagrangian of the constrained system can be written as

$$\mathcal{L} = \bar{\mathcal{L}} + \lambda \phi(\boldsymbol{x}), \tag{2.51}$$

where $\bar{\mathcal{L}}$ is the lagrangian of the unconstrained system and λ is the lagrangian multiplier. The lagrangian equation becomes

$$\boldsymbol{\mathcal{B}}(\boldsymbol{x})\ddot{\boldsymbol{x}} + \bar{\boldsymbol{\mathcal{C}}}(\boldsymbol{x}, \dot{\boldsymbol{x}})\dot{\boldsymbol{x}} + \bar{\boldsymbol{\gamma}}(\boldsymbol{x}) + \lambda \left(\frac{\partial \phi}{\partial \boldsymbol{x}}\right)^{\mathrm{T}} = \bar{\boldsymbol{\xi}}_x, \tag{2.52}$$

where $\bar{\boldsymbol{\mathcal{C}}}$, according to [63], is computed as

$$\bar{\mathcal{C}}_{i,j}(\boldsymbol{x}, \dot{\boldsymbol{x}}) = \sum_{k=1}^{n} \frac{1}{2} \left(\frac{\partial b_{i,j}}{\partial x_k} + \frac{\partial b_{jk}}{\partial x_i} - \frac{\partial b_{j,k}}{\partial x_i} \right) \dot{x}_k, \tag{2.53}$$

$\bar{\boldsymbol{\gamma}}$ is given by

$$\bar{\boldsymbol{\gamma}}(\boldsymbol{x}) = \left(\partial \mathcal{T} / \partial \boldsymbol{x}\right)^{\mathrm{T}}, \tag{2.54}$$

while the term $\bar{\boldsymbol{\xi}}_x$ is the vector of the generalized forces acting along the lagrangian coordinates $\boldsymbol{x}$. By noting that

$$\frac{\partial \phi}{\partial \boldsymbol{x}} = -\boldsymbol{Q}^{\mathrm{T}} \boldsymbol{Q} \boldsymbol{x},$$

equation (2.52) can be rewritten as

$$\boldsymbol{\mathcal{B}}(\boldsymbol{x})\ddot{\boldsymbol{x}} + \bar{\boldsymbol{\mathcal{C}}}(\boldsymbol{x}, \dot{\boldsymbol{x}})\dot{\boldsymbol{x}} + \bar{\boldsymbol{\gamma}}(\boldsymbol{x}) = \bar{\boldsymbol{\xi}}_x + \lambda \boldsymbol{Q}^{\mathrm{T}} \boldsymbol{Q} \boldsymbol{x}, \tag{2.55}$$

from which λ can be computed by pre-multiplying the (2.55) by $\boldsymbol{x}^{\mathrm{T}}$, obtaining

$$\lambda = \boldsymbol{x}^{\mathrm{T}} \left(\boldsymbol{\mathcal{B}}(\boldsymbol{x})\ddot{\boldsymbol{x}} + \bar{\boldsymbol{\mathcal{C}}}(\boldsymbol{x}, \dot{\boldsymbol{x}})\dot{\boldsymbol{x}} + \bar{\boldsymbol{\gamma}}(\boldsymbol{x}) - \bar{\boldsymbol{\xi}}_x \right). \tag{2.56}$$

By folding (2.56) into (2.55) and after few algebraic steps, it yields

$$\boldsymbol{\mathcal{B}}(\boldsymbol{x})\ddot{\boldsymbol{x}} + \boldsymbol{\mathcal{C}}(\boldsymbol{x}, \dot{\boldsymbol{x}})\dot{\boldsymbol{x}} + \boldsymbol{\gamma}(\boldsymbol{x}) = \boldsymbol{\xi}_x - \boldsymbol{\mathcal{B}}(\boldsymbol{x})\boldsymbol{x}\dot{\boldsymbol{x}}^{\mathrm{T}} \boldsymbol{Q}^{\mathrm{T}} \boldsymbol{Q} \dot{\boldsymbol{x}}, \tag{2.57}$$

$$\begin{aligned}
\boldsymbol{\mathcal{C}} &= \left(\boldsymbol{I}_{7+f} - \boldsymbol{Q}^{\mathrm{T}} \boldsymbol{Q} \boldsymbol{x} \boldsymbol{x}^{\mathrm{T}} \right) \bar{\boldsymbol{\mathcal{C}}}, \\
\boldsymbol{\gamma} &= \left(\boldsymbol{I}_{7+f} - \boldsymbol{Q}^{\mathrm{T}} \boldsymbol{Q} \boldsymbol{x} \boldsymbol{x}^{\mathrm{T}} \right) \bar{\boldsymbol{\gamma}}, \\
\boldsymbol{\xi}_x &= \left(\boldsymbol{I}_{7+f} - \boldsymbol{Q}^{\mathrm{T}} \boldsymbol{Q} \boldsymbol{x} \boldsymbol{x}^{\mathrm{T}} \right) \bar{\boldsymbol{\xi}}_x,
\end{aligned} \tag{2.58}$$

where the following relationship has been exploited

$$\boldsymbol{x}^{\mathrm{T}} \boldsymbol{Q}^{\mathrm{T}} \boldsymbol{Q} \ddot{\boldsymbol{x}} = -\dot{\boldsymbol{x}}^{\mathrm{T}} \boldsymbol{Q}^{\mathrm{T}} \boldsymbol{Q} \dot{\boldsymbol{x}},$$

obtained by differentiating twice the constraint (2.50). If the system reaches a static equilibrium, the virtual work is null

$$-\boldsymbol{v}_c^{\mathrm{T}} \boldsymbol{h}_c + \dot{\boldsymbol{q}}_f^{\mathrm{T}} \boldsymbol{\tau}_f - \boldsymbol{v}_a^{\mathrm{T}} \boldsymbol{h}_a = 0, \tag{2.59}$$

where $\boldsymbol{v}_c \in \Re^{6n_c}$ is the vector stacking the finger velocities at each contact point, n_c is the number of contact points, $\boldsymbol{h}_c \in \Re^{6n_c}$ is the vector stacking the contact wrenches, $\boldsymbol{\tau}_f \in \Re^l$ is the vector of commanded torques (l is the number of hand DOFs), $\boldsymbol{v}_a \in \Re^6$ is the vector of generalized wrist velocities, $\boldsymbol{h}_a$ represents the wrist wrench. The contact generalized velocities (twists) can be further expressed as

$$\begin{aligned} \boldsymbol{v}_c &= \boldsymbol{G}_a^{\mathrm{T}}(\boldsymbol{r}_a)\boldsymbol{v}_a + \boldsymbol{v}_{c,h} \\ \boldsymbol{v}_{c,h} &= \boldsymbol{J}_{f_c}\dot{\boldsymbol{q}}_f, \end{aligned} \tag{2.60}$$

where $\boldsymbol{r}_a$ is the vector stacking the position of each contact point with respect to the wrist frame,

$$\boldsymbol{G}_a(\boldsymbol{r}_a) = \Big[\boldsymbol{G}_{a_1}(\boldsymbol{r}_{a_1}) \;\; \boldsymbol{G}_{a_2}(\boldsymbol{r}_{a_2}) \;\; \dots \;\; \boldsymbol{G}_{a_{n_c}}(\boldsymbol{r}_{a_{n_c}})\Big],$$

$$\boldsymbol{G}_{a_i}(\boldsymbol{r}_{a_i}) = \begin{bmatrix} \boldsymbol{I}_3 & \boldsymbol{O}_3 \\ \boldsymbol{S}(\boldsymbol{r}_{a_i}) & \boldsymbol{I}_3 \end{bmatrix},$$

$\boldsymbol{J}_{f_c}$ is the hand jacobian mapping the joint velocities into contact point twists. The principle of virtual works becomes

$$-\boldsymbol{v}_a^{\mathrm{T}}\left(\boldsymbol{h}_a + \boldsymbol{G}_a(\boldsymbol{r}_a)\boldsymbol{h}_c\right) + \dot{\boldsymbol{q}}_f^{\mathrm{T}}\left(\boldsymbol{\tau}_f - \boldsymbol{J}_{f_c}^{\mathrm{T}}\boldsymbol{h}_c\right) = 0. \tag{2.61}$$

By recalling (2.46), it yields

$$-\dot{\boldsymbol{x}}_a^{\mathrm{T}}\boldsymbol{L}_a^{\mathrm{T}}\left(\boldsymbol{h}_a + \boldsymbol{G}_a(\boldsymbol{r}_a)\boldsymbol{h}_c\right) + \dot{\boldsymbol{q}}_f^{\mathrm{T}}\left(\boldsymbol{\tau}_f - \boldsymbol{J}_{f_c}^{\mathrm{T}}\boldsymbol{h}_c\right) = 0, \tag{2.62}$$

which could be rewritten in a more compact form as

$$\begin{bmatrix} \dot{\boldsymbol{x}}_a^{\mathrm{T}} & \dot{\boldsymbol{q}}_f^{\mathrm{T}} \end{bmatrix} \begin{bmatrix} -\boldsymbol{L}_a^{\mathrm{T}}\left(\boldsymbol{h}_a + \boldsymbol{G}_a(\boldsymbol{r}_a)\boldsymbol{h}_c\right)) \\ \boldsymbol{\tau}_f - \boldsymbol{J}_{f_c}^{\mathrm{T}}\boldsymbol{h}_c \end{bmatrix} = 0; \tag{2.63}$$

from which it could be recognized that

$$\boldsymbol{\xi}_x = \begin{bmatrix} -\boldsymbol{L}_a^{\mathrm{T}}\left(\boldsymbol{h}_a + \boldsymbol{G}_a(\boldsymbol{r}_a)\boldsymbol{h}_c\right)) \\ \boldsymbol{\tau}_f - \boldsymbol{J}_{f_c}^{\mathrm{T}}\boldsymbol{h}_c \end{bmatrix}, \tag{2.64}$$

since $\dot{\boldsymbol{x}}^{\mathrm{T}}\boldsymbol{\xi}_x = 0$.

2.6 Contact analysis

The detailed dynamics of the grasped object can be expressed as

$$\boldsymbol{B}_o\dot{\boldsymbol{v}}_o + \boldsymbol{C}(\boldsymbol{v}_o)\boldsymbol{v}_o + \boldsymbol{g}_o = \boldsymbol{G}_c(\boldsymbol{r}_o)\boldsymbol{h}_c - \boldsymbol{h}_e, \tag{2.65}$$

where $\boldsymbol{B}_o = \text{diag}\{m_o\boldsymbol{I}_3, \boldsymbol{M}_o\}$, $m_o \in \Re$ and $\boldsymbol{M}_o \in \Re^{3\times3}$ are the mass and inertia tensor of the object respectively, $\boldsymbol{v}_o \in \Re^6$ is the generalized velocity of the frame Σ_o attached to the center of gravity (CoG) of the object, $\boldsymbol{C}(\boldsymbol{v}_o) \in \Re^{6\times6}$ is the matrix collecting the centrifugal and Coriolis terms, $\boldsymbol{g}_o \in \Re^6$ is the gravity generalized force, $\boldsymbol{G}_c(\boldsymbol{r}_o) \in \Re^{6\times6n_c}$ is the grasp matrix

$$\begin{aligned}\boldsymbol{G}_c(\boldsymbol{r}_o) &= \begin{bmatrix} \boldsymbol{G}_{c_1}(\boldsymbol{r}_{o_1}) & \boldsymbol{G}_{c_2}(\boldsymbol{r}_{o_2}) & \dots & \boldsymbol{G}_{c_{n_c}}(\boldsymbol{r}_{o_{n_c}}) \end{bmatrix}, \\ \boldsymbol{G}_{c_i}(\boldsymbol{r}_{o_i}) &= \begin{bmatrix} \boldsymbol{I}_3 & \boldsymbol{O}_3 \\ \boldsymbol{S}(\boldsymbol{r}_{o_i}) & \boldsymbol{I}_3 \end{bmatrix},\end{aligned} \tag{2.66}$$

$\boldsymbol{r} = \begin{bmatrix}\boldsymbol{r}_{o_1}^{\mathrm{T}} \boldsymbol{r}_{o_2}^{\mathrm{T}} \dots \boldsymbol{r}_{o_{n_c}}^{\mathrm{T}}\end{bmatrix}^{\mathrm{T}}$ and $\boldsymbol{r}_{o_i} \in \Re^3$ is the relative position of the ith contact point with respect to the origin of Σ_o. The other terms in (2.65) are $\boldsymbol{h}_c$, the contact wrenches, and $\boldsymbol{h}_e$, which is the environmental interaction wrench, i.e. it takes into account the case in which the grasped object collides with other bodies populating the external environment.

Depending on the contact model, (2.65) can be rewritten by considering only the force transmitted to the object through the contact

$$\boldsymbol{B}_o\dot{\boldsymbol{v}}_o + \boldsymbol{C}(\boldsymbol{v}_o)\boldsymbol{v}_o + \boldsymbol{g}_o = \boldsymbol{G}(\boldsymbol{r}_o)\boldsymbol{h}_t - \boldsymbol{h}_e, \tag{2.67}$$

where $\boldsymbol{h}_t = \begin{bmatrix}\boldsymbol{h}_{t_1}^{\mathrm{T}} \boldsymbol{h}_{t_2}^{\mathrm{T}} \dots \boldsymbol{h}_{t_{n_c}}^{\mathrm{T}}\end{bmatrix}^{\mathrm{T}}$ denotes the vector stacking the transmitted forces, and

$$\boldsymbol{G}(\boldsymbol{r}_o) = \begin{bmatrix} \boldsymbol{G}_1(\boldsymbol{r}_{o_1}) & \boldsymbol{G}_2(\boldsymbol{r}_{o_2}) & \dots & \boldsymbol{G}_{n_c}(\boldsymbol{r}_{o_{n_c}}) \end{bmatrix},$$

where the expression of $\boldsymbol{G}_i(\boldsymbol{r}_{o_i}) \in \Re^{n_t}$, $\boldsymbol{h}_{t_i} \in \Re^{n_t}$ and n_t depend on the chosen contact model; it could be useful to consider 4 cases:

- Point contact without friction: only normal forces are transmitted. Thus, $n_t = 1$ and

$$h_{t_i} = \boldsymbol{n}_i^{\mathrm{T}} \boldsymbol{h}_{c_i},$$
$$\boldsymbol{G}_i = \begin{bmatrix} \boldsymbol{n}_i \\ \boldsymbol{S}(\boldsymbol{r}_{o_i})\boldsymbol{n}_i \end{bmatrix},$$

  where $\boldsymbol{n}_i$ is the unit vector normal to the object surface at contact point i.

- Point contact with friction: only forces (no moments) are transmitted. Thus, $n_t = 3$ and

$$\boldsymbol{h}_{t_i} = \boldsymbol{H}_3 \boldsymbol{h}_{c_i},$$
$$\boldsymbol{G}_i(\boldsymbol{r}_{o_i}) = \begin{bmatrix} \boldsymbol{I}_3 \\ \boldsymbol{S}(\boldsymbol{r}_{o_i}) \end{bmatrix},$$

  where $\boldsymbol{H}_\alpha$ a selector operator which extracts the first α components

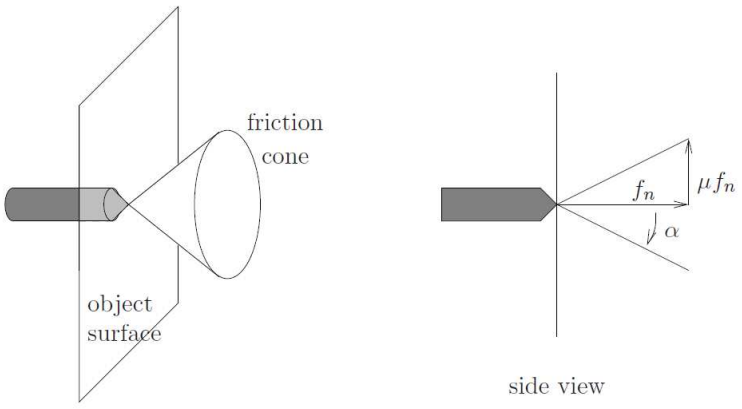

Figure 2.2: Friction cone. $\boldsymbol{f}_n$ represent the normal forces where μ is the friction coefficient

  from a vector of dimension $\beta \geq \alpha$, $\boldsymbol{H}_\alpha = \begin{bmatrix} \boldsymbol{I}_\alpha & \boldsymbol{O}_{\alpha,n-\alpha} \end{bmatrix}$. The friction law imposes that the components of the total force transmitted to the object through the contact, should lie in a limit surface, called *friction*

cone, $\mathcal{F}_i$ as shown in Figure 2.2. Let $\boldsymbol{R}_{c_i} = [\boldsymbol{n}_i^{\mathrm{T}}\, \boldsymbol{t}_i^{\mathrm{T}}\, \boldsymbol{k}_i^{\mathrm{T}}]^{\mathrm{T}}$ be the rotation matrix representing the orientation of contact point i on the object surface, where $\boldsymbol{n}_i$ is the outward normal to the object surface while $\boldsymbol{t}_i$ and $\boldsymbol{k}_i$ are the unit vector spanning the tangent plane, then the friction cone can be written as

$$\mathcal{F}_i = \left\{ \boldsymbol{h}_{t_i} \in \Re^3 \colon \frac{1}{\mu_i} \sqrt{|\boldsymbol{t}_i^{\mathrm{T}} \boldsymbol{h}_{t_i}|^2 + |\boldsymbol{k}_i^{\mathrm{T}} \boldsymbol{h}_{t_i}|^2} \leq \mu_i |\boldsymbol{n}^{\mathrm{T}} \boldsymbol{h}_{t_i}| \right\}, \tag{2.68}$$

where μ_i is the friction coefficient.

- Soft finger: in this case, not only forces are transmitted but also the moment around the normal axis. Thus, $n_t = 4$ and

$$\boldsymbol{h}_{t_i} = \begin{bmatrix} \boldsymbol{I}_3 & \boldsymbol{O}_3 \\ 0 & \boldsymbol{n}_i^{\mathrm{T}} \end{bmatrix} \boldsymbol{h}_{c_i}$$
$$\boldsymbol{G}_i(\boldsymbol{r}_{o_i}) = \begin{bmatrix} \boldsymbol{I}_3 & \boldsymbol{O}_3 \\ \boldsymbol{S}(\boldsymbol{r}_{o_i}) & \boldsymbol{n}_i \end{bmatrix}.$$

  The transmitted force can be written in terms of components $\boldsymbol{h}_{t_i} = [\boldsymbol{f}_{t_i}\, m_{t_i}]^{\mathrm{T}}$ where $\boldsymbol{f}_{t_i} \in \Re^3$ is the contact forces and m_{t_i} the torsional moment, around $\hat{\boldsymbol{n}}_i$; thus, a definition of the friction cone, according to [52], can be stated as

$$\mathcal{F}_i = \left\{ \boldsymbol{h}_{t_i} \in \Re^4 \colon \frac{1}{\mu_i} \sqrt{|\boldsymbol{t}_i^{\mathrm{T}} \boldsymbol{h}_{t_i}|^2 + |\boldsymbol{k}_i^{\mathrm{T}} \boldsymbol{h}_{t_i}|^2} + \frac{1}{s\nu_i} |m_{t_i}| \leq |\boldsymbol{n}_i^{\mathrm{T}} \boldsymbol{h}_{t_i}| \right\}, \tag{2.69}$$

  where ν_i is torsional friction coefficient and a is a characteristic length of the object that makes measurement units consistent.

- Rigid contact: the finger can be thought as "welded" on the object. Thus, $n_t = 6$

$$\boldsymbol{h}_{t_i} = \boldsymbol{I}_3 \boldsymbol{h}_{c_i}$$
$$\boldsymbol{G}_i(\boldsymbol{r}_{o_i}) = \boldsymbol{G}_{c_i}(\boldsymbol{r}_{o_i}).$$

From equation (2.67), assuming that $\text{rank}(\boldsymbol{G}(\boldsymbol{r}_o)) = 6$ and the null space of $\boldsymbol{G}(\boldsymbol{r}_o)$, hereafter $\mathcal{N}(\boldsymbol{G})$, is not trivial, contact generalized forces can be computed via the following

$$\boldsymbol{h}_t = \boldsymbol{G}_W^{\dagger}(\boldsymbol{r}_o)\left(\boldsymbol{B}_o\dot{\boldsymbol{v}}_o + \boldsymbol{C}(\boldsymbol{v}_o)\boldsymbol{v}_o + \boldsymbol{g}_o - \boldsymbol{h}_e\right) + \boldsymbol{N}_{G_W}\boldsymbol{h}_{t_I}, \tag{2.70}$$

where $\boldsymbol{G}_W^{\dagger}$ and $\boldsymbol{N}_{G_w}$ represent a weighted right pseudo-inverse and a null projector of the grasp matrix, respectively, while the matrix of weights, $\boldsymbol{W}$, depends on the contact model and can be chosen according to [4]; $\boldsymbol{h}_{t_I} \in \Re^{6N}$, i.e. the internal contact forces, are wrenches not affecting the object motion, that represent internal stresses applied to the object. On the other hand, contact forces which generate the object motion,

$$\boldsymbol{h}_{t_E} = \boldsymbol{G}_W^{\dagger}(\boldsymbol{r}_o)\left(\boldsymbol{B}_o\dot{\boldsymbol{v}}_o + \boldsymbol{C}(\boldsymbol{v}_o)\boldsymbol{v}_o + \boldsymbol{g}_o - \boldsymbol{h}_e\right), \tag{2.71}$$

are called external contact forces, $\boldsymbol{h}_{c_E}$. The forces exerted by fingertips on the object are the sum of the internal contact forces and the external ones

$$\boldsymbol{h}_t = \boldsymbol{h}_{t_E} + \boldsymbol{h}_{t_I}. \tag{2.72}$$

2.6.1 Grasp restraint

The most fundamental requirements in grasping and dexterous manipulation are the abilities to hold an object in equilibrium and control the position and orientation of the grasped object relative to the palm of the hand. The two most useful characterizations of grasp restraint are *force closure* and *form closure*.

Form closure

According to [52], a grasp has form closure if and only if

$$\left.\begin{array}{c} \boldsymbol{G}_{t_n}\boldsymbol{h}_{t_n} = -\boldsymbol{h}_{ext} \\ \boldsymbol{h}_{t_n} \geq \boldsymbol{0}_{n_c} \end{array}\right\} \ \forall \boldsymbol{h}_{ext} \in \Re^6, \tag{2.73}$$

where the subscript t_n emphasizes that contact point without friction has been considered and $\boldsymbol{h}_{ext}$ is an arbitrary vector of $\Re^6$ representing all possible external forces acting on the object. It is worth pointing out that inequalities referred to vectors, as in (2.73), should be considered element-wise. The physical interpretation of this condition is that equilibrium can be maintained under the conservative assumption that the contacts are frictionless as shown if Figure 2.3.

Figure 2.3: Example of form closure. Image extracted from the Handbook of Robotics [52].

Under the hypothesis that $\boldsymbol{G}_{t_n}$ is full row rank, i.e., $\text{rank}(\boldsymbol{G}_{t_n}) = 6$, and has more columns than rows, it is well known that the general solution of (2.73) is of the form

$$\boldsymbol{h}_{t_n} = \boldsymbol{h}_{np} + \alpha_h \boldsymbol{h}_{n0}, \tag{2.74}$$

where $\boldsymbol{h}_{np}$ is the particular solution representing the vector stacking contact forces which balance the external wrench, i.e. $\boldsymbol{G}_{t_n}\boldsymbol{h}_{np} = -\boldsymbol{h}_{ext}$, $\alpha_h \boldsymbol{h}_{n0}$ is the homogeneous solution, $\alpha_h > 0$ is a scalar and $\boldsymbol{h}_{n0}$ is a vector of normal contact forces which lies in the null space $\mathcal{N}(\boldsymbol{G}_{t_n})$ of $\boldsymbol{G}_{t_n}$. More in detail, if the dimension of $\mathcal{N}(\boldsymbol{G}_{t_n})$ is h (i.e., $\dim(\mathcal{N}(\boldsymbol{G}_{t_n})) = h$), then the vector of internal forces $\boldsymbol{h}_{n0}$ can be written as

$$\boldsymbol{h}_{n0} = \boldsymbol{h}_h + \frac{\alpha_{h-1}}{\alpha_h}\boldsymbol{h}_{h-1} + \ldots + \frac{\alpha_1}{\alpha_h}\boldsymbol{h}_1, \tag{2.75}$$

where α_i $(i = 1, 2, \ldots, h)$ are scalars and the set $\{\boldsymbol{h}_1, \boldsymbol{h}_2, \ldots, \boldsymbol{h}_h\}$ forms a basis for $\mathcal{N}(\boldsymbol{G}_{t_n})$.

By using the same argument used in [35], it is easy to show that if there exists a suitable choice of coefficients $\{\alpha_1, \ldots, \alpha_{h-1}\}$ such that $\boldsymbol{h}_{n0} > \boldsymbol{0}$, $\boldsymbol{h}_{t_n}$ can be made non negative by choosing α_h large enough; thus, the following equivalent condition for form closure can be stated

$$\begin{array}{rcl} \boldsymbol{G}_{t_n}\boldsymbol{h}_{n0} & = & \boldsymbol{0}_6, \\ \boldsymbol{h}_{n0} & > & \boldsymbol{0}_{n_c}. \end{array} \tag{2.76}$$

The geometric interpretation of form closure suggests that the positive span of the columns of $\boldsymbol{G}_{t_n}$ must include the origin of the wrench space. This means that there exists a set of strictly compressive normal contact forces in the null space of $\boldsymbol{G}_{t_n}$. In other words, the object can be squeezed as tightly as desired while maintaining equilibrium.

Let us consider the case in which the object is constrained, along some directions, by means of a bilateral constraint. A bilateral constraint, acting at some point on the object, can be expressed, at velocity level, as

$$\boldsymbol{F}^{\mathrm{T}}\boldsymbol{v}_o = \boldsymbol{0}, \tag{2.77}$$

where $\boldsymbol{F} \in \Re^{6\times n_\rho}$ is the matrix whose columns define the direction along which the object is constrained and n_ρ represents the number of degrees of freedom lost. It is reasonable to assume that $n_\rho = \mathrm{rank}(\boldsymbol{F})$, since otherwise the constraints would be redundant.

An object twist which satisfies (2.77) must lie in the null space of $\boldsymbol{F}^{\mathrm{T}}$

$$\boldsymbol{v}_o = \boldsymbol{N}\left(\boldsymbol{F}^{\mathrm{T}}\right)\boldsymbol{\rho}, \tag{2.78}$$

where $\boldsymbol{N}\left(\boldsymbol{F}^{\mathrm{T}}\right) \in \Re^{6\times n_\rho}$ is a matrix whose columns form a basis for the null space of $\boldsymbol{F}^{\mathrm{T}}$ denoted as $\mathcal{N}\left(\boldsymbol{F}^{\mathrm{T}}\right)$, $\boldsymbol{\rho}$ is an arbitrary vector in $\Re^{n_\rho}$. Note that the dimension $\mathcal{N}\left(\boldsymbol{F}^{\mathrm{T}}\right)$ is $n_\rho = 6 - n_\rho$. Since the columns of $\boldsymbol{N}\left(\boldsymbol{F}^{\mathrm{T}}\right)$

form a basis for $\mathcal{N}(\boldsymbol{F})$, i.e., $\boldsymbol{F}^{\mathrm{T}}\boldsymbol{N}\left(\boldsymbol{F}^{\mathrm{T}}\right)=\boldsymbol{O}$, it can be recognized that also $\boldsymbol{A}_F\boldsymbol{F}=\boldsymbol{O}$ with $\boldsymbol{A}_F=\left(\boldsymbol{N}\left(\boldsymbol{F}^{\mathrm{T}}\right)\right)^{\mathrm{T}}$, and thus (2.78) can be rewritten as

$$\boldsymbol{v}_o=\boldsymbol{A}_F^{\mathrm{T}}\boldsymbol{\rho}. \tag{2.79}$$

A definition of form closure similar to (2.73) can be derived by considering the grasped object at the equilibrium and applying the Principle of Virtual Work. Since the system is in equilibrium, the virtual work, δU, associated with a small displacement of the object $\delta\boldsymbol{u}$, compatible with the constraint, must be zero

$$\delta U=\delta\boldsymbol{u}^{\mathrm{T}}(\boldsymbol{G}_{t_n}\boldsymbol{h}_{t_n}+\boldsymbol{F}\boldsymbol{h}_b+\boldsymbol{h}_{ext})=0, \tag{2.80}$$

where $\boldsymbol{h}_b\in\Re^{n_\rho}$ is the vector of the bilateral constraint reactions, $\boldsymbol{h}_{ext}$ is an arbitrary vector in $\Re^6$ representing an external wrench acting on the object. For small virtual displacement the following equality holds

$$\delta\boldsymbol{u}=\boldsymbol{v}_o\delta t, \tag{2.81}$$

which allows one to rewrite (2.80) as

$$\delta U=\delta t\,\boldsymbol{v}_o^{\mathrm{T}}(\boldsymbol{G}_{t_n}\boldsymbol{h}_{n_c}+\boldsymbol{F}\boldsymbol{h}_b+\boldsymbol{h}_{ext})=0, \tag{2.82}$$

By recalling (2.79) and the fact that $\boldsymbol{A}_F\boldsymbol{F}=\boldsymbol{O}$, or equivalently, the fact that the virtual work of bilateral constraints must be zero, the (2.82) becomes

$$\boldsymbol{\rho}^{\mathrm{T}}\boldsymbol{A}_F(\boldsymbol{G}_{t_n}\boldsymbol{h}_{n_c}+\boldsymbol{h}_{ext})=0. \tag{2.83}$$

By defining $\overline{\boldsymbol{G}}_{t_n}\in\Re^{6n_\rho\times n_c}$ as

$$\overline{\boldsymbol{G}}_{t_n}=\boldsymbol{A}_F\boldsymbol{G}_{t_n},$$

and $\overline{\boldsymbol{h}}_{ext}\in\Re^{n_\rho}$ as

$$\overline{\boldsymbol{h}}_{ext}=\boldsymbol{A}_F\boldsymbol{h}_{ext},$$

equation (2.83) yields

$$\overline{\boldsymbol{G}}_{t_n}\boldsymbol{h}_n = -\overline{\boldsymbol{h}}_{ext}. \tag{2.84}$$

It is worth remarking that $\text{rank}(\overline{\boldsymbol{G}}_{t_n}) \leq n_\rho < 6$, since the bilateral constraints remove some of the object's degrees of freedom. Hence, the definition of form closure for bilateral constrained objects can be stated as follows

$$\begin{array}{rcl} \overline{\boldsymbol{G}}_{t_n}\boldsymbol{h}_{t_n} & = & -\overline{\boldsymbol{h}}_{ext}, \\ \boldsymbol{h}_{t_n} & \geq & \boldsymbol{0}_{n_c}. \end{array} \tag{2.85}$$

which is formally analogous to the definition given in [52].

Under the assumption that $\overline{\boldsymbol{G}}_{t_n}$ is full row rank, i.e., $\text{rank}(\overline{\boldsymbol{G}}_{t_n}) = n_\rho$, and has more columns than rows, it is well known that the general solution of (2.84) is of the form

$$\boldsymbol{h}_{t_n} = \boldsymbol{h}_{np} + \alpha_h \boldsymbol{h}_{n0}, \tag{2.86}$$

where $\boldsymbol{h}_{np}$ is the particular solution, i.e. $\overline{\boldsymbol{G}}_{t_n}\boldsymbol{h}_{np} = -\overline{\boldsymbol{h}}_{ext}$, $\alpha_h \boldsymbol{h}_{n0}$ is the homogeneous solution, being $\alpha_h > 0$ a scalar and $\boldsymbol{h}_{n0}$ a vector of normal contact forces which lies in the null space $\mathcal{N}(\overline{\boldsymbol{G}}_{t_n})$ of $\overline{\boldsymbol{G}}_{t_n}$. More in detail, if the dimension of $\mathcal{N}(\overline{\boldsymbol{G}}_{t_n})$ is h (i.e., $\dim(\mathcal{N}(\overline{\boldsymbol{G}}_{t_n})) = h$), then the vector of internal forces $\boldsymbol{h}_{n0}$ can be written as

$$\boldsymbol{h}_{n0} = \boldsymbol{h}_h + \frac{\alpha_{h-1}}{\alpha_h}\boldsymbol{h}_{h-1} + \ldots + \frac{\alpha_1}{\alpha_h}\boldsymbol{h}_1, \tag{2.87}$$

where α_i $(i = 1, 2, \ldots, h)$ are scalars and the set $\{\boldsymbol{h}_1, \boldsymbol{h}_2, \ldots, \boldsymbol{h}_h\}$ forms a basis for $\mathcal{N}(\overline{\boldsymbol{G}}_{t_n})$. By using the same argument used in [35], it is easy to show that if there exists a suitable choice of coefficients $\{\alpha_1, \ldots, \alpha_{h-1}\}$ such that $\boldsymbol{h}_{n0} > \boldsymbol{0}$, $\boldsymbol{h}_{t_n}$ can be made non negative by choosing α_h large enough; thus, the following equivalent condition for form closure can be stated

$$\begin{array}{rcl} \overline{\boldsymbol{G}}_{t_n}\boldsymbol{h}_{n0} & = & \boldsymbol{0}_{n_\rho}, \\ \boldsymbol{h}_{n0} & > & \boldsymbol{0}_{n_c}. \end{array} \tag{2.88}$$

The geometric interpretation of form closure with bilateral constraints is analogous to that adopted in the case without bilateral constraints - the positive span of the columns of $\overline{\boldsymbol{G}}_{t_n}$ must include the origin of the wrench space. This is the wrench space of reduced dimension formed by eliminating the wrench space associated with the bilateral constraints. Also, it is convenient to express the null space of $\overline{\boldsymbol{G}}_{t_n}$ as follows

$$\mathcal{N}\left(\overline{\boldsymbol{G}}_{t_n}\right) = \mathcal{R}(\boldsymbol{G}_{t_n}) \cap \mathcal{N}\left(\boldsymbol{A}_F\right). \tag{2.89}$$

where $\mathcal{R}$ denotes the range of a matrix.

Frictional form closure and force closure

The common definition of frictional form closure can be written as

$$\left.\begin{array}{c} \boldsymbol{G}_t\boldsymbol{h}_t = -\boldsymbol{h}_{ext} \\ \boldsymbol{h}_t \in \mathcal{F} \end{array}\right\} \ \forall\ \boldsymbol{h}_{ext} \in \Re^6, \tag{2.90}$$

where $\mathcal{F}$ is the composite friction cone defined as:

$$\mathcal{F} = \mathcal{F}_1 \times \cdots \times \mathcal{F}_{n_c} = \{\boldsymbol{h}_t \in \Re^{n_t} \mid \boldsymbol{h}_i \in \mathcal{F}_i; i = 1, ..., n_c\},$$

being $\mathcal{F}_i$ the friction cone at the ith contact point. This definition requires that each contact force must lie in its friction cone and does not consider the hand's ability to control contact forces, since there is no dependency on the manipulation system.

A grasp has force closure if and only

$$\left.\begin{array}{c} \boldsymbol{G}_t\boldsymbol{h}_t = -\boldsymbol{h}_{ext} \\ \boldsymbol{h}_t \in \mathcal{F} \\ \mathcal{N}(\boldsymbol{G}_t) \cap \mathcal{N}(\boldsymbol{J}_{f_c}^{\mathrm{T}}) = \ \boldsymbol{0} \end{array}\right\} \ \forall\ \boldsymbol{h}_{ext} \in \Re^6. \tag{2.91}$$

The force closure definition is similar but stricter than frictional form closure; as depicted in Figure 2.4, it additionally requires that the hand be able to

Figure 2.4: Example of force closure. Image extracted from the Handbook of Robotics [52].

control the internal object forces as required by the last condition in (2.91).

In the case of bilateral constrained objects, the principle of virtual works, with reference to an equilibrium configuration of the object, allows one to write

$$\delta U = \delta t \; \boldsymbol{\rho}^{\mathrm{T}} \boldsymbol{A}_F (\boldsymbol{G}_t \boldsymbol{h}_t + \boldsymbol{F} \boldsymbol{h}_b + \boldsymbol{h}_{ext}) = 0. \tag{2.92}$$

where $\boldsymbol{G}_t \in \Re^{6 \times n_t n_c}$ is the grasp matrix, $\boldsymbol{h}_t \in \Re^{n_t n_c}$ is the vector stacking all contact wrenches including friction components. By recognizing that the virtual work associated to the bilateral constraints must be zero, it follows that

$$\delta U = \boldsymbol{\rho}^{\mathrm{T}} \boldsymbol{A}_F (\boldsymbol{G}_t \boldsymbol{h}_t + \boldsymbol{h}_{ext}) = 0; \tag{2.93}$$

thus, by defining $\overline{\boldsymbol{G}_t} = \boldsymbol{A}_F \boldsymbol{G}_t$, the following definitions can be stated:

- Frictional form closure. A grasp is said to have frictional form closure

if and only if

$$\left.\begin{array}{c} \overline{\boldsymbol{G}}_t \boldsymbol{h}_t = -\boldsymbol{h}_{ext} \\ \boldsymbol{h}_t \in \mathcal{F} \end{array}\right\} \quad \forall\ \boldsymbol{h}_{ext} \in \Re^6, \tag{2.94}$$

- Force closure. A grasp is said to have force closure if and only if

$$\left.\begin{array}{c} \overline{\boldsymbol{G}}_t \boldsymbol{h}_t = -\boldsymbol{h}_{ext} \\ \boldsymbol{h}_t \in \mathcal{F} \\ \mathcal{N}(\overline{\boldsymbol{G}}_t) \cap \mathcal{N}(\boldsymbol{J}_{f_c}^{\mathrm{T}}) = \ \boldsymbol{0} \end{array}\right\} \quad \forall\ \boldsymbol{h}_{ext} \in \Re^6, \tag{2.95}$$

where $\mathcal{F}$ denotes the composite friction cone and $\boldsymbol{J}_{f_c}$ is the hand jacobian.

Chapter 3

Control Scheme with redundancy resolution

Multi-arm systems equipped with robotics hands are, generally, kinematically redundant, i.e. they have more DOFs then those required by the assigned task. The redundancy is often a desired feature: it allows to achieve secondary objectives (e.g., maximize dexterity, avoid obstacles) in addition to the primary manipulation task. In this chapter, an on-line planner is proposed in order to execute multiple tasks at different priority, by ensuring, at the same time, that both environmental (obstacles or human in the robots' workspace) and mechanical constraints (e.g., joint limits) are always satisfied. Moreover, since the number of active tasks can change dynamically, smooth behavior of the system is guaranteed when a task is deactivated/reactivated. Forces are controlled via a parallel force/position scheme.

3.1 Control architecture

In order to exploit the redundancy of the multi-arm/hand system, the following two-stage control architecture is proposed:

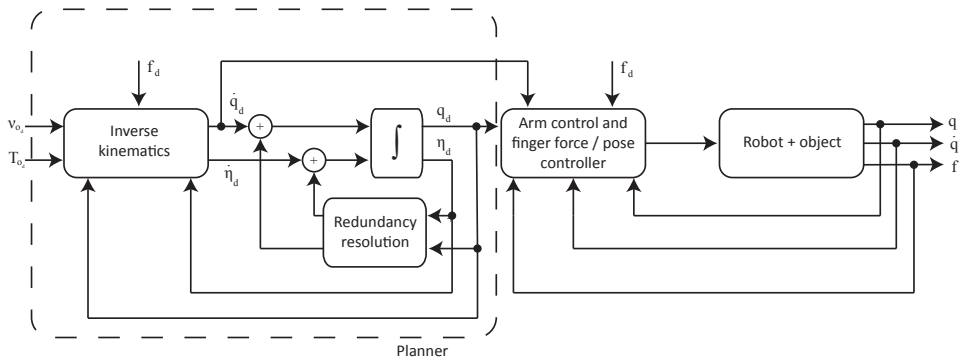

Figure 3.1: Block scheme of the control architecture

- the first stage is a *motion planner*, given by a closed-loop inverse kinematics algorithm with redundancy resolution; the algorithm computes the joint references for the active joints corresponding to a desired object's motion –assigned in terms of the homogeneous transformation matrix $\boldsymbol{T}_{o_d}$ and the corresponding twist velocity vector $\boldsymbol{v}_{o_d}$– and to the desired contact normal force $\boldsymbol{f}_d = \begin{bmatrix} f_{d_1} & \cdots & f_{d_N} \end{bmatrix}^{\mathrm{T}}$ for the fingers;
- the second stage is a *parallel control* scheme, composed by a PD position controller and a PI tip force controller; the controller ensures tracking of the desired joint motion references computed in the first stage and the desired contact forces.

In ideal conditions, the joint references computed by the inverse kinematics stage ensure tracking of the desired object motion. Tracking of the desired contact forces is guaranteed by force control, assuming that force sensors at the fingertips are available. In principle, the joint references of the overall

manipulation system could be controlled; however, it is reasonable to design a force controller acting only on the joints of the fingers.

3.1.1 Planner

As it will be detailed int next section, a force control strategy is adopted to ensure a desired constant contact forces f_{d_j} along the direction normal to the contact point. Hence, by assuming point contact model and that $\Delta l_j = \Delta l_{d_j} = f_{d_j}/k_j$ is fixed ($\Delta \dot{l}_j = 0$) Equation (2.18) can be rewritten as

$$\boldsymbol{J}_{F_j}(\boldsymbol{q}_j)\dot{\boldsymbol{q}}_j + \boldsymbol{J}_{\eta_j}(\boldsymbol{\eta}_j, \boldsymbol{q}_j, \Delta l_j)\dot{\boldsymbol{\eta}}_j = \widetilde{\boldsymbol{G}}_j^{\mathrm{T}}(\boldsymbol{\eta}_j, \Delta l_j)\boldsymbol{\upsilon}_o, \tag{3.1}$$

where the subscript j labels the finger. It is worth recalling that equation (3.1) can be seen as the differential kinematics of an extended finger which includes the arm kinematic chain, the j finger active and passive foint. Let be $N = \sum_{j=1}^{n_a} N_j$ the total number of finger, or equivalently of contact points, with N_i number of finger belonging to the ith arm/hand system and n_a number of arms composing the manipulation system, then the differential kinematics of the whole system can be written as

$$\widetilde{\boldsymbol{J}}(\widetilde{\boldsymbol{q}}, \Delta \boldsymbol{l})\dot{\widetilde{\boldsymbol{q}}} = \widetilde{\boldsymbol{G}}^{\mathrm{T}}(\boldsymbol{\eta}, \Delta \boldsymbol{l})\widetilde{\boldsymbol{\upsilon}}_o, \tag{3.2}$$

where $\widetilde{\boldsymbol{q}} = \begin{bmatrix}\boldsymbol{q}^{\mathrm{T}} & \boldsymbol{\eta}^{\mathrm{T}}\end{bmatrix}^{\mathrm{T}}$, $\widetilde{\boldsymbol{J}} = \begin{bmatrix}\boldsymbol{J} & \boldsymbol{J}_{\eta}\end{bmatrix}$, $\boldsymbol{J}$ is the Jacobian of the arm-hand system defined in (2.6), $\boldsymbol{J}_{\eta} = \mathrm{diag}\{\boldsymbol{J}_{\eta_1}, \cdots, \boldsymbol{J}_{\eta_N}\}$ is a block-diagonal matrix corresponding to the vector of passive joint velocities , $\dot{\boldsymbol{\eta}} = \begin{bmatrix}\dot{\boldsymbol{\eta}}_1^{\mathrm{T}} & \cdots & \dot{\boldsymbol{\eta}}_N^{\mathrm{T}}\end{bmatrix}^{\mathrm{T}}$, $\widetilde{\boldsymbol{G}}$ is the block-diagonal grasp matrix $\widetilde{\boldsymbol{G}} = \mathrm{diag}\{\boldsymbol{G}_1, \cdots, \boldsymbol{G}_N\}$, $\Delta \boldsymbol{l} = \begin{bmatrix}\Delta l_1 & \cdots \Delta l_N\end{bmatrix}^{\mathrm{T}}$ and $\widetilde{\boldsymbol{\upsilon}}_o = \begin{bmatrix}\boldsymbol{\upsilon}_o^{\mathrm{T}} & \cdots & \boldsymbol{\upsilon}_o^{\mathrm{T}}\end{bmatrix}^{\mathrm{T}}$. If a minimal representation is chosen to parametrize object orientation, from (3.2) the following closed-loop inverse kinematics algorithm can be derived

$$\begin{aligned}\dot{\widetilde{\boldsymbol{q}}}_d &= \widetilde{\boldsymbol{J}}^{\dagger}(\widetilde{\boldsymbol{q}}_d, \Delta \boldsymbol{l}_d)\widetilde{\boldsymbol{G}}^{\mathrm{T}}(\boldsymbol{\eta}_d, \Delta \boldsymbol{l}_d)\dot{\boldsymbol{x}}_c + \boldsymbol{N}_o\boldsymbol{\sigma}, \\ \dot{\boldsymbol{x}}_c &= \widetilde{\boldsymbol{\Gamma}}\,(\widetilde{\boldsymbol{x}}_o)\,(\dot{\widetilde{\boldsymbol{x}}}_{o_d} + \boldsymbol{K}_o\widetilde{\boldsymbol{e}}_o),\end{aligned} \tag{3.3}$$

where the symbol † denotes a weighted right pseudo-inverse, $\boldsymbol{K}_o$ is a diagonal and positive definite matrix gain, $\boldsymbol{N}_o = \boldsymbol{I} - \widetilde{\boldsymbol{J}}^{\dagger}\widetilde{\boldsymbol{J}}$ is a projector onto the null space of the Jacobian matrix $\widetilde{\boldsymbol{J}}$ and

$$\widetilde{\boldsymbol{x}}_{o_d} = \begin{bmatrix} \boldsymbol{x}_{o_d} \\ \vdots \\ \boldsymbol{x}_{o_d} \end{bmatrix}, \ \widetilde{\boldsymbol{x}}_o = \begin{bmatrix} \boldsymbol{x}_{o_1} \\ \vdots \\ \boldsymbol{x}_{o_N} \end{bmatrix}, \ \widetilde{\boldsymbol{e}}_o = \begin{bmatrix} \boldsymbol{e}_{o_1} \\ \vdots \\ \boldsymbol{e}_{o_N} \end{bmatrix}, \tag{3.4}$$

$$\widetilde{\boldsymbol{\Gamma}}\left(\widetilde{\boldsymbol{x}}_o\right) = \mathrm{diag}\{\boldsymbol{\Gamma}\left(\boldsymbol{x}_{o_1}\right), \ldots, \boldsymbol{\Gamma}\left(\boldsymbol{x}_{o_N}\right)\}, \tag{3.5}$$

where $\boldsymbol{x}_{o_d}$ and $\boldsymbol{x}_{o_j}$ are the planned and the actual object poses, respectively, $\boldsymbol{e}_{o_j} = \boldsymbol{x}_{o_d} - \boldsymbol{x}_{o_j}$ and $\boldsymbol{\Gamma}\left(\boldsymbol{x}_{o_j}\right)$ is the transformation between $\dot{\boldsymbol{x}}_{o_j}$ and the object velocity $\boldsymbol{v}_{o_j}$, computed on the basis of the kinematics of finger i. The quantity $\Delta\boldsymbol{l}_d$ in (3.3) is the vector collecting the finger elastic pad deformations $\Delta l_{d_j} = f_{d_j}/k_j$ corresponding to the desired contact force f_{d_j}.

If a quaternion based representation is chosen, the expression of $\dot{\boldsymbol{x}}_c$ results to be slightly different with respect to that in (3.3)

$$\begin{aligned} \dot{\widetilde{\boldsymbol{q}}}_d &= \widetilde{\boldsymbol{J}}^{\dagger}(\widetilde{\boldsymbol{q}}_d, \Delta\boldsymbol{l}_d)\widetilde{\boldsymbol{G}}^{\mathrm{T}}(\boldsymbol{\eta}_d, \Delta\boldsymbol{l}_d)\dot{\boldsymbol{x}}_c + \boldsymbol{N}_o\boldsymbol{\sigma}, \\ \dot{\boldsymbol{x}}_c &= \dot{\widetilde{\boldsymbol{x}}}_{o_d} + \boldsymbol{K}_o\widetilde{\boldsymbol{e}}_o, \end{aligned} \tag{3.6}$$

where the error $\widetilde{\boldsymbol{e}_{o_j}}$ is defined as

$$\widetilde{\boldsymbol{e}}_{o_j} = \begin{bmatrix} \boldsymbol{p}_{o_d} - \boldsymbol{p}_{o_j} \\ \widetilde{\boldsymbol{\epsilon}}_{o_j} \end{bmatrix},$$

where $\boldsymbol{p}_{o_d}$ and $\boldsymbol{p}_{o_j}$ are the palanned and the actual positions while $\widetilde{\boldsymbol{\epsilon}}_{o,j}$ is the vector part of the unit quaternion $\widetilde{\mathcal{Q}}_{o_j}$ extract from the rotation matrix $\widetilde{\boldsymbol{R}}_{o_j} = \boldsymbol{R}_{o_d}^{\mathrm{T}}\boldsymbol{R}_{o_j}$, with $\boldsymbol{R}_{o_d}$ and $\boldsymbol{R}_{o_j}$ representing the desired and actual object orientation, computed via the forward kinematics of the extended finger.

Since the system may be highly redundant, multiple tasks could be fulfilled, provided that they are suitably arranged in a priority order. Consider m secondary tasks, each expressed by a task function $\boldsymbol{\sigma}_{t_h}(\widetilde{\boldsymbol{q}})$ $(h = 1, \ldots, m)$.

According to the *augmented projection method* [2], the null projection can be better detailed as

$$\dot{\widetilde{\boldsymbol{q}}}_d = \widetilde{\boldsymbol{J}}^{\dagger}(\widetilde{\boldsymbol{q}}_d, \Delta\boldsymbol{l}_d)\widetilde{\boldsymbol{G}}^{\mathrm{T}}(\boldsymbol{\eta}_d, \Delta\boldsymbol{l}_d)\dot{\boldsymbol{x}}_c + \sum_{h=1}^{m} \boldsymbol{N}(\boldsymbol{J}_{t_h}^A)\boldsymbol{J}_{t_h}^{\dagger}\boldsymbol{K}_{t_h}\boldsymbol{e}_{t_h}, \tag{3.7}$$

where $\boldsymbol{J}_{t_h}$ is the hth task Jacobian, $\boldsymbol{J}_{t_h}^A$ is the augmented Jacobian, given by

$$\boldsymbol{J}_{t_h}^A = \begin{bmatrix} \widetilde{\boldsymbol{J}}^{\mathrm{T}} & \boldsymbol{J}_{t_1}^{\mathrm{T}} & \dots & \boldsymbol{J}_{t_{h-1}}^{\mathrm{T}} \end{bmatrix}^{\mathrm{T}}. \tag{3.8}$$

$\boldsymbol{N}(\boldsymbol{J}_{t_h}^A)$ is a null projector of the matrix $\boldsymbol{J}_{t_h}^A$, $\boldsymbol{K}_{t_h}$ is a positive definite gain matrix and $\boldsymbol{e}_{t_h} = \boldsymbol{\sigma}_{t_{h\,d}} - \boldsymbol{\sigma}_{t_h}$ is the task error, being $\boldsymbol{\sigma}_{t_{h\,d}}$ the desired value of the hth task variable.

The augmented projection method can be also adopted to fulfill mechanical or environmental constraints, such as joint limits and obstacle (i.e., other fingers or the grasped object) avoidance. To this aim, each constraint can be described by means of a cost function, $\mathcal{C}(\widetilde{\boldsymbol{q}})$, which increases when the manipulator is close to violate the constraint. In order to minimize the cost function, the manipulator could be moved according to $-\nabla_{\widetilde{\boldsymbol{q}}}^{\mathrm{T}}\mathcal{C}(\widetilde{\boldsymbol{q}})$, that could be considered as a fictitious force moving the manipulator away from configurations violating the constraints. In order to include the constraints in (3.7), an overall cost function $\mathcal{C}_\Sigma$, given by

$$\mathcal{C}_\Sigma(\widetilde{\boldsymbol{q}}) = \sum_s \gamma_s \mathcal{C}_s(\widetilde{\boldsymbol{q}}), \tag{3.9}$$

is introduced, where γ_s and $\mathcal{C}_s$ are a positive weight and a cost function, respectively, referred to the sth constraint. Therefore, the following term can be added to (3.7)

$$\dot{\widetilde{\boldsymbol{q}}}_c = -k_\nabla \boldsymbol{N}(\boldsymbol{J}_{t_{m+1}}^A)\nabla_{\widetilde{\boldsymbol{q}}_d}^{\mathrm{T}}\mathcal{C}_\Sigma, \tag{3.10}$$

where k_∇ is a positive gain.

If the system is close to violate a constraint, a high level supervisor has

to remove some secondary tasks and relax enough DOFs to fulfill the constraints [34]. To manage in a correct way removal/insertion of tasks from/into the stack (task sequencing), a task supervisor, based on a two-layer architecture, can be designed: the lower layer determines when some tasks must be removed from the stack and the tasks to be removed; then, the upper layer verifies if the previously removed tasks can be pushed back into the stack.

Removal and insertion of the tasks

The first layer verifies if the planned trajectory will cause a constraint violation at the next time step. Hence, a task must be removed from the stack when the predicted value of the overall cost function at the next time step is above a suitable defined threshold, $\overline{\mathcal{C}}$. Let T be the sampling time and κT the actual time (where κ is an integer), the configuration at the time instant $(\kappa+1)T$ can be estimated as follows

$$\widehat{\widetilde{\boldsymbol{q}}}_d(\kappa+1) = \widetilde{\boldsymbol{q}}_d(\kappa) + T\dot{\widetilde{\boldsymbol{q}}}_d(\kappa). \tag{3.11}$$

Hence, a task must be removed from the stack if

$$\mathcal{C}_\Sigma\left(\widehat{\widetilde{\boldsymbol{q}}}_d(\kappa+1)\right) \geq \overline{\mathcal{C}}. \tag{3.12}$$

Once it has been ascertained that a task must be removed from the stack, the problem is to detect which task has to be removed. To the purpose, different criteria have been proposed in [34], with the aim of verifying the conflict between the constraints and each task. In detail, in [34] two criteria are presented: the first one compares the velocities induced by a subtask and by the gradient of $\mathcal{C}_\Sigma$; the second criterion considers the projection of the gradient onto the null space of the task Jacobians. A new criterion is presented. Given two generic tasks, whose Jacobians are $\boldsymbol{J}_{t_x}$ and $\boldsymbol{J}_{t_y}$, respectively, they are defined as *annihilating* [2] if

$$\boldsymbol{J}_{t_x}\boldsymbol{J}_{t_y}^{\dagger} = \boldsymbol{O}. \tag{3.13}$$

The annihilation condition can be considered as a compatibility condition between the tasks, since it is equivalent to the orthogonality condition between the subspaces spanned by $\boldsymbol{J}_{t_x}^{\mathrm{T}}$ and $\boldsymbol{J}_{t_y}^{\mathrm{T}}$. Therefore, in order to select the secondary task less compatible with the constraints, the following compatibility metric can be introduced

$$\mathcal{M}_{t_h} = \left\| \nabla_{\widetilde{\boldsymbol{q}}_d}^{\mathrm{T}} \mathcal{C}_\Sigma \; \boldsymbol{J}_{t_h}^{\dagger} \right\|, \quad h = 1, \ldots, m. \tag{3.14}$$

The more $\mathcal{M}_{t_h}$ is close to zero the more the hth task is compatible with the constraints: hence, the task having the maximum value of $\mathcal{M}_{t_h}$ is removed.

The tasks removed by the first layer must be reinserted into the stack as soon as possible, provided that the reinsertion does not cause constraint violation. To this aim, a prediction of the evolution of $\mathcal{C}_\Sigma$ at the next time step is evaluated by considering the effect of each task currently out of the stack, i.e.,

$$\widehat{\widetilde{\boldsymbol{q}}}_{t_h}(\kappa + 1) = \widetilde{\boldsymbol{q}}_d(\kappa) + \boldsymbol{J}_{t_h}^{\dagger} \boldsymbol{e}_{t_h}(\kappa). \tag{3.15}$$

Therefore, let $\underline{\mathcal{C}} < \overline{\mathcal{C}}$ be a suitably chosen threshold, a task is pushed back into the stack if

$$\mathcal{C}_\Sigma \left(\widehat{\widetilde{\boldsymbol{q}}}_{t_h}(\kappa + 1) \right) \leq \underline{\mathcal{C}}. \tag{3.16}$$

Smooth transition

Task sequencing might cause discontinuities in the planned joint velocities due to the change of active tasks in the stack [34, 64]. In order to achieve a smooth behavior of the motion planner output, for each task a variable gain, ρ_{t_h}, is defined in such a way to behave according to the following dynamics

- reactivation

$$\dot{\rho}_{t_h} + \mu \rho_{t_h} = \mu \delta_{-1}(t - \tau), \; \rho_{t_h}(0) = 0, \tag{3.17}$$

- deactivation

$$\dot{\rho}_{t_h} + \mu \rho_{t_h} = \mu - \mu \delta_{-1}(t - \tau'), \; \rho_{t_h}(0) = 1, \tag{3.18}$$

where τ and τ' are the time instant in which the task is inserted into the stack and the time instant in which it is removed, respectively, and $1/\mu$ is a time constant. Since the sistems defined in (3.17) and (3.18) are linear first order system, it is trivial to show that the time evolution of ρ_{t_h} is the following

$$\rho_{t_h}(t) = \begin{cases} 1 - \mathrm{e}^{-\mu(t-\tau)}, & \text{reactivation requested at time istant } \tau, \\ \mathrm{e}^{-\mu(t-\tau')}, & \text{deactivation requested at time instant } \tau', \end{cases} \tag{3.19}$$

These gains guarantee the continuity of the planned joint velocity, $\dot{\widetilde{\boldsymbol{q}}}_d$, during the insertion and removal of the tasks.

In sum, the planned joint reference vector for the controller is computed via

$$\begin{aligned} \dot{\widetilde{\boldsymbol{q}}}_d = {} & \widetilde{\boldsymbol{J}}^{\dagger}(\widetilde{\boldsymbol{q}}_d, \Delta\boldsymbol{l}_d)\widetilde{\boldsymbol{G}}^{\mathrm{T}}(\boldsymbol{\eta}_d, \Delta\boldsymbol{l}_d)\dot{\boldsymbol{x}}_c + \sum_{h=1}^{m} \rho_{t_h} \boldsymbol{N}(\boldsymbol{J}^A_{t_h}) \boldsymbol{J}^{\dagger}_{t_h} \boldsymbol{K}_{t_h} \boldsymbol{e}_{t_h} \\ & - k_{\nabla} \boldsymbol{N}(\boldsymbol{J}^A_{t_{m+1}}) \nabla^{\mathrm{T}}_{\widetilde{\boldsymbol{q}}_d} \mathcal{C}_{\Sigma}. \end{aligned} \tag{3.20}$$

3.1.2 Parallel force/pose control

Since the motion planner provides joint references (i.e., $\boldsymbol{q}_d$ and $\dot{\boldsymbol{q}}_d$) of the overall dual-arm/hand system, any kind of joint motion control can be adopted for the arms, while joint torques for the jth finger are computed according to the following parallel force/pose control law in the operational space

$$\begin{aligned} & \boldsymbol{J}_j^{\mathrm{T}}(\boldsymbol{q}_j) \Big(\boldsymbol{K}_P \Delta\boldsymbol{x}_j - \boldsymbol{K}_D \dot{\boldsymbol{x}}_j + \boldsymbol{f}_{dj} + k_F \Delta\boldsymbol{f}_{nj} \\ & + k_I \int_0^t \Delta\boldsymbol{f}_{nj} \mathrm{d}\zeta + \boldsymbol{g}_j(\boldsymbol{q}_j) \Big), \end{aligned} \tag{3.21}$$

where $\boldsymbol{g}_j(\boldsymbol{q}_j)$ is the vector of the generalized gravity force acting on finger j, $\Delta\boldsymbol{x}_j$ denotes the pose error of finger j between the desired value $\boldsymbol{x}_{j_d}$, corresponding to $\boldsymbol{q}_{d_j}$, and the current one, $\boldsymbol{x}_j$, with respect to the palm frame

Σ_{rh} (or Σ_{lh}), $\boldsymbol{K}_P$, $\boldsymbol{K}_D$ are gain matrices, k_F, k_I are positive scalar gains and $\Delta \boldsymbol{f}_{n_j} = \left[\Delta f_{n_j} \hat{\boldsymbol{n}}_j^{\mathrm{T}} \quad \boldsymbol{0}^{\mathrm{T}}\right]^{\mathrm{T}}$, being Δf_{n_j} the projection of the force error along the normal to the object surface, $\hat{\boldsymbol{n}}_j$, at the contact point j.
Control law (3.21) allows to track the assigned contact forces which are, in turn, imposed to avoid contact breaks or excessive stresses on the manipulated object, even in the presence of uncertainties.

3.1.3 Stability analysis

In order to prove stability of the system under the control law (3.21) the dynamic model in the operational space [63] of the ith finger should be considered

$$\boldsymbol{M}_j(\boldsymbol{x}_j)\ddot{\boldsymbol{x}}_j + \boldsymbol{C}_j\left(\boldsymbol{x}_j, \dot{\boldsymbol{x}}_j\right)\dot{\boldsymbol{x}}_j + \boldsymbol{g}_j(\boldsymbol{x}_j) = \boldsymbol{u}_j - \boldsymbol{f}_j, \tag{3.22}$$

where $\boldsymbol{M}_j$ is the (6×6) inertia matrix of the jth finger, $\boldsymbol{C}_j$ is the (6×6) matrix collecting the centrifugal and Coriolis terms, $\boldsymbol{f}_j$ is the (6×1) vector of generalized contact forces (acting at the fingertip), $\boldsymbol{u}_j$ is the (6×1) vector of driving generalized forces, through which the control torques can be obtained via

$$\boldsymbol{\tau}_j = \boldsymbol{J}_j^{\mathrm{T}}(\boldsymbol{q}_j)\boldsymbol{u}_j. \tag{3.23}$$

Hereafter the subscript j will be dropped for notation compactness. The following properties hold [30, 62, 63]:

1. $\boldsymbol{M}$ is symmetric and positive definite; therefore, if $\lambda_m(\cdot)$ ($\lambda_M(\cdot)$) denotes the minimum (maximum) eigenvalue, it is

$$0 < \lambda_m(\boldsymbol{M})\,\boldsymbol{I}_6 \leq \boldsymbol{M}(\boldsymbol{x}) \leq \lambda_M(\boldsymbol{M})\,\boldsymbol{I}_6, \tag{3.24}$$

   where $\lambda_M(\boldsymbol{M}) < \infty$ if all joints are revolute.

2. There always exists a choice of $\boldsymbol{C}$ such that

$$\dot{\boldsymbol{M}}(\boldsymbol{x}) = \boldsymbol{C}\left(\boldsymbol{x}, \dot{\boldsymbol{x}}\right) + \boldsymbol{C}^{\mathrm{T}}\left(\boldsymbol{x}, \dot{\boldsymbol{x}}\right), \tag{3.25}$$

moreover, $\boldsymbol{C}$ can be upper-bounded as follows $\dot{\boldsymbol{x}}$

$$\|\boldsymbol{C}\left(\boldsymbol{x}, \dot{\boldsymbol{x}}\right)\| \leq k_c \|\dot{\boldsymbol{x}}\|, \tag{3.26}$$

with $k_c > 0$.

The following assumptions have been considered

Assumption 1. *Pose and force references are constant, i.e.,* $\dot{\boldsymbol{x}}_d = \dot{\boldsymbol{f}}_d = \mathbf{0}$.

Assumption 2. *Quasi-static object manipulation, i.e.,* $\dot{\boldsymbol{\upsilon}}_o = \boldsymbol{\upsilon}_o = \mathbf{0}$.

Assumption 3. *The force along the normal to the contact surface is assumed of elastic type, i.e.,* $\boldsymbol{f}_n = k\Delta l \hat{\boldsymbol{n}} = f_n \hat{\boldsymbol{n}}$.

Assumption 4. *The object has a convex surface. For this kind of objects and for quasi-static manipulation the time derivative of the unit vector normal to object surface at contact point (see the Appendix A.1 for further details), can be norm bounded as follows*

$$\|\dot{\hat{\boldsymbol{n}}}\| \leq k_n \|\dot{\boldsymbol{p}}_f\|, \tag{3.27}$$

where $\boldsymbol{p}_f = \boldsymbol{o}_{f_j} - \boldsymbol{o}_h$ *is the position of* Σ_{f_j} *with respect to the palm frame* Σ_h *expressed in base frame coordinates.*

By taking into account the elasticity of the normal force (Assumption 3) and by considering the object quasi-static (Assumption 2) the following relationship between the force and position errors can be derived

$$\Delta f_n = k\left(\Delta l_d - \Delta l\right) = k\boldsymbol{n}^T \Delta \boldsymbol{x}, \tag{3.28}$$

where $\boldsymbol{n} = \begin{bmatrix} \hat{\boldsymbol{n}}^{\mathrm{T}} & \mathbf{0}^{\mathrm{T}} \end{bmatrix}^{\mathrm{T}}$ is a (6×1) unit vector. By virtue of the integral action in (3.21) and equation (3.28), the system (3.22) under the control law (3.21) has a unique equilibrium at $\boldsymbol{x}_\infty = \boldsymbol{x}_d$ and $\boldsymbol{f}_{n_\infty} = \boldsymbol{f}_d$ (see Appendix A.2).

In order to study the stability of the equilibrium, it is convenient to consider a (13×1) state vector [62]

$$\mathbf{z} = \begin{bmatrix} \boldsymbol{z}_1 \\ \boldsymbol{z}_2 \\ z_3 \end{bmatrix} = \begin{bmatrix} \Delta\dot{\boldsymbol{x}} \\ \Delta\boldsymbol{x} \\ \Delta s \end{bmatrix}, \tag{3.29}$$

where

$$\Delta s = s_\infty - s = s_\infty - \int_0^t \left(\Delta f_n - \frac{k}{\rho} \dot{\boldsymbol{n}}^{\mathrm{T}} \Delta\boldsymbol{x} \right) d\zeta, \tag{3.30}$$

ρ is a positive constant, k is the stiffness of the elastic pad and s_∞ is the value of s at the equilibrium (the explicit expression of s_∞ is given in Appendix A.3). The augmented state dynamics is thus given by

$$\dot{\boldsymbol{z}} = \boldsymbol{A}\boldsymbol{z} + \boldsymbol{b}, \tag{3.31}$$

with

$$\boldsymbol{A} = \begin{bmatrix} -\boldsymbol{M}^{-1}(\boldsymbol{C} + \boldsymbol{K}_D) & -\boldsymbol{M}^{-1}(\boldsymbol{K}_P + \boldsymbol{F}) & k_I \boldsymbol{M}^{-1}\boldsymbol{n} \\ \boldsymbol{I} & \boldsymbol{O} & \boldsymbol{0} \\ 0 & -k\left(\boldsymbol{n} - \dfrac{\dot{\boldsymbol{n}}}{\rho}\right)^{\mathrm{T}} & 0 \end{bmatrix}, \tag{3.32}$$

$$\boldsymbol{b} = \begin{bmatrix} k_I I_n \left(\boldsymbol{M}^{-1}\boldsymbol{n}\right)^{\mathrm{T}} & \boldsymbol{0}^{\mathrm{T}} & 0 \end{bmatrix}^{\mathrm{T}}, \tag{3.33}$$

where the dependencies of $\boldsymbol{M}$ and $\boldsymbol{C}$ upon $\boldsymbol{x}$ and $\dot{\boldsymbol{x}}$ have been dropped, $\boldsymbol{F} = (1 + k_f) k \boldsymbol{n}\boldsymbol{n}^T$ and

$$I_n = -s_\infty - \int_0^t \frac{k}{\rho} \dot{\boldsymbol{n}}^{\mathrm{T}} \Delta\boldsymbol{x} d\zeta. \tag{3.34}$$

Theorem 1. *There exists a set of parameters $\boldsymbol{K}_P$, $\boldsymbol{K}_D$, k_f and k_I such that $\boldsymbol{z}_1$ and $\boldsymbol{z}_2$ are locally asymptotically convergent to $\boldsymbol{0}$.*

Proof of Theorem 1 is given in Appendix A.4.

Since $\Delta\dot{\boldsymbol{x}}$ and $\Delta\boldsymbol{x}$ are asymptotically convergent to $\mathbf{0}$, by recalling (3.28) it can be seen that Δf_n asymptotically converges to 0 as well.

It is worth noticing that, differently from [62], it has been proven that system (3.22), under the control law (3.21), is locally stable even when a non-planar convex surface is considered.

3.2 Case study

The proposed scheme has been tested in simulation on a dual-arm/hand manipulation system (Figure 3.2) grasping a cardboard box. The manipulation system is composed by two identical planar arm, with 2 DOFs each, and two planar two-fingered hands, with 3+2 DOFs each, resulting in a total of $N = 4$ fingers and 14 active joints.

3.2.1 Set-up configuration

It is assumed that, in its initial configuration, the system grasps the object with tips 1 and 2, ensuring force closure, since the contact normal forces are acting on the same straight line, while tips 3 and 4 are also in contact but in arbitrary way. The main task consists in keeping the object still, thanks to fingers 1 and 2, while tips 3 and 4 move in order to achieve a force closure condition upon the object in a dexterous configuration, without violating a certain number of limits and constraints. The force control loop ensures that the planned forces are applied on the object. In this case study, the desired forces for tips 3 and 4 are set close to zero, since they have to slide, but not exactly zero, because contact continuity should be ensured during the whole motion. Concerning fingers 1 and 2, higher values of contact forces have been considered in such a way to hold the object without excessive stresses.

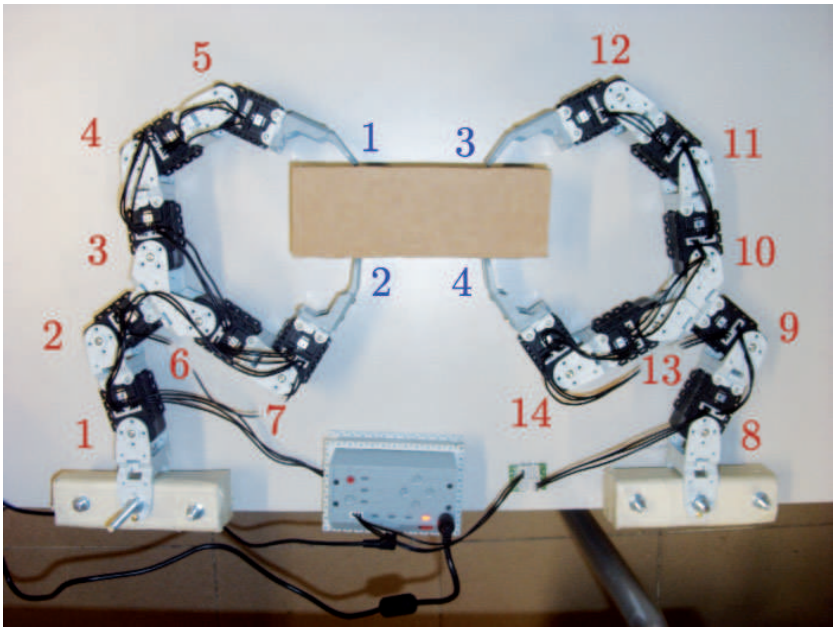

Figure 3.2: Dual-arm/hand experimental set-up which has been built by using the Bioloid© Expert Kit. The red numbers label the joints. The blue numbers indicate the tips of the fingers.

The planner ((3.20)) and the controller ((3.21)) have been developed in the Matlab© environment, while GRASPIT! has been used as dynamic simulator.

3.2.2 Dynamic simulation environment

GRASPIT! offers a dynamic engine which allows to deal with contact mechanics in a realistic way, since it is possible to simulate hard finger contacts (as well as point contacts without friction) fulfilling non-penetration constraints. Frictional forces and non-penetration constraints are expressed via inequalities; thus, a Linear Complementary Problem (LCP) is solved by GRASPIT!, at each time step, by using Lemke's algorithm [37]. Moreover,

a collision detection system acts in such a way to prevent collisions within bodies as well as to identify and mark contact regions.

GRASPIT! also provides C-MEX functions which allow communication with Matlab©: it is possible to assign joint torques (only when the dynamic mode is enabled) to the manipulation system, as well as, to read joint positions and contact forces. Some modifications to the source code of the simulation software have been done in order to retrieve end-effector pose, choose the reference frame in which contact forces are provided to Matlab© and include the prismatic dynamic joint class[1].

The dual-arm/hand system model has been added to the GRASPIT! robot library; accurate values of mass and geometric parameters have been set on the basis of available datasheets.

The elastic contact, described in Section 2.3.2, has been modeled by using a rotational joint and a prismatic one, acting like a spring-damper systems, isuch that the elastic force acts only along the direction of the object surface normal at each contact point.

3.2.3 Secondary tasks and constraints

Different secondary tasks have been considered: the first two, aimed at choosing the optimal contact points, are related to the grasp force-closure condition, the other one is related to a measure of the grasp quality, while the last one regards the manipulability of the dual-arm/hand system. On the other hand, two physical constraints have been considered: joint limits and collision avoidance.

Unit frictionless equilibrium. By moving the contact points on the object surface until the unit frictionless equilibrium is reached, it is possible to

[1]The modified source code of GRASPIT! is available for download for Linux at `http://www.unibas.it/automatica/laboratory.html`

guarantee the grasp force-closure condition [42]. Such equilibrium is satisfied when two positive indices, called frictionless force (ε_f) and moment (ε_m) residuals, are zero [18, 50]

$$\begin{aligned} \varepsilon_f &= \frac{1}{2}\boldsymbol{f}^{\mathrm{T}}\boldsymbol{f} \qquad & \boldsymbol{f} &= \sum_{i=1}^{N} \hat{\boldsymbol{n}}_i^o, \\ \varepsilon_m &= \frac{1}{2}\boldsymbol{m}^{\mathrm{T}}\boldsymbol{m} \qquad & \boldsymbol{m} &= \sum_{i=1}^{N} \boldsymbol{c}_i^o \times \hat{\boldsymbol{n}}_i^o, \end{aligned} \tag{3.35}$$

where $N = 4$ is the number of fingers and $\hat{\boldsymbol{n}}_i^o(\boldsymbol{\xi}_i)$ is the surface normal of the ith contact point, referred to the object frame. It has been shown that, for two or more contact points, unit frictionless equilibrium is a force closure condition for any nonzero friction coefficient [50, 51].

The Jacobian matrix of the unit frictionless force residual is given by

$$\boldsymbol{J}_{\varepsilon_f} = \frac{\partial \varepsilon_f}{\partial \widetilde{\boldsymbol{q}}} = \frac{\partial \varepsilon_f}{\partial \boldsymbol{f}} \frac{\partial \boldsymbol{f}}{\partial \boldsymbol{\xi}} \frac{\partial \boldsymbol{\xi}}{\partial \widetilde{\boldsymbol{q}}} = \boldsymbol{f}^{\mathrm{T}} \frac{\partial \boldsymbol{f}}{\partial \boldsymbol{\xi}} \frac{\partial \boldsymbol{\xi}}{\partial \widetilde{\boldsymbol{q}}}, \tag{3.36}$$

where $\boldsymbol{\xi} = \begin{bmatrix} \boldsymbol{\xi}_1^{\mathrm{T}} & \cdots & \boldsymbol{\xi}_N^{\mathrm{T}} \end{bmatrix}^{\mathrm{T}}$ and $\dfrac{\partial \boldsymbol{f}}{\partial \boldsymbol{\xi}} = \begin{bmatrix} \dfrac{\partial \hat{\boldsymbol{n}}_1^o}{\partial \boldsymbol{\xi}_1} & \cdots & \dfrac{\partial \hat{\boldsymbol{n}}_N^o}{\partial \boldsymbol{\xi}_N} \end{bmatrix}$. As for the unit frictionless momentum residual the Jacobian can be computed as

$$\boldsymbol{J}_{\varepsilon_m} = \frac{\partial \varepsilon_m}{\partial \widetilde{\boldsymbol{q}}} = \frac{\partial \varepsilon_m}{\partial \boldsymbol{m}} \frac{\partial \boldsymbol{m}}{\partial \boldsymbol{\xi}} \frac{\partial \boldsymbol{\xi}}{\partial \widetilde{\boldsymbol{q}}} = \boldsymbol{m}^{\mathrm{T}} \frac{\partial \boldsymbol{m}}{\partial \boldsymbol{\xi}} \frac{\partial \boldsymbol{\xi}}{\partial \widetilde{\boldsymbol{q}}}, \tag{3.37}$$

with $\dfrac{\partial \boldsymbol{m}}{\partial \boldsymbol{\xi}} = \begin{bmatrix} \dfrac{\partial (\boldsymbol{c}_1^o \times \hat{\boldsymbol{n}}_1^o)}{\partial \boldsymbol{\xi}_1} & \cdots & \dfrac{\partial (\boldsymbol{c}_N^o \times \hat{\boldsymbol{n}}_N^o)}{\partial \boldsymbol{\xi}_N} \end{bmatrix}$.

It is worth noticing that, since the considered object is rectangular and the opposite fingers of each hand are on the opposite sides of the rectangle, the force residual index is always zero during the whole case study, therefore it is not considered in the following.

Grasp quality. The unit frictionless equilibrium is necessary to achieve the positions of the fingertips on the object surface ensuring that the external wrenches acting on the object can be balanced by the fingers. A subset of these positions might be selected according to a grasp quality index. In

general, several indexes can be considered: in this case study, the fingers are commanded to reach a symmetric position with respect to the object's center. In detail, the following task function is considered

$$\sigma_{s_i} = \begin{cases} |\xi_{d_i} - \xi_i| & \text{if } |\xi_{d_i} - \xi_i| > \overline{\xi}_i, \\ 0 & \text{otherwise,} \end{cases} \tag{3.38}$$

where $\overline{\xi}_i$ is a threshold for the task activation and ξ_{d_i} is the desired value for the ith finger contact variable, with $i = 3, 4$. The desired value, $\sigma_{d_{s_i}}$, is zero. The meaning of (3.38) is that the contact variables for fingers 3 and 4, the only fingers that can slide, should reach the desired position on the object, represented by the values ξ_{d_3} and ξ_{d_4}, on the basis of the positions of the fingers 1 and 2 on the object, denoted by the constant values ξ_1 and ξ_2, respectively.

Let $\boldsymbol{\sigma}_s = \begin{bmatrix} \sigma_{s_3} & \sigma_{s_4} \end{bmatrix}^{\mathrm{T}}$, the Jacobian $\boldsymbol{J}_{\sigma_s}(\boldsymbol{\xi})$ for the symmetric grasp subtask can be computed as

$$\boldsymbol{J}_{\sigma_s}(\boldsymbol{\xi}) = \frac{\partial \boldsymbol{\sigma}_s}{\partial \boldsymbol{\xi}} \frac{\partial \boldsymbol{\xi}}{\partial \widetilde{\boldsymbol{q}}}, \tag{3.39}$$

where

$$\frac{\partial \sigma_{s_i}}{\partial \xi_j} = \begin{cases} 0, \text{ if } i \neq j \\ \dfrac{\partial \sigma_{s_i}}{\partial \xi_i}, \text{ if } i = j \end{cases},$$

and

$$\frac{\partial \sigma_{s_i}}{\partial \xi_i} = \begin{cases} -\text{sign}(\xi_{d_i} - \xi_i), \text{ if } |\xi_{d_i} - \xi_i| > \overline{\xi}_i \\ 0, \text{ otherwise} \end{cases}.$$

Manipulability. In order to keep the manipulation system far from singularities, the manipulability index presented in [63] can be considered for the ith finger

$$w_i(\boldsymbol{q}_i) = \sqrt{det\left(\boldsymbol{J}_{F_i}(\boldsymbol{q}_i)\boldsymbol{J}_{F_i}^{\mathrm{T}}(\boldsymbol{q}_i)\right)}, \quad i = 1, \ldots, 4. \tag{3.40}$$

However, a simplified manipulability index, computationally simpler than (3.40) but still describing in an effective way the distance from kinematic singularities, is adopted for the considered set-up, i.e.,

$$\begin{aligned} w_1 &= 0.5\,(s_2^2 + s_3^2 + s_4^2 + s_5^2) \\ w_2 &= 0.5\,(s_2^2 + s_6^2 + s_7^2) \\ w_3 &= 0.5\,(s_9^2 + s_{10}^2 + s_{11}^2 + s_{12}^2) \\ w_4 &= 0.5\,(s_9^2 + s_{13}^2 + s_{14}^2) \end{aligned} \tag{3.41}$$

where $s_\alpha = \sin(q_\alpha)$.

Hence, the following task function is considered

$$\sigma_{w_i} = \begin{cases} |w_{d_i} - w_i| & \text{if } |w_{d_i} - w_i| > \overline{w}_i, \\ 0 & \text{otherwise,} \end{cases} \tag{3.42}$$

where $\overline{w}_i$ is a threshold for the task activation and w_{d_i} is the desired value for the ith finger manipulability, with $i = 1, \ldots, 4$. The desired value, $\sigma_{d_{w_i}}$, is zero and a vectorial task function $\boldsymbol{\sigma}_w = \begin{bmatrix} \sigma_{w_1} & \ldots & \sigma_{w_4} \end{bmatrix}^{\mathrm{T}}$ is considered.

The Jacobian $\boldsymbol{J}_{\sigma_w}(\boldsymbol{q})$ for the manipulability subtask can be computed as

$$\boldsymbol{J}_{\sigma_w}(\boldsymbol{q}) = \frac{\partial \boldsymbol{\sigma}_w}{\partial \boldsymbol{q}} \frac{\partial \boldsymbol{q}}{\partial \widetilde{\boldsymbol{q}}}, \tag{3.43}$$

where

$$\frac{\partial w_{s_i}}{\partial q_j} = \begin{cases} 0, \text{ if } i \neq j \\ \dfrac{\partial \sigma_{w_i}}{\partial q_i}, \text{ if } i = j \end{cases},$$

and

$$\frac{\partial \sigma_{w_i}}{\partial q_i} = \begin{cases} -\text{sign}(w_{d_i} - w_i) \dfrac{\partial w_i}{\partial q_i}, \text{ if } |w_{d_i} - w_i| > \overline{w}_i \\ 0, \text{ otherwise} \end{cases}.$$

Joint-limit avoidance. A physical constraint to the motion of the system is imposed by the mechanical joint limits. The system configuration is considered safe if $q_j \in [\underline{q}_j, \overline{q}_j]$, for $j = 1, \ldots, 14$, with $\underline{q}_j$ and $\overline{q}_j$ suitable chosen

values far enough from the mechanical limits. The related cost function is chosen as follows

$$\mathcal{C}_{JL}(\boldsymbol{q}) = \sum_{j=1}^{14} c_j(q_j),$$
$$c_j(q_j) = \begin{cases} k_j e^{\delta(q_j - \underline{q}_j)^2} - 1, & \text{if } \; q_j \leq \underline{q}_j, \\ 0, & \text{if } \; \underline{q}_j < q_j \leq \overline{q}_j, \\ k_j e^{\delta(q_j - \overline{q}_j)^2} - 1, & \text{if } \; q_j > \overline{q}_j, \end{cases} \tag{3.44}$$

where k_j and δ are positive constants.

Collision avoidance. In order to avoid collisions between the fingers, a value of the distance between the fingers larger than a safety value, d_s it is imposed; hence, if $d_{ii'}$ denotes the distance between the ith and the i'th finger, the following cost function can be considered

$$\mathcal{C}_{CA}(\widetilde{\boldsymbol{q}}) = \sum_{i,i'} c_{ii'}(\widetilde{\boldsymbol{q}}), \tag{3.45}$$

where the sum is extended to all the couples of fingers,

$$c_{ii'}(d_{ii'}) = \begin{cases} k_{ii'} \dfrac{d_s - d_{ii'}}{d_{ii'}^2}, & \text{if } \; d_{ii'} \leq d_s, \\ 0, & \text{if } \; d_{ii'} > d_s, \end{cases} \tag{3.46}$$

and $k_{ii'}$ is a positive gain.

3.2.4 Simulation results

Parameters. The elastic contact parameters are: 1000 N/m for the spring elastic coefficients, 20 Ns/m for the spring damper coefficients of all fingers, while $l_i = 24.5 \cdot 10^{-3}$ m is the spring rest position, with $i = 1, \ldots, 4$. Concerning the planner (3.20), the gain for the object pose error has been tuned to $\boldsymbol{K}_o = 450 \boldsymbol{I}_{12}$, while the pseudo-inverse of $\widetilde{\boldsymbol{J}}$, $\widetilde{\boldsymbol{J}}^{\dagger} = \boldsymbol{W}^{-1} \widetilde{\boldsymbol{J}}^{\mathrm{T}} \left(\widetilde{\boldsymbol{J}} \boldsymbol{W}^{-1} \widetilde{\boldsymbol{J}}^{\mathrm{T}} \right)^{-1}$,

has been weighted by a matrix $\boldsymbol{W} = \text{diag}\left(\begin{bmatrix} 4 & 4 & \boldsymbol{e}_{11} & 4 & 4 & \boldsymbol{e}_{11} \end{bmatrix}\right)$, where $\boldsymbol{e}_\alpha$ is a $(1 \times \alpha)$ vector of ones, in order to limit the motion of the arms with respect to that of fingers, assuming that fingers motion is less demanding in terms of power consumption. The object is required to keep its initial position $\begin{bmatrix} 0 & 0.1 \end{bmatrix}^{\mathrm{T}}$ m and orientation of 0 rad during the whole task.

The parameters used to define the secondary tasks are chosen as follows: $\overline{\xi}_i = 0$, with $i = 3, 4$, $\xi_{d_3} = -30 \cdot 10^{-3}$ m, $\xi_{d_4} = 84.5 \cdot 10^{-3}$ m, for the quality index subtask, $\overline{w}_i = 0$, with $i = 1, \ldots, 4$, $w_{d_1} = w_{d_3} = 1.80$, $w_{d_2} = w_{d_4} = 1.30$, for the manipulability subtask. Notice that both the activation thresholds have been put to zero in order to precisely reach their null error conditions. Subtasks gains are set as follows: $k_{t_1} = 30$, $\boldsymbol{K}_{t_2} = 73.5\boldsymbol{I}_2$ and $\boldsymbol{K}_{t_3} = 180\boldsymbol{I}_4$.

Since the mechanical limits of each joint are about ± 1.74 rad, the following safety thresholds for joint limits avoidance have been set: $\overline{q}_j = 1.6$ rad, $\underline{q}_j = -1.6$ rad; moreover, the other parameters in (3.44) are $\delta = 2.2$ and $k_j = 2$ for $j = 1, \ldots, 14$. As for the collision avoidance, the safety distance d_s has been set to $50 \cdot 10^{-3}$ m and the gain $k_{ii'}$ is equal to 1 for all couples of fingers.

The task has a duration of 4 s. A Runge-Kutta integration method, with time step of 0.2 ms, has been used to simulate the system.

The trajectories of the active joints computed by the motion planner are the references for the control law ((3.21)). The parameters in such equation are chosen as follows: $\boldsymbol{K}_P = 2 \cdot 10^5 \boldsymbol{I}_3$, $\boldsymbol{K}_D = 150\boldsymbol{I}_3$, $k_{F_1} = k_{F_2} = 12.5$, $k_{F_3} = k_{F_4} = 1.25$, $k_I = 10$. The desired values for the contact normal forces are 2 N, -2 N, 0.2 N and -0.2 N for the fingers 1, 2, 3 and 4 respectively. The desired values of the first two contact normal forces are bigger since the corresponding fingers have to keep the object still while the other two are required to slide along the surface (i.e., small contact normal forces values are required) in order to reach a force closure condition.

Motion planner. The planner performance are summarized in Figure 3.3

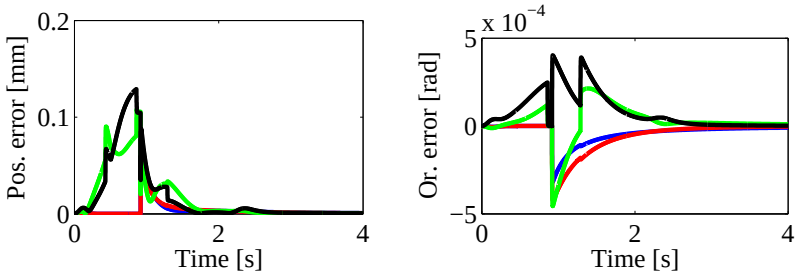

Figure 3.3: Object's pose error computed on the basis of the direct kinematics of each extended finger. Left, norm of the object's position error; right, object's orientation error. Finger 1 is represented in blue, 2 in red, 3 in green and 4 in black.

and Figure 3.4. In detail, Figure 3.3 shows the time history of the norm of the object's pose error computed on the basis of the direct kinematics of each finger. It can be noticed that the error asymptotically goes to zero for each extended finger.

Figure 3.4(a) reports the time history of the stack status. The main task, with priority 1, is never removed from the stack, while the other tasks, numbered from 2 to 4 are removed when some constraints are near to be violated. Notice that task 3 is never removed from the stack since, in this case, it never affects the constraints. When the system is in a safe condition with respect to the constraints, the tasks are re-inserted in the stack maintaining their previous priorities. Moreover, it can be noticed that the peaks in the time histories of the object's pose error correspond to task insertion and/or removal.

Figure 3.4(b) and Figure 3.4(c) show the cost functions related to the joint limits and collision avoidance constraints, respectively. In a first phase, their values increase; for this reason, the tasks farthest from the annihilating condition are removed from the stack. When their values become almost

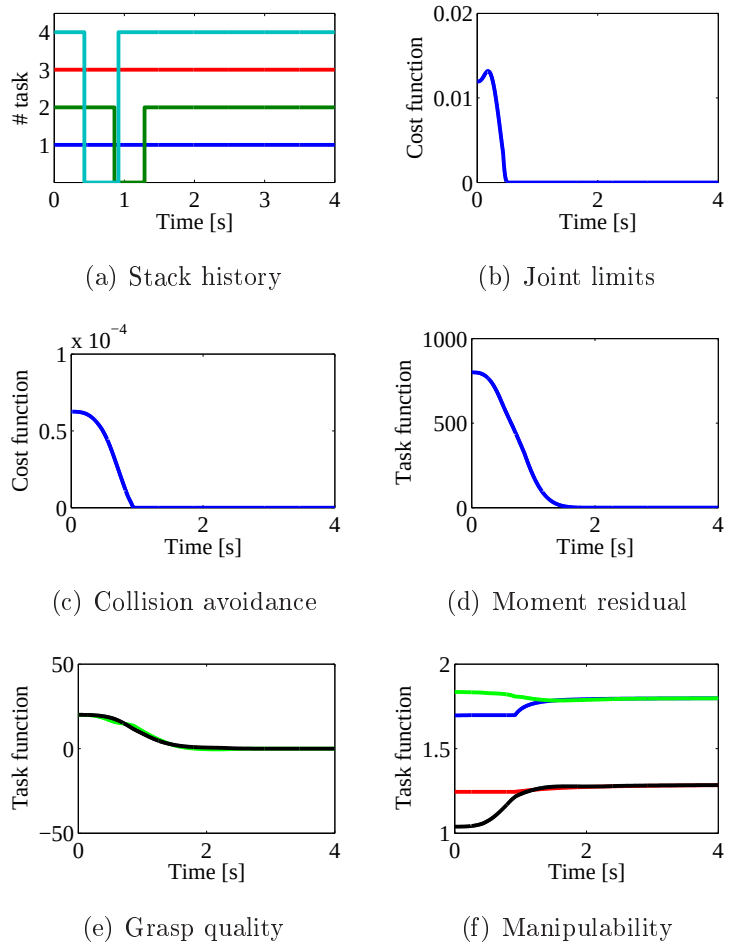

(a) Stack history (b) Joint limits

(c) Collision avoidance (d) Moment residual

(e) Grasp quality (f) Manipulability

Figure 3.4: Time histories of the constraints and secondary tasks. Subfigures (e) and (f) use the some color legend as Figure 3.3.

zero, the removed tasks are re-inserted into the stack.

Figure 3.4(d) shows the moment residual ϵ_m. This asymptotically converges to zero, i.e., fingers 3 and 4 reach a force closure condition. Figure 3.4(e) reports the time histories of the grasp quality indexes σ_{s_3} and σ_{s_4}. Such values converge to zero, since both fingers 3 and 4 reach a symmetric position with respect to the object's center from fingers 1 and 2, respectively.

Finally, Figure 3.4(f) shows the time history of the manipulability measures w_i, with $i = 1, \ldots, 4$, for each finger. The depicted values are equal or above the desired ones w_{d_i}. *Controller.* The controller performance are summarized

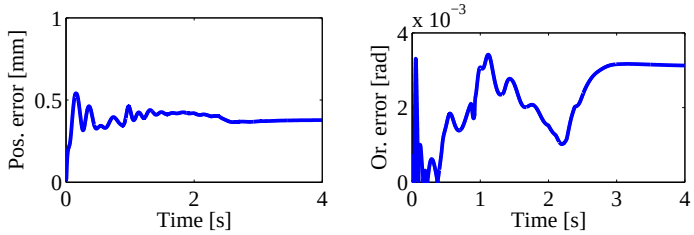

Figure 3.5: Object's pose error. Left, norm of the object's position error; right, object's orientation error.

in Figures 3.5-3.7. In detail, Figure 3.5 shows the time history of the norm of the object's pose error. It can be noticed that the errors do not converge

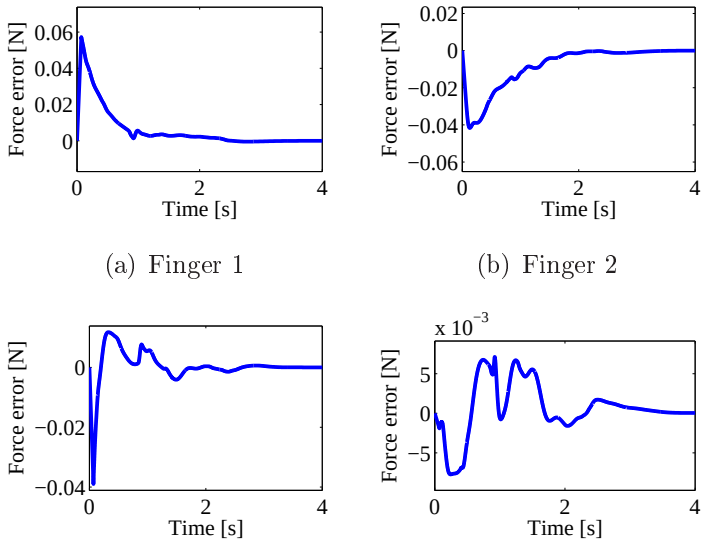

(a) Finger 1 (b) Finger 2

(c) Finger 3 (d) Finger 4

Figure 3.6: Time histories of the contact normal forces errors.

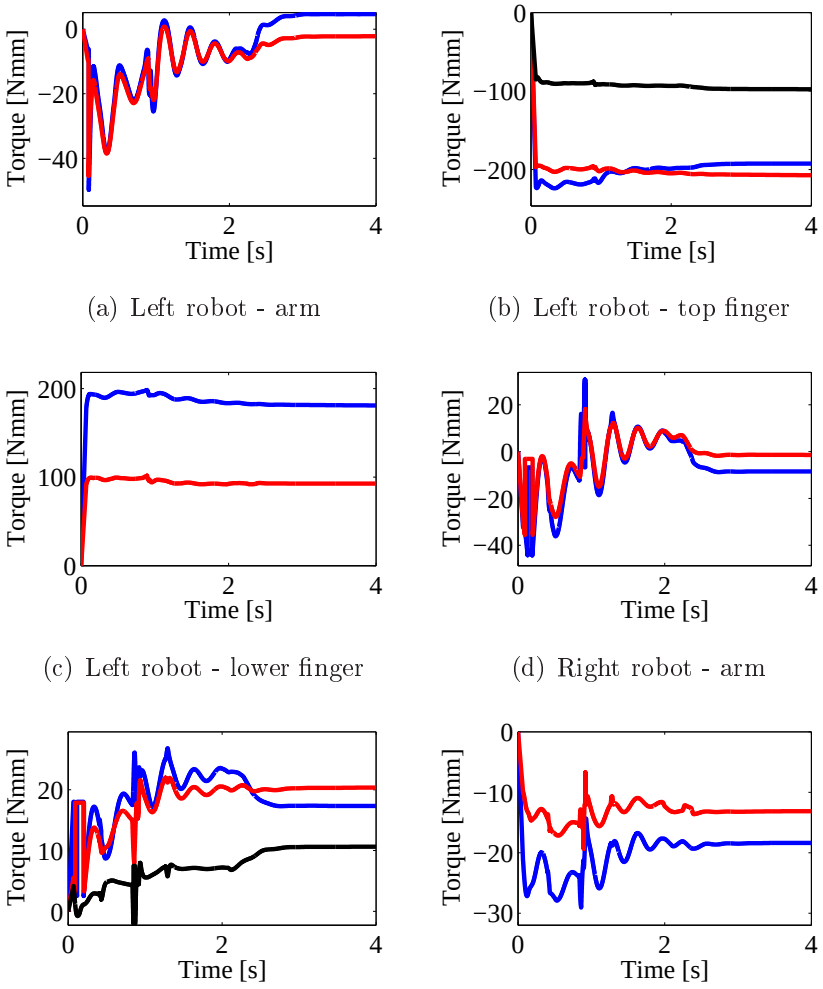

(a) Left robot - arm

(b) Left robot - top finger

(c) Left robot - lower finger

(d) Right robot - arm

(e) Right robot - top finger

(f) Right robot - lower finger

Figure 3.7: Time histories of the joint torques. Color legend for subfigures (a) and (d): blue are the joint torques 1 and 8, red 2 and 9. Color legend for subfigures (b) and (e): blue are the joint torques 3 and 10, red 4 and 11, black 5 and 12. Color legend for subfigures (c) and (f): blue are the joint torques 6 and 13, red 7 and 14.

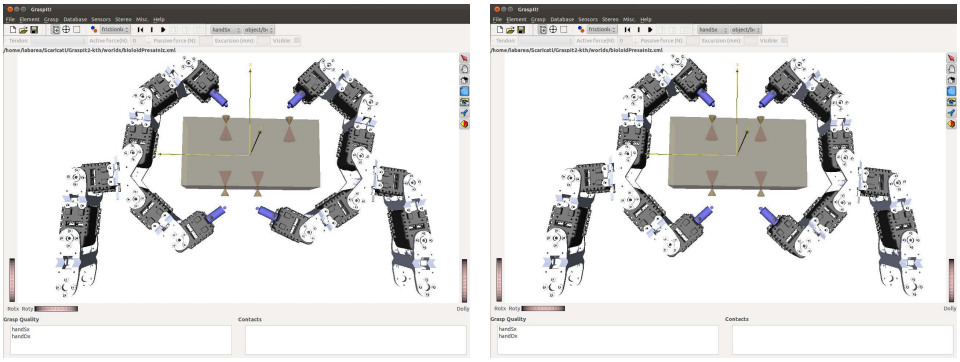

(a) Initial configuration (b) Final configuration

Figure 3.8: GRASPIT! screenshots depicting the system in its initial and final configuration. Prismatic joints, that model the fingers elastic pads, have not been drawn.

to zero, but they present a constant offset. This is due to the absence, in the control scheme, of the feedback of the object pose. In fact, sliding of fingers 3 and 4 affects the object's motion, while the planner cannot take into account these disturbances.

Figure 3.6 depicts the time histories of the errors of the normal contact forces with respect to the desired ones. It could be noticed that all the errors converge asymptotically to zero. Some peaks occur in correspondence of task removal/insertion from/in the stack.

Figure 3.7 shows the time histories of the joint actuation torques. Their values are smooth and compatible with state-of-the-art joint actuators.

Finally, Figure 3.8 shows the initial and final configurations of the system. It can be noticed that fingers 3 and 4 move along the object surface until their tips are on the same straight line on the opposite sides of the object, in such a way to ensure both force closure and a symmetric position with respect to the object's center.

Chapter 4

Control scheme with force control and object impedance

The control scheme described in previous chapter does not guarantee that environmental interaction forces remain bounded, by being based on parallel force/position control; thus, a different control strategy is also proposed with the purpose of controlling normal contact forces and making the overall system compliant in the case of an environmental interaction. In detail, external forces which ensure tracking of the planned trajectory for the grasped object, and internal forces, which prevent contact breaks and/or excessive stresses on the object, are regulated. An impedance behavior, enforced at object level, ensures that interaction forces, between the object itself and the environment, are kept bounded.

4.1 Control architecture

The considered control scheme is aimed at exploiting direct force control to regulate normal internal forces, in order to stabilize the grasp, and external

forces, so as to achieve the desired impedance at object level, as well as improve grasp quality via suitably defined virtual tangential forces.

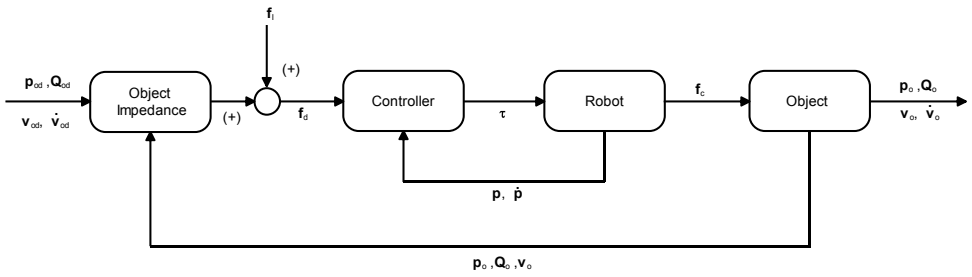

Figure 4.1: Block scheme of the overall control system

4.1.1 Object impedance

When the grasped object comes in contact with the external environment, interaction forces may arise, leading to excessive mechanical stresses. Hence, a compliant behavior of the object is wished so as to keep contact forces bounded. On the other hand, during free-space motion, tracking of the desired trajectory of the object is required, specified in terms of desired position, $\boldsymbol{p}_{od}(t)$, and orientation, $\boldsymbol{R}_{od}(t)$, as well as in terms of the desired generalized velocity, $\boldsymbol{v}_{od}(t)$, and acceleration, $\dot{\boldsymbol{v}}_{od}(t)$. To this aim, normal contact forces can be planned in such a way to impose an impedance behavior to the manipulated object. Namely, the desired external contact forces are computed via the equation

$$\begin{aligned} \boldsymbol{f}_{c_E d} &= \boldsymbol{G}^{\dagger}(\boldsymbol{r})\left(\boldsymbol{C}(\boldsymbol{v}_o)\boldsymbol{v}_o + \boldsymbol{g}_o + \boldsymbol{B}_o\dot{\boldsymbol{v}}_{od} + \right. \\ &\quad \left. \boldsymbol{K}_v\Delta\boldsymbol{v}_o + \boldsymbol{h}_{\Delta}(\Delta\boldsymbol{p}_o, \Delta\mathcal{Q}_o)\right), \end{aligned} \tag{4.1}$$

where $\boldsymbol{f}_{c_E d} = [\boldsymbol{f}^{\mathrm{T}}_{c_E d_1}, \boldsymbol{f}^{\mathrm{T}}_{c_E d_2}, \ldots, \boldsymbol{f}^{\mathrm{T}}_{c_E d_N}]^{\mathrm{T}}$ is the vector stacking the desired external contact forces for each finger, $\boldsymbol{G}^{\dagger}(\boldsymbol{r})$ is a consistent right pseudo-inverse of $\boldsymbol{G}(\boldsymbol{r})$ [4], $\Delta\boldsymbol{v}_o = \boldsymbol{v}_{od} - \boldsymbol{v}_o \in \Re^6$ is the velocity error, $\boldsymbol{K}_v$ is a

positive definite gain matrix, $\Delta \boldsymbol{p}_o = \boldsymbol{p}_{od} - \boldsymbol{p}_o \in \Re^3$ is the object position error, $\Delta \mathcal{Q}_o = \{\Delta\eta_o, \Delta\boldsymbol{\varepsilon}_o\}$ is the unit quaternion representing the orientation error [8], i.e., extracted form the mutual orientation matrix $\boldsymbol{R}_o^{\mathrm{T}}\boldsymbol{R}_{od}$, $\Delta\eta_o \in \Re$ is the scalar part of $\Delta\mathcal{Q}_o$ and $\Delta\boldsymbol{\varepsilon}_o \in \Re^3$ is its vector part. The term $\boldsymbol{h}_\Delta(\Delta\boldsymbol{p}_o, \Delta\mathcal{Q}_o)$ represents an elastic force, defined as in [11]

$$\begin{aligned}
\boldsymbol{h}_\Delta &= \begin{bmatrix} \boldsymbol{K}_p' & \boldsymbol{O}_3 \\ \boldsymbol{K}_{po}' & \boldsymbol{K}_o' \end{bmatrix} \begin{bmatrix} \Delta\boldsymbol{p}_o \\ \Delta\boldsymbol{\varepsilon}_o \end{bmatrix}, \\
\boldsymbol{K}_p' &= \frac{1}{2}\boldsymbol{R}_{od}\boldsymbol{K}_p\boldsymbol{R}_{od}^{\mathrm{T}} + \frac{1}{2}\boldsymbol{R}_o\boldsymbol{K}_p\boldsymbol{R}_o^{\mathrm{T}}, \\
\boldsymbol{K}_{po}' &= \frac{1}{2}\boldsymbol{S}(\Delta\boldsymbol{p}_o)\boldsymbol{R}_{od}\boldsymbol{K}_p\boldsymbol{R}_{od}^{\mathrm{T}}, \\
\boldsymbol{K}_o' &= 2(\Delta\eta_o\boldsymbol{I}_3 - \boldsymbol{S}(\Delta\boldsymbol{\varepsilon}_o))\boldsymbol{R}_o\boldsymbol{K}_o\boldsymbol{R}_o^{\mathrm{T}},
\end{aligned}$$

where $\boldsymbol{K}_p$ and $\boldsymbol{K}_o$ are positive definite matrices.

From (4.1) and (2.65), the following closed-loop dynamics is obtained

$$\boldsymbol{B}_o\Delta\dot{\boldsymbol{v}}_o + \boldsymbol{K}_v\Delta\boldsymbol{v}_o + \boldsymbol{h}_\Delta = \boldsymbol{h}_e + \boldsymbol{G}\Delta\boldsymbol{f}_{c_E}, \tag{4.2}$$

where $\Delta\boldsymbol{f}_{c_E} = [\Delta\boldsymbol{f}_{c_{E_1}}^{\mathrm{T}}, \Delta\boldsymbol{f}_{c_{E_2}}^{\mathrm{T}}, \ldots, \Delta\boldsymbol{f}_{c_{E_N}}^{\mathrm{T}}]^{\mathrm{T}}$ and $\Delta\boldsymbol{f}_{c_{E_j}} = \boldsymbol{f}_{c_E d_j} - \boldsymbol{f}_{c_{E_j}}$ is the force error for the jth finger. Equation (4.2) clearly shows that a six-degree-of-freedom mechanical impedance behavior is enforced. Assuming null force tracking errors ($\Delta\boldsymbol{f}_{c_E} = \boldsymbol{0}_{3N}$), equation (4.2) guarantees asymptotic trajectory tracking in the absence of object/environment interaction forces ($\boldsymbol{h}_e = \boldsymbol{0}_6$), while a suitable compliant behavior is obtained when $\boldsymbol{h}_e \neq \boldsymbol{0}_6$.

4.1.2 Grasp quality

A major issue in multi-fingered robotic manipulation is that of positioning the contacts on the object surface to obtain an optimal (or near optimal) grasp quality and robustness. In the absence of any off-line accurate planning, initial contact locations are, in general, non-optimal and thus fingers

should slide on the object surface to improve grasp quality as well as grasp robustness. A conventional way to measure grasp quality is the use of suitably defined indexes. A quality index, ε, is a function of the contact configuration, i.e., $\varepsilon(\boldsymbol{r}) \in \mathcal{R}$, which defines the quality of the current grasp, on the basis of the chosen measurable parameters. In [18, 50] the so-called *unit frictionless equilibrium residuals* are introduced: these indexes relate normal unit forces to the grasp quality, such that the optimal location is achieved when the static equilibrium is reached. However, other indexes related to contact points location can be found in the literature [38] and new ones could be defined as well. On the basis these indexes, it is possible to find a set of optimal contact configurations $\mathcal{S} = \{\boldsymbol{r}_k^* : \varepsilon(\boldsymbol{r}_k^*) = \varepsilon^*, k = 1, 2, ..., m_{\mathcal{S}}\}$, where $\boldsymbol{r}_k^*$ is an optimal configuration, ε^* is the optimal value of the quality index and $m_{\mathcal{S}}$ is the cardinality of $\mathcal{S}$, The optimal configurations can be characterized by defining a convex non-negative scalar function $U(\boldsymbol{r})$, whose minimum is attained at the optimal contact configurations $\boldsymbol{r}_k^* \in \mathcal{S}$. In other words, $U(\boldsymbol{r})$ takes into account the distance of the actual contact configuration from the optimal one. The objective is that of minimizing the cost function $U(\boldsymbol{r})$, by considering a virtual force defined as

$$\boldsymbol{f}_{\nabla} = -\nabla_{\boldsymbol{r}} U(\boldsymbol{r}), \tag{4.3}$$

where $\nabla_{\boldsymbol{r}}$ is the gradient operator with respect to the variables $\boldsymbol{r}_j$, $j = 1, \ldots, N$. It can be easily shown that the virtual forces always lie in the plane tangent at each contact point. To this aim, consider a parametrization of the object surface (as in Section 2.2) given by two independent parameters u_j and v_j; the position of each contact point can be expressed as $\boldsymbol{r}_j = \boldsymbol{r}_j(u_j, v_j)$; therefore, $U = U(\boldsymbol{r}_1(u_1, v_1), \ldots, \boldsymbol{r}_N(u_N, v_N))$. Assuming that $\boldsymbol{r}_j(u_j, v_j)$ is at

least of class $\mathcal{C}^1$, its gradient, expressed in the local reference frame, is

$$\nabla_{\boldsymbol{r}} U(\boldsymbol{r}) = \begin{bmatrix} \frac{1}{h_{u_1}} \frac{\partial U}{\partial u_1} \hat{\boldsymbol{u}}_1 + \frac{1}{h_{v_1}} \frac{\partial U}{\partial v_1} \hat{\boldsymbol{v}}_1 \\ \vdots \\ \frac{1}{h_{u_N}} \frac{\partial U}{\partial u_N} \hat{\boldsymbol{u}}_N + \frac{1}{h_{v_N}} \frac{\partial U}{\partial v_N} \hat{\boldsymbol{v}}_N \end{bmatrix}, \tag{4.4}$$

where $\hat{\boldsymbol{u}}_j = (\partial \boldsymbol{r}_j / \partial u_j)/h_{u_j}$, $\hat{\boldsymbol{v}}_j = (\partial \boldsymbol{r}_j / \partial v_j)/h_{v_j}$ are the unit vectors spanning the tangent plane at the jth contact point and $h_{u_j} = \|\partial \boldsymbol{r}_j / \partial u_j\|$, $h_{v_j} = \|\partial \boldsymbol{r}_j / \partial v_j\|$. Derivation of (4.4) is detailed in Appendix B.1. Since the virtual forces act in the direction opposite to the gradient of the cost function, they bring the fingertips to the nearest optimal contact location, i.e., the minimum of $U(\boldsymbol{r})$ (as shown by Theorem 1 in Section 4.1.3).

4.1.3 Controller

In order to achieve tracking of both the planned normal contact forces and the virtual forces, a direct force control law with dynamic compensation of all non-linear terms [63] is adopted

$$\boldsymbol{\tau} = \boldsymbol{B}(\boldsymbol{q})\boldsymbol{y} + \boldsymbol{C}(\boldsymbol{q}, \dot{\boldsymbol{q}})\dot{\boldsymbol{q}} + \boldsymbol{g}(\boldsymbol{q}) + \boldsymbol{J}^{\mathrm{T}} \boldsymbol{h}_c, \tag{4.5}$$

where $\boldsymbol{y}$ is computed as follows

$$\begin{aligned} \boldsymbol{y} &= \boldsymbol{J}_p^{-1} \boldsymbol{M}_d^{-1} \Big(\boldsymbol{K}_{p_f} (\boldsymbol{p}_{fc} + \boldsymbol{p}_{f\nabla}) - \boldsymbol{K}_d \dot{\boldsymbol{p}} - \boldsymbol{M}_d \dot{\boldsymbol{J}}_p \dot{\boldsymbol{q}} \Big), \\ \boldsymbol{p}_{fc} &= k_{fc} \boldsymbol{P}_n \left(\boldsymbol{f}_{cd} - \boldsymbol{f}_c \right), \\ \boldsymbol{p}_{f\nabla} &= -k_{f\nabla} \boldsymbol{f}_{\nabla}, \end{aligned} \tag{4.6}$$

where $\boldsymbol{M}_d$, $\boldsymbol{K}_d$, $\boldsymbol{K}_{p_f}$ are positive definite diagonal matrices, $\boldsymbol{p} = [\boldsymbol{p}_1^{\mathrm{T}}, \boldsymbol{p}_2^{\mathrm{T}}, \ldots, \boldsymbol{p}_N^{\mathrm{T}}]^{\mathrm{T}}$, $\boldsymbol{p}_i \in \Re^3$ is the position of the jth fingertip, k_{fc}, $k_{f\nabla}$, are scalar gains, the desired value of the virtual force is set to zero,

$$\boldsymbol{P}_n = \mathrm{diag} \left(\boldsymbol{n}_1 \boldsymbol{n}_1^{\mathrm{T}}, \boldsymbol{n}_2 \boldsymbol{n}_2^{\mathrm{T}}, \ldots, \boldsymbol{n}_N \boldsymbol{n}_N^{\mathrm{T}} \right),$$

and $\boldsymbol{n}_i$ is the unit vector normal to object surface at the ith contact point.

Remark 1. *If the manipulation system is functionally redundant, i.e.,* $\boldsymbol{J}_p$ *has more columns than rows, control input* (4.6) *should be suitably modified as*

$$\begin{aligned}\boldsymbol{y} &= \boldsymbol{J}_p^{\dagger}\boldsymbol{M}_d^{-1}\Big(\boldsymbol{K}_{pf}(\boldsymbol{p}_{fc}+\boldsymbol{p}_{f\nabla}) - \\ &\quad - \boldsymbol{K}_d\dot{\boldsymbol{p}} - \boldsymbol{M}_d\dot{\boldsymbol{J}}_p\dot{\boldsymbol{q}}\Big) - \boldsymbol{N}(\boldsymbol{J}_p)\boldsymbol{K}_{q0}\dot{\boldsymbol{q}},\end{aligned} \tag{4.7}$$

where $\boldsymbol{J}_p^{\dagger}$ *represents a right pseudo-inverse of* $\boldsymbol{J}_p$*,* $\boldsymbol{N}(\boldsymbol{J}_p)$ *represents a projector onto the null space of* $\boldsymbol{J}_p$*, while* $\boldsymbol{K}_{q0}\dot{\boldsymbol{q}}_0$ *is a damping term added to stabilize the internal motions.*

Theorem 2. *Under the assumption of quasi-static manipulation (i.e.,* $\boldsymbol{v}_o = \dot{\boldsymbol{v}}_o = \boldsymbol{0}_6$*, where* $\boldsymbol{v}_o$ *is the object generalized velocity), control law* (4.5) *ensures the convergence of contact point positions to an optimal configuration.*

The proof of Theorem 2 is given in Appendix B.

4.2 Case study

The effectiveness of the proposed control scheme has been proven in a number of simulation case studies developed in the Matlab/Simulink© environment. The fingers should slide on the object surface in order to minimize a cost function defined on the basis of unit frictionless force and moment residuals, described in Section 3.2, and, simultaneously, to apply the correct normal contact forces in such a way to drive the object along the planned trajectory. Contact forces are modeled by means of software springs connecting each finger to the object's boundary and friction has been modeled by considering a constant static and a viscous term, both acting against the fingers'sliding motion. Hence, tangential contact forces are present and act like uncertainties, since the object impedance design does not take them into account. Two cases have been considered: in the first one environmental interaction forces are not present, while in the second case an elastic force acts on the

object CoG (i.e., contact with a purely elastic environment is considered). The bimanual planar 14 DOFs arm/hand manipulation system, described in Section 3.2.1, has been considered.

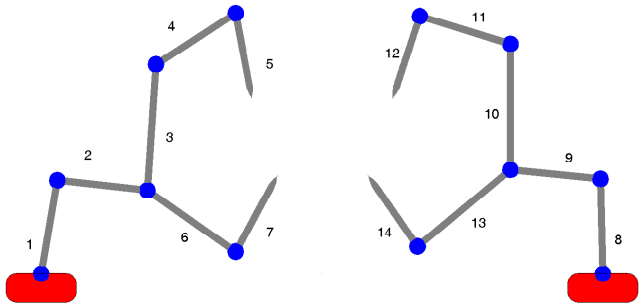

Figure 4.2: Bimanual arm/hand system.

Geometrical and inertial effective parameters of the manipulation system are reported in Table 4.1. The the elliptic shaped object has mass $m_o = 1$ kg , inertia moment $M_o = 10$ kgm^2, semi-major axis $70 \cdot 10^{-3}$ m, semi-minor axis $28 \cdot 10^{-3}$ m. The controller has been designed by using a nominal model in which the nominal link masses are equal to the 90% of the real masses, while the nominal object's mass and inertia moment have been considered to be the 95 % of the real ones. The third and seventh link lengths of each manipulator have been considered to be the 95% and 105% of the nominal ones. Sensor noise has been simulated by superimposing a normal distributed noise with zero mean and standard deviation equal to $5 \cdot 10^{-4}$ rad to joint positions, while, for contact forces a normal distributed noise with zero mean and standard deviation equal to $5 \cdot 10^{-3}$ N has been considered. As concerns object position (orientation), a normal distributed measurement error with zero mean and standard deviation equal to 0.01 mm (rad) has been added to the simulator output.

The control gains are chosen as $\boldsymbol{M}_d = \boldsymbol{I}_4$, $\boldsymbol{K}_d = 900\boldsymbol{I}_4$, $\boldsymbol{K}_{pf} = 800\boldsymbol{I}_4$,

Table 4.1: Parameters of the manipulation system

Link	$m_i \cdot 10^3$ [kg]	$M_i \cdot 10^6$[kgm^2]	$a_i \cdot 10^3[m]$
1,3,4,6,8,10,11,13	72	445	67.50
2,9	56	245	64.50
5,7,12,14	75	595	62

$k_{fc} = k_{f\nabla} = 30$. The object impedance gains are $\boldsymbol{K}_v = \text{diag}\{120\ 120\ 4\}$, $\boldsymbol{K}_p = 3 \cdot 10^3 \boldsymbol{I}_2$, $k_o = 12$ (scalar, since the orientation is represented by the angle around the axis normal to the plane of the manipulation system).

The cost function U is chosen as

$$U(\boldsymbol{r}) = \exp\left(\frac{1}{2}\rho_f(\boldsymbol{r}) + \frac{1}{2}\frac{\rho_m(\boldsymbol{r})}{\|\boldsymbol{r}\|^2}\right) - 1, \tag{4.8}$$

where $\rho_f(\boldsymbol{r})$ and $\rho_m(\boldsymbol{r})$ are the so-called unit frictionless force and moment residuals, respectively, defined as follows

$$\begin{aligned} \rho_f(\boldsymbol{r}) &= \sum_{i=1}^{N} \boldsymbol{n}_i(\boldsymbol{r}_i)^{\mathrm{T}} \boldsymbol{n}_i(\boldsymbol{r}_i) \\ \rho_m(\boldsymbol{r}) &= \sum_{i=1}^{N} \left(\boldsymbol{r}_i \times \boldsymbol{n}_i(\boldsymbol{r}_i)\right)^{\mathrm{T}} \left(\boldsymbol{r}_i \times \boldsymbol{n}_i(\boldsymbol{r}_i)\right). \end{aligned} \tag{4.9}$$

In (4.8) $\rho_m(\boldsymbol{r})$ has been normalized to obtain a dimensionless quantity homogeneous to $\rho_f(\boldsymbol{r})$. It is worth noticing that both the residuals are non-negative and thus the cost function reaches its minimum when both are zero.

In order to test the controller performance, three different simulations have been carried out. In the first one, initial contact locations on the object surface are arbitrary and non-optimal (non-null unit force and moment residuals), and thus fingers slide on the object surface in order to minimize U. In the second case, starting from the optimal contact configuration previously obtained, the object is moved along a smooth trajectory in the absence

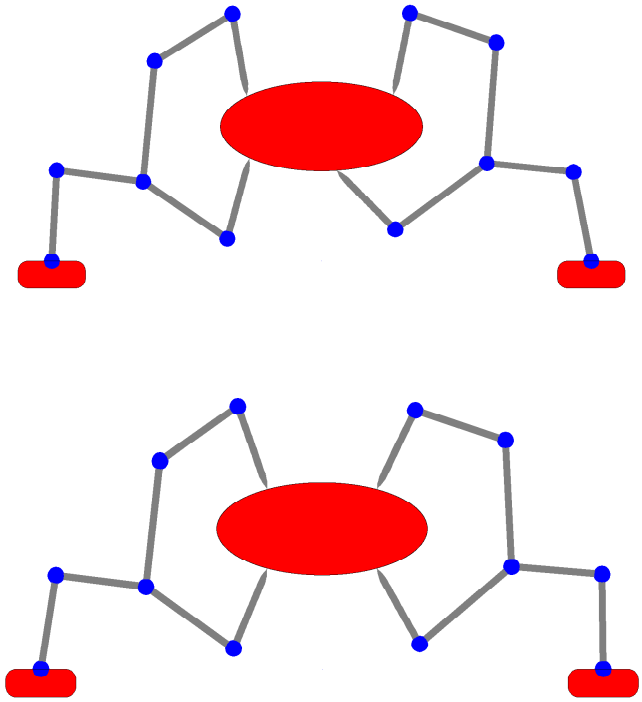

Figure 4.3: Bimanual arm/hand system in initial condition (top) and final condition (bottom).

of interaction with the external environment. Finally, the same trajectory planned for the second case is executed in the presence of environmental forces acting on the object.

4.2.1 Regrasping

The objective is that of keeping the object still, while fingers are sliding from their initial configuration, shown in Figure 4.3 (top), to reach the optimal one depicted in Figure 4.3 (bottom). Moreover, the controller is re-

quired to ensure a certain amount of internal normal contact forces set as $\boldsymbol{f}_{c_I d} = f_o \boldsymbol{N}(\boldsymbol{G})\boldsymbol{n}$, where $\boldsymbol{N}(\boldsymbol{G})$ is the projector onto the null space of $\boldsymbol{G}$ [4, 11], i.e., $\boldsymbol{N}(\boldsymbol{G}) = \boldsymbol{I}_{3N} - \boldsymbol{G}^{\dagger}\boldsymbol{G}$, $f_o = 10$ N and $\boldsymbol{n} = [\boldsymbol{n}_1^{\mathrm{T}}, \boldsymbol{n}_2^{\mathrm{T}}, \boldsymbol{n}_3^{\mathrm{T}}, \boldsymbol{n}_4^{\mathrm{T}}]^{\mathrm{T}}$. Figure 4.4 reports the time history of the norm of the normal force errors, which converge to zero at steady state. Fingers motion on the object sur-

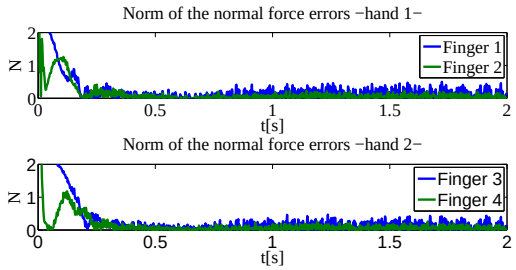

Figure 4.4: Norm of the normal force error for fingers 1,2 (top) and 3,4 (bottom).

face induces force disturbances causing object position errors, depicted in Figure 4.5; however, these errors are effectively counteracted by the object impedance controller.
Figure 4.6 reports the time history of the virtual forces and the cost function

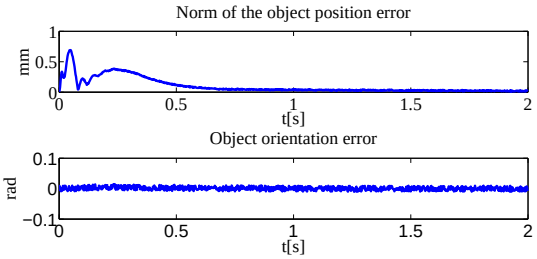

Figure 4.5: Norm of the object position error (top) and of the object orientation error (bottom).

U: it can be easily recognized that an optimal configuration is reached at steady state.

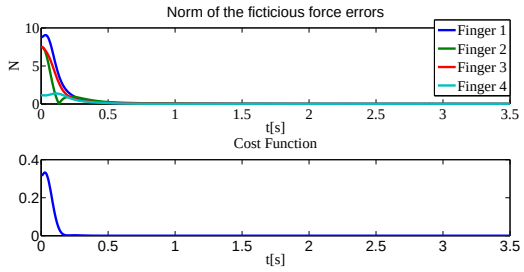

Figure 4.6: Norm of the virtual force errors (top) and cost function (bottom).

4.2.2 Object Motion

A smooth trajectory is planned for the object, consisting in a 50 mm displacement along the horizontal direction and a 100 mm displacement along the vertical one; the initial position is $\boldsymbol{p}_o = [0\ 150]^{\mathrm{T}}$ mm.
The controller ensures accurate tracking of the object planned trajectory in the absence of interaction forces, as shown in Figure 4.7. Figure 4.8 depicts

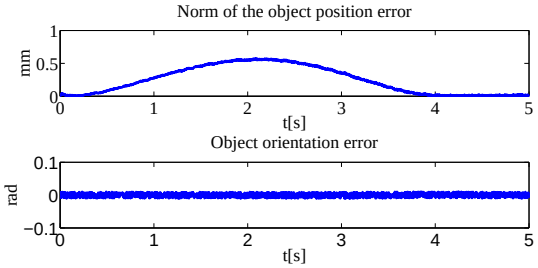

Figure 4.7: Norm of the object position errors (top) and of the object orientation error (bottom).

the norm of the normal force errors: it can be recognized that the desired force are tracked with small errors, which become null at steady state. By considering the total forces acting on each fingertip (of the order of 10 N), the presence of model uncertainties, and tacking into account the maximum length when the system is fully extended (of the order of 30 cm), the maximum force and pose errors can be considered fully acceptable.

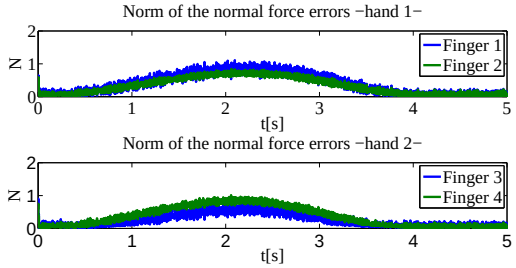

Figure 4.8: Norm of the normal force errors for fingers 1,2 (top) and 3,4 (bottom).

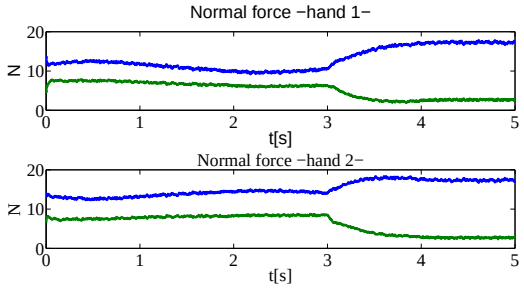

Figure 4.9: Norm of the normal forces for fingers 1,2 (top) and 3,4 (bottom).

Then, an elastic force acting at the object CoG is introduced

$$\boldsymbol{h}_e = -\boldsymbol{K}_e(\boldsymbol{x}_o - \boldsymbol{x}_r), \tag{4.10}$$

where $\boldsymbol{K}_e = \text{diag}\{5\,\text{N/mm}, 5\,\text{N/mm}, 0\,\text{Nmm/rad}\}$ models the environment

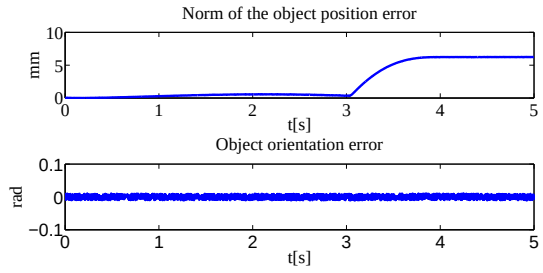

Figure 4.10: Norm of the object position error (top) and of the object orientation error (bottom).

stiffness, $\boldsymbol{x}_o$ is the pose of the object CoG and $\boldsymbol{x}_r = [0, 60, 0]$ (positions are measured in mm while orientation in rad) is the spring rest pose. In the presence of interaction, Figure 4.9 shows that the controller ensures limited interaction forces at the expense of a position error, as shown in Figure 4.10.

Chapter 5

Control scheme with internal force and wrist impedance control

Both the previous controllers, described in Chapters 3 and 4, consider each arm-hand system as a unique mechanical system, while the third control law described in this chapter deals with the two subsystems (the arm and the hand) separately. The proposed control strategy enforces an impedance behavior at the arm wrist to make the system compliant in the case of an interaction between the object and the external environment. At the same time, internal contact forces are regulated at a desired value in order to firmly hold the object.

5.1 Control architecture

Grasping and manipulation of an object require fine control of internal contact forces, in order to stabilize the grasp when the object is moved along a planned trajectory. Internal force control should prevent contact breaks and/or excessive stresses on the object.

The control system should be able to safely handle environmental or hu-

man interaction. A way to guarantee a safe behavior of the manipulation system is that of considering the arm and the hand as different subsystems: an impedance control scheme for the arm, ensures good tracking of the reference trajectory in absence of interaction, while enforcing a compliant behavior when an unexpected interaction happens; as concerns the hand, internal force control guarantees a firm grasp.

5.1.1 Hand control

Robotic hands are complex systems whose dynamics may be not known with the accuracy needed in order to design a model-based controller: due to space limitation, actuation systems results to be very complex and, thus, source of uncertainties (they can present mechanical coupling between DOFS through springs, clutches or tendons). To this aim, it would be useful to compute motion references of the fingers through a dynamic planner. Then, a low level controller will be in charge of tracking joint references. By assuming that only fingertips are involved in grasping (fine manipulation), i.e. the number of contact points and of fingers is the same, the dynamic planner for finger j, designed to control internal forces, is given by

$$\begin{aligned} &\boldsymbol{M}_{d_f}\dot{\boldsymbol{\nu}}_{d_j}^{c_j} + \boldsymbol{K}_{d_f}\boldsymbol{\nu}_{d_j}^{c_j} + \boldsymbol{K}_{p_f}\Delta\boldsymbol{x}_{d_j}^{c_j} = \boldsymbol{K}_p\boldsymbol{x}_{f_j}^{c_j} \\ &\boldsymbol{x}_{f_j}^{c_j} = \boldsymbol{C}_f(\boldsymbol{h}_{I_{d_j}}^{c_j} - \boldsymbol{h}_{I_j}^{c_j}) + \boldsymbol{C}_I\int_0^t(\boldsymbol{h}_{I_{d_j}}^{c_j} - \boldsymbol{h}_{I_j}^{c_j})\mathrm{d}\sigma, \end{aligned} \tag{5.1}$$

where the superscript c_j means that vectors are expressed with respect to Σ_{c_j}, $\dot{\boldsymbol{\nu}}_{d_j}^{c_j} \in \Re^{6\times1}$ ($\boldsymbol{\nu}_{d_j}^{c_j} \in \Re^{6\times1}$) is the relative reference accelerations (velocities) of contact points with respect to arm wrist, $\Delta\boldsymbol{x}_{d_j} = \left[\Delta\boldsymbol{r}_{d_j}^{\mathrm{T}}\ \Delta\boldsymbol{\epsilon}_{d_j}^{\mathrm{T}}\right]^{\mathrm{T}}$, $\Delta\boldsymbol{r}_{d_j} = \boldsymbol{r}_{d_j} - \boldsymbol{r}_{s_j}$, where $\boldsymbol{r}_{s_j}$, $\boldsymbol{r}_{d_j}$ have the meaning of rest and reference positions relative to Σ_a, $\Delta\boldsymbol{\epsilon}_{re} = \left[\Delta\boldsymbol{\epsilon}_{r_1}^{\mathrm{T}}\ \Delta\boldsymbol{\epsilon}_{r_2}^{\mathrm{T}}\ \ldots\ \Delta\boldsymbol{\epsilon}_{r_{n_c}}^{\mathrm{T}}\right]^{\mathrm{T}}$, $\Delta\boldsymbol{\epsilon}_{r_j}$ is the vector part of the quaternion $\Delta\mathcal{Q}_j = \mathcal{Q}_{a,s_j} * \mathcal{Q}_{a,d_j}^{-1}$ (i.e. the orientation error of finger j), where $\mathcal{Q}_{a,s_j}$, $\mathcal{Q}_{a,d_j}$ represent the rest and the reference orientation, of the contact

frame with respect to Σ_a. The other terms in (5.1) $\boldsymbol{M}_{d_f}$, $\boldsymbol{K}_{d_f}$, $\boldsymbol{K}_{p_f}$, $\boldsymbol{C}_f$, $\boldsymbol{C}_I$ are positive definite matrices of gains, $\boldsymbol{h}_{I_{d_j}} = [\boldsymbol{f}_{c_I d_j}^{\mathrm{T}} \ \boldsymbol{0}_3^{\mathrm{T}}]^{\mathrm{T}}$ is vector of desired internal generalized forces, $\boldsymbol{h}_{I_j} = [\boldsymbol{f}_{c_I j}^{\mathrm{T}} \ \boldsymbol{0}_3^{\mathrm{T}}]^{\mathrm{T}}$ is the vector of measured internal generalized forces. Desired internal forces can be achieved via standard grasp force optimization techniques [45], to avoid slippage and excessive mechanical stresses on the object.

By integrating equation (5.1) motion references (i.e. $\mathcal{Q}_{a,d_j}$, $\boldsymbol{r}_{d_j}$, $\boldsymbol{\nu}_{d_j}$, $\dot{\boldsymbol{\nu}}_{d_j}$) in cartesian space, which ensure internal force regulation, are available to feed an Inverse Kinematics, hereafter IK, algorithm.

5.1.2 Arm control

The aim is that of making the wrist able to track the desired trajectory with good accuracy in the absence of interaction, while a compliant behavior must be if interactions occur. This objective could be achieved via an impedance control law. More in detail, an impedance filter is adopted in order to make the controller performance independent from the knowledge of the dynamic model, while a pure motion controller is in charge of tracking the motion references. The impedance has the following dynamics

$$\boldsymbol{M}_d \Delta\dot{\boldsymbol{v}}_a + \boldsymbol{K}_d \Delta\boldsymbol{v}_a + \boldsymbol{h}_{\Delta p} = \boldsymbol{h}_a - \boldsymbol{h}_{comp}, \tag{5.2}$$

where $\Delta\dot{\boldsymbol{v}}_a$ ($\Delta\boldsymbol{v}_a$) is the acceleration (velocity) error, computed as the difference between the desired acceleration (velocity) $\dot{\boldsymbol{v}}_{a_d}$ ($\boldsymbol{v}_{a_d}$) planned off-line and the reference one $\dot{\boldsymbol{v}}_{a_r}$ ($\boldsymbol{v}_{a_r}$),

$$\begin{aligned}
\boldsymbol{h}_{\Delta p} &= \begin{bmatrix} \boldsymbol{K}_p^{'} & \boldsymbol{O}_3 \\ \boldsymbol{K}_{po}^{'} & \boldsymbol{K}_o^{'} \end{bmatrix} \begin{bmatrix} \Delta\boldsymbol{p}_{dr} \\ \Delta\boldsymbol{\varepsilon}_{dr} \end{bmatrix}, \\
\boldsymbol{K}_p^{'} &= \frac{1}{2}\boldsymbol{R}_{a_d}\boldsymbol{K}_p\boldsymbol{R}_{a_d}^T + \frac{1}{2}\boldsymbol{R}_{a_r}\boldsymbol{K}_p\boldsymbol{R}_{a_r}^T, \\
\boldsymbol{K}_{po}^{'} &= \frac{1}{2}\boldsymbol{S}(\Delta\boldsymbol{p}_{dr})\boldsymbol{R}_{a_d}\boldsymbol{K}_p\boldsymbol{R}_{a_d}^T, \\
\boldsymbol{K}_o^{'} &= 2(\widetilde{\eta}_{dr}\boldsymbol{I}_3 - \boldsymbol{S}(\Delta\boldsymbol{\varepsilon}_{dr}))\boldsymbol{R}_{a_r}\boldsymbol{K}_o\boldsymbol{R}_{a_r}^T,
\end{aligned}$$

where $\boldsymbol{K}_p$, $\boldsymbol{K}_o$, are positive definite matrices of gains, $\Delta\boldsymbol{p}_{dr}$ is the error between the desired wrist position (depending on the planned position for the grasped object) and the reference one, $\Delta\mathcal{Q}_{dr} = \begin{bmatrix}\Delta\eta_{dr} & \Delta\boldsymbol{\epsilon}_{dr}^{\mathrm{T}}\end{bmatrix}^{\mathrm{T}}$ is the quaternion extracted from the rotation matrix $\boldsymbol{R}_{dr} = \boldsymbol{R}_{a_d}\boldsymbol{R}_{a_r}^{\mathrm{T}}$, which represents the orientation error being $\boldsymbol{R}_{a_d}$ and $\boldsymbol{R}_{a_r}$ the desired and reference orientation of the frame Σ_a, respectively. The other terms in (5.3) are $\boldsymbol{h}_a$, which is the wrench measured by the sensor and $\boldsymbol{h}_{comp}$=$-\left(\boldsymbol{G}_a(\boldsymbol{r}_a)\boldsymbol{h}_c + (\boldsymbol{L}_a\boldsymbol{L}_a^{\mathrm{T}})^{-1}\boldsymbol{L}_a\boldsymbol{H}_7\boldsymbol{\xi}_x\right)$ computed through (2.52), being $\boldsymbol{H}_\alpha$ the already introduced (in Section 2.6) selector operator. $\boldsymbol{h}_{comp}$ compensates the effects on the wrist due to hand dynamics and contact forces. Once the motion references are known, they could be passed to a motion controller directly designed in the operational space. An alternative is that of adopting an IK algorithm to compute the joint reference trajectories for a joint space controller.

Remark 2. *If the dynamic parameters of the hand are not available, it could be enough to compensate the static effects of the hand and the contact forces,*

$$\boldsymbol{h}_{comp} = -\left(\boldsymbol{G}_a(\boldsymbol{r}_a)\boldsymbol{h}_c + (\boldsymbol{L}_a\boldsymbol{L}_a^{\mathrm{T}})^{-1}\boldsymbol{L}_a\boldsymbol{H}_7\boldsymbol{g}(\boldsymbol{x})\right). \tag{5.3}$$

Remark 3. *If a measure of the contact forces is not available, by considering that internal forces do not act on the wrist, under the hypothesis that* $\mathrm{rank}(\boldsymbol{G}(\boldsymbol{r})) = 6$*, the external contact forces can be estimated via*

$$\boldsymbol{f}_{c_E} = \boldsymbol{G}^{\dagger}(\boldsymbol{r})\left(\boldsymbol{B}_o\dot{\boldsymbol{v}}_o + \boldsymbol{C}(\boldsymbol{v}_o)\boldsymbol{v}_o + \boldsymbol{g}_o\right), \tag{5.4}$$

or, in the case of non perfect knowledge of the object dynamics, as

$$\boldsymbol{f}_{c_E} = \boldsymbol{G}(\boldsymbol{r})^{\dagger}\boldsymbol{g}_o, \tag{5.5}$$

and substituted in (2.52) *or, alternatively, in* (5.3)*. It is worth noting that* $\boldsymbol{G}(\boldsymbol{r})^{\dagger}$ *in* (5.4) *and* (5.5) *represents a right pseudo-inverse of* $\boldsymbol{G}(\boldsymbol{r})$ *while* $\boldsymbol{G}_a\boldsymbol{h}_c = \boldsymbol{G}_a\boldsymbol{h}_{c_E} = \boldsymbol{G}_a\begin{bmatrix}\boldsymbol{f}_{c_E}^{\mathrm{T}} & \boldsymbol{0}_3^{\mathrm{T}}\end{bmatrix}^{\mathrm{T}}$.

5.1.3 Joint references

Since (5.1) and (5.2) provide motion cartesian references, an IK algorithm is needed to compute suitable joint references in order to feed a low level controller, as shown in Figure 5.1. A possible choice is given by the a law similar to that in (3.3)

$$\begin{aligned} \ddot{\boldsymbol{q}}_r &= \bar{\boldsymbol{J}}^{-1}\boldsymbol{x}_c, \\ \boldsymbol{x}_c &= \dot{\boldsymbol{v}}_r + \boldsymbol{K}_v\boldsymbol{e}_v + \boldsymbol{K}\boldsymbol{e}_p - \dot{\bar{\boldsymbol{J}}}\dot{\boldsymbol{q}}_r, \end{aligned} \tag{5.6}$$

where $\boldsymbol{q}_r = [\boldsymbol{q}_{a_r}^{\mathrm{T}}\ \boldsymbol{q}_{f_r}^{\mathrm{T}}]^{\mathrm{T}}$ is the vector stacking joint positions of the arm ($\boldsymbol{q}_{a_r}$

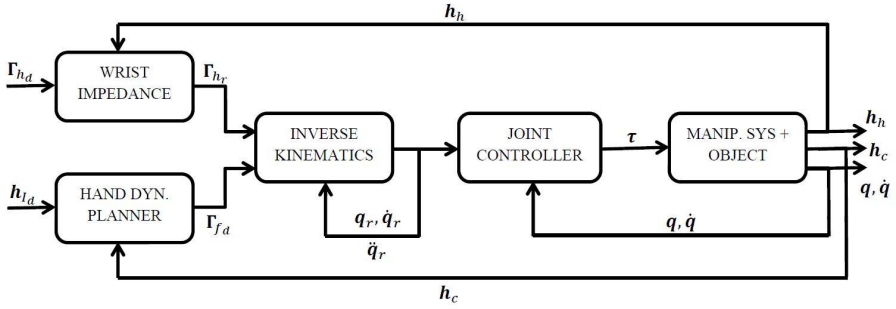

Figure 5.1: Block scheme of the control architecture. Γ_{a_d} represents the desired trajectory, in terms of pose, velocities and accelerations, for the wrist, while Γ_{a_r} (Γ_{f_d}) represent the reference trajectory for the wrist (contact points)

and hand $\boldsymbol{q}_{f_a}$), $\bar{\boldsymbol{J}}$ is the following Jacobian

$$\bar{\boldsymbol{J}} = \begin{bmatrix} \boldsymbol{J}_a & \boldsymbol{O}_{6n\times l} \\ \boldsymbol{O}_{6n_c\times n_a} & \boldsymbol{J}_f \end{bmatrix},$$

n_a is the number of arm DOFs, $l = \sum_{j=1}^{N} f_j$ is the number of hand DOFs, $\boldsymbol{v}_r = \left[\boldsymbol{v}_{a_r}^{\mathrm{T}}\ \boldsymbol{\nu}_d^{\mathrm{T}}\right]^{\mathrm{T}}$, $\boldsymbol{\nu}_d \in \Re^{6n_c}$ is the vector stacking all relative reference finger twists, $\boldsymbol{e}_v$ is the velocity error i.e. $\boldsymbol{e}_v = \boldsymbol{v}_r - \bar{\boldsymbol{J}}\dot{\boldsymbol{q}}_r$, $\boldsymbol{e}_p = \left[\Delta\boldsymbol{p}_a^{\mathrm{T}}\ \Delta\boldsymbol{\epsilon}_a^{\mathrm{T}}\ \Delta\boldsymbol{r}_{re}^{\mathrm{T}}\ \Delta\boldsymbol{\epsilon}_{re}^{\mathrm{T}}\right]^{\mathrm{T}}$,

$\Delta \boldsymbol{p}_a$ ($\Delta \boldsymbol{r}_{re}$) is the position error of the wrist (finger) (i.e. the difference between the reference value and that computed via the forward kinematics on the basis of $\boldsymbol{q}_{a_r}$ ($\boldsymbol{q}_{f_r}$)), $\Delta \boldsymbol{\epsilon}_a$ is the vector part of the unit quaternion $\Delta \mathcal{Q}_a = \mathcal{Q}_{r_a} * \mathcal{Q}_{e_a}^{-1}$, where $\mathcal{Q}_{r_a}$ and $\mathcal{Q}_{e_a}$ represent, respectively, the reference orientation and that computed via the forward kinematics on the basis of $\boldsymbol{q}_{a_r}$, $\Delta \boldsymbol{\epsilon}_{re} = \left[\Delta \boldsymbol{\epsilon}_{r_1}^{\mathrm{T}} \, \Delta \boldsymbol{\epsilon}_{r_2}^{\mathrm{T}} \, \ldots \, \Delta \boldsymbol{\epsilon}_{r_{n_c}}^{\mathrm{T}}\right]^{\mathrm{T}}$ and $\Delta \boldsymbol{\epsilon}_{r_j}$ is the vector part of the quaternion $\Delta \mathcal{Q}_{rj} = \mathcal{Q}_{r_j} * \mathcal{Q}_{e_j}^{-1}$ representing the orientation error of finger j, where $\mathcal{Q}_{r_j}$ and $\mathcal{Q}_{e_j}$ the reference and that computed via the forward kinematics on the basis of $\boldsymbol{q}_{f_r}$.

Remark 4. *If the arm/hand system is redundant, i.e.* $\bar{\boldsymbol{J}}$ *has more columns than rows,* (5.6) *should be suitably modified*

$$\begin{aligned} \ddot{\boldsymbol{q}}_r &= \bar{\boldsymbol{J}}^{\dagger} \boldsymbol{a}_c + \boldsymbol{N}(\bar{\boldsymbol{J}})(\boldsymbol{\beta} - k_s \dot{\boldsymbol{q}}) \\ \boldsymbol{a}_c &= \dot{\boldsymbol{v}}_r + \boldsymbol{K}_v \boldsymbol{e}_v + \boldsymbol{K} \boldsymbol{e}_p - \dot{\bar{\boldsymbol{J}}} \dot{\boldsymbol{q}}_r \ , \\ \boldsymbol{\beta} &= -\dot{\boldsymbol{N}} \dot{\boldsymbol{q}} \end{aligned} \tag{5.7}$$

where $\bar{\boldsymbol{J}}^{\dagger}$ *is a right pseudo-inverse of* $\bar{\boldsymbol{J}}$, $\boldsymbol{N}(\bar{\boldsymbol{J}})$ *is a null space projector and* $\boldsymbol{\beta} - k_s \dot{\boldsymbol{q}}$ *is a term designed to stabilize internal motions..*

A theoretical proof of (5.6) is reported in Appendix C.

5.2 Experimental case study

A case study has been conducted in order to test the performance of the proposed scheme. The experimental setup, available at the Computer Science Robotics Laboratory of the Rensselaer Polytechnic Institute (RPI), Troy, New York, consists of a 7-DOFs Barret WAM and a Barrett Hand 280 attached to the arm wrist. The available feedback consists of joint positions, sampled at 500 Hz for the arm and 100 Hz for the hand, force/torque at the wrist, sampled at 500 Hz and tactile pressure on the fingertip and palm (4

matrices of 24 sensors each), sampled at 40 Hz. Robot Operating System (ROS) [53] is used as software platform.

Tactile pressures are integrated onto the fingertip surfaces, in order to estimate the normal contact forces. Since the hand is underactuated and only normal contact forces are available as feedback, the control law (5.1) has been projected along the unit vector normal to the object surface at each contact point, (hereafter called simply contact normal). It is worth noting that the hand has 4 motors, one for each finger and the forth for the spread, which is the motion of fingers 1 and 2 around the axis normal to the palm. The spread has been kept constant and set to zero. By neglecting the spread contribution, the positional part of the hand Jacobian, $\boldsymbol{J}_f^p \in \Re^{9\times 3}$, can be written as

$$\boldsymbol{J}_f^p = \begin{bmatrix} \boldsymbol{J}_{f_1}^p & \mathbf{0}_3 & \mathbf{0}_3 \\ \mathbf{0}_3 & \boldsymbol{J}_{f_2}^p & \mathbf{0}_3 \\ \mathbf{0}_3 & \mathbf{0}_3 & \boldsymbol{J}_{f_3}^p \end{bmatrix} \tag{5.8}$$

where $\boldsymbol{J}_{f_j}^p \in \Re^3$ the jth finger Jacobian. Because of the underactuation, each $\boldsymbol{J}_{f_j}^p$ has been projected along the contact normal, therefore the Jacobian to be considered in (5.6) is

$$\bar{\boldsymbol{J}} = \begin{bmatrix} \boldsymbol{J}_h & \boldsymbol{O}_{6\times 3} \\ \boldsymbol{O}_{3\times n_h} & \boldsymbol{J}_f^n \end{bmatrix},$$

where $\boldsymbol{J}_f^n = \mathrm{diag}\{J_{f_1}^n, J_{f_2}^n, J_{f_3}^n\}$, $J_{f_j}^n = \boldsymbol{n}_j^{\mathrm{T}} \boldsymbol{J}_{f_j}^p$ and $\boldsymbol{n}_j$ is the jth contact normal.

The performed case study consists of a first phase in which the object is grasped by the hand and the contact forces are regulated to suitable values; after the grasp is made, the object is moved along a planned trajectory while a human operator interacts with the object itself: the idea is that of ensuring a compliant behavior maintaining, at the same time, a firm grasp. At the end of the trajectory the object is pressed against a planar surface without neither sliding on it nor human operator interaction.

5.2.1 Experimental results

The hand grasps the object in such a configuration that the fingertips are symmetric with respect to the object CoG, as depicted in Figure 5.2; contact normal forces are regulated to 5 N for finger 1 and 2 and 10 N for the thumb. It can be recognized that the desired normal forces are a set of internal

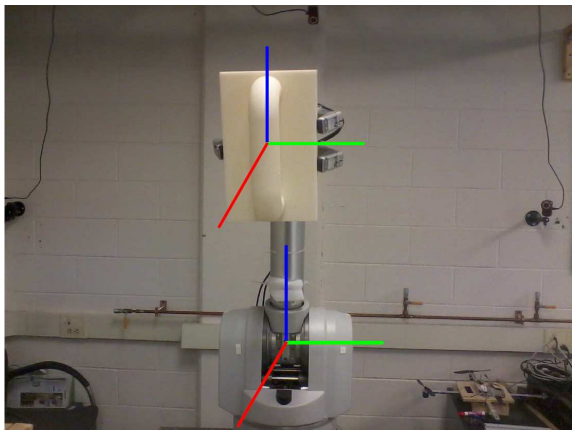

Figure 5.2: Experimental setup in the initial configuration. The reference frames are visible: base frame on the bottom and object frame on the top. The axes are ordered as follows: x red, y green, z blue

forces since they constitute a self-balancing system (i.e. the total force and momentum are zero). Despite the low rate at which the tactile pressures data are sampled, 40 Hz, the controller, which runs at 100 Hz, is able to drive the contact forces to the desired values, within an acceptable error, as shown in Figure 5.3. For the first 24 s the object is grabbed and the normal contact forces are regulated, in the last 16 s the trajectory is executed. After the object has been grasped, starting from the initial configuration, depicted in Figure 5.4(a), the object should be moved of -0.5 m along the z axis and 0.3 m along the x axis of the base frame (Figure 5.2) while maintaining the position along the y axis.

The final orientation should be such that the x axis of the object frame is

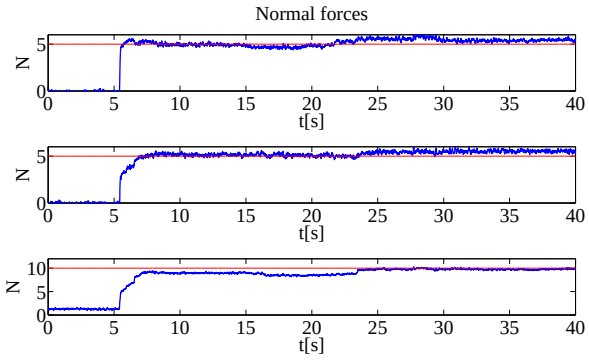

Figure 5.3: Time history of the normal contact forces: finger 1 on the top, finger 2 on the middle and thumb on the bottom

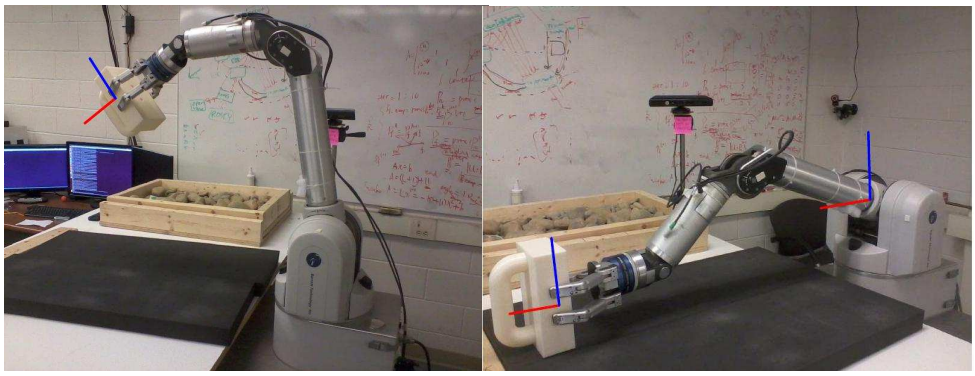

(a) Initial configuration (b) Final configuration

Figure 5.4: Initial configuration (a) and final configuration (b) of the system

parallel to the x axis of the world frame. The trajectory has been generated using fifth order polynomial time profile. During the motion, a human operator interacts with the object, by pushing or pulling the handle attached on it, as it could be recognized in Figure 5.5. It is worth noting that only static compensation has been performed according to (5.3). The manipulation system should not be compliant along and around the y axis of the base frame, thus the measured component of wrist forces and moment are not fed to the impedance filter. Figure 5.6 reports the IK errors of the object, defined as

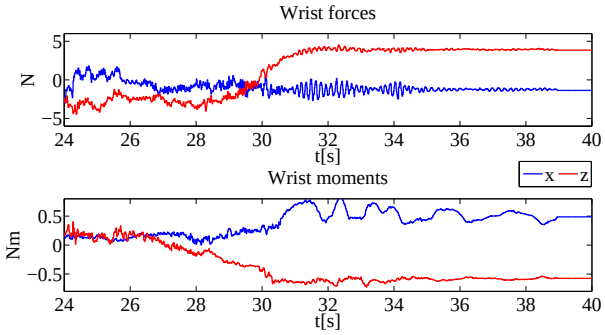

Figure 5.5: Time history of the interaction wrist forces and torques

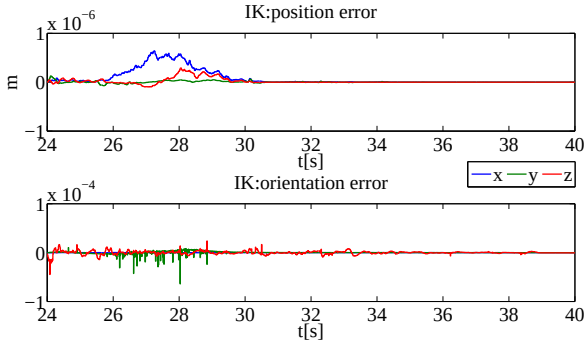

Figure 5.6: Time history of closed loop inverse kinematics error

$$\begin{aligned} \Delta \boldsymbol{p}_o &= \boldsymbol{p}_{o_d} - \boldsymbol{p}_{o_r}, \\ \Delta \mathcal{Q}_o &= \mathcal{Q}_{o_d} * \mathcal{Q}_{o_r}^{-1}, \end{aligned} \tag{5.9}$$

where $\boldsymbol{p}_{o_d}$ ($\mathcal{Q}_{o_d}$) are the desired position (quaternion representing the orientation) of the object, while $\boldsymbol{p}_{o_r}$ ($\mathcal{Q}_{o_r}$) is the object position (quaternion) computed on the basis of direct kinematics of the arm/hand system, through the planned joint positions obtained by solving the differential equation (5.6). Figure 5.7 shows the pose error of the object, which can be computed exploiting (5.9) by substituting $\boldsymbol{p}_{o_r}$ ($\mathcal{Q}_{o_r}$) with measured ones $\boldsymbol{p}_o$ ($\mathcal{Q}_o$); it could be recognized that along the y direction there is a good tracking of the planned

position, while an error is observed along the compliant directions. Around $32s$ the object interacts with a planar horizontal surface: this explains the large error at steady state. The same consideration can be done for the orientation error: the presence of the steady state error can be justified considering that the surface is not either perfectly horizontal or planar.

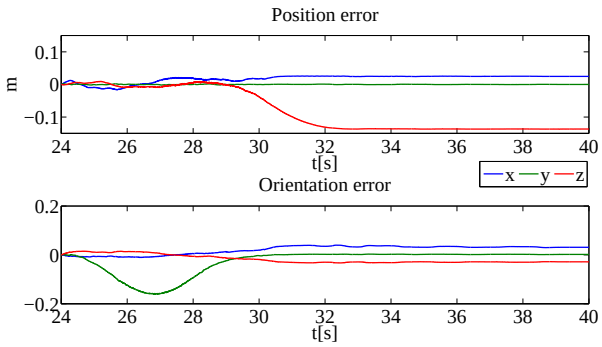

Figure 5.7: Time history of the object pose error

In summary, the experimental case study shows that exploiting the impedance paradigm together with internal force control allows to achieve a compliant behavior and, at the same time, a firm grasp of the grabbed object. It is worth noting that the interaction has been done by a human operator pushing/pulling the object and by hitting a planar surface at the end of the trajectory: experimental results clearly demonstrate that the object is held in any case.

Conclusions and future work

In this thesis, modeling and control of multi-arm systems equipped with robotic hands have been tackled. Kinematic and dynamics model of such complex systems are not trivial matters, since each arm equipped with a robotic hand is composed of multiple interconnected kinematic chains.

Cooperative arm/hand systems are often kinematically redundant: in this thesis a planner has been proposed to properly handle the redundancy in such a way to safely fulfill multiple tasks. By exploiting null space projection techniques, several tasks, even conflicting, can be simultaneously accomplished with a certain priority order. Mechanical and environmental constraints have been taken into account via mathematical cost functions: when one or more task would bring the system close to violate the constraints, those tasks must be disengaged and engaged again, if possible, when the system configuration is far enough from the critical ones. Suitable metrics have been defined in order to quantify the degree of interaction between tasks and constraints. Smooth transition of the control variables has been guaranteed by using time varying gains.

The approach discussed above, even if capable to avoid constraints violation, still needs the a priori knowledge of the whole environmental scenario; this means that the control architecture will not guarantee a safe behavior in the case of unexpected collision or interaction. To this aim, the impedance paradigm has been exploited to safely handle interaction and collisions. If

the compliance involves the whole arm/hand system, a good regulation of internal forces (i.e., those which do not contribute to the object motion) is required, in order to keep the object still while the interaction takes place. A control law has been proposed with the aim of regulating the internal forces to a desired constant value, while the external one are controlled so as to make the object behave like a mechanical impedance.

A different approach is that of separating the control of the hand from that of the arm: the strategy is that of regulating internal forces only by using the fingers actuators, while full compliance is imposed to the arm.

In summary, redundancy has been exploited only to fulfill multiple tasks by fulfilling environmental and mechanical constraints. A further improvement could be that of achieving a certain degree of fault tolerance if some actuator functionality is lost.

Another important improvement would be that of merging the concepts of task sequencing and object impedance: a planner, in charge of computing object pose references, can be designed at the highest hierarchical level with the aim of ensuring the desired behavior of the system.

In order to guarantee safe operation of the multi-arm system, in view of tight human-robot cooperation, it would be useful to ensure the compliance of the whole system, even in the absence of joint torque sensors.

Appendices

Appendix A

A.1 Time derivative of $\boldsymbol{n}$

The linear velocity of the ith fingertip with respect to the palm frame can be expressed as follows (subscript i will be dropped for simplicity)

$$\dot{\boldsymbol{p}}_f = \boldsymbol{G}_l^{\mathrm{T}} \boldsymbol{v}_{o,p} + \boldsymbol{R}_o \frac{\partial \boldsymbol{c}^o}{\partial \boldsymbol{\xi}} \dot{\boldsymbol{\xi}} + (l - \Delta l) \boldsymbol{R}_o \dot{\hat{\boldsymbol{n}}}^o - \boldsymbol{R}_o \hat{\boldsymbol{n}}^o \Delta \dot{l}, \tag{A.1}$$

where $\boldsymbol{G}_l^{\mathrm{T}}$ is the matrix composed by the first three rows of $\boldsymbol{G}^{\mathrm{T}}$, $\boldsymbol{v}_{o,p}$ is the object relative velocity with respect to the palm and $\dot{\hat{\boldsymbol{n}}}^o(\boldsymbol{c}^o(\boldsymbol{\xi}))$ is given by

$$\dot{\hat{\boldsymbol{n}}}^o = \frac{\partial \hat{\boldsymbol{n}}^o}{\partial \boldsymbol{c}^o} \frac{\partial \boldsymbol{c}^o}{\partial \boldsymbol{\xi}} \dot{\boldsymbol{\xi}}. \tag{A.2}$$

Since the time derivative of the unit normal vector belongs to the tangent plane of the object at contact point, by projecting Equation (A.2) in such a plane, a suitable expression for $\dot{\hat{\boldsymbol{n}}}$ can be derived

$$\dot{\hat{\boldsymbol{n}}} = \boldsymbol{L}_o \boldsymbol{v}_o + \boldsymbol{L}_f \dot{\boldsymbol{p}}_f, \tag{A.3}$$

with

$$\boldsymbol{A}_n = \boldsymbol{I} + (l - \Delta l)\frac{\partial \hat{\boldsymbol{n}}}{\partial \boldsymbol{c}}, \tag{A.4}$$

$$\boldsymbol{P}_t = \boldsymbol{I} - \hat{\boldsymbol{n}}\hat{\boldsymbol{n}}^T,$$

$$\boldsymbol{L}_f = \frac{\partial \hat{\boldsymbol{n}}}{\partial \boldsymbol{c}}\boldsymbol{A}_n^{-1}\boldsymbol{P}_t, \tag{A.5}$$

$$\boldsymbol{L}_o = \left[\boldsymbol{L}_f \ , \quad \boldsymbol{S}(\hat{\boldsymbol{n}}) + \boldsymbol{L}_f\left((l - \Delta l)\boldsymbol{S}(\hat{\boldsymbol{n}}) - \boldsymbol{S}(\boldsymbol{c})\right)\right]. \tag{A.6}$$

It can be noticed that matrix $\boldsymbol{A}_n$ is always full rank for convex objects bounded by a smooth surface. Let $f(\boldsymbol{c})$ be the function describing the surface of the object, the normal at each point of the frontier, can be written as $\hat{\boldsymbol{n}} = \frac{\partial f}{\partial \boldsymbol{c}}$, and thus the gradient in (A.4) can be rewritten as

$$\frac{\partial \hat{\boldsymbol{n}}}{\partial \boldsymbol{c}} = \boldsymbol{H}_f(\boldsymbol{c}),$$

with $\boldsymbol{H}_f(\boldsymbol{c})$ the hessian matrix of $f(\boldsymbol{c})$. It is well known that for convex function, the hessian matrix is positive semi-definite which, in turn, allows us to state that $\boldsymbol{A}_n$ is always invertible for regular convex surfaces, since it is positive definite. Moreover, it could be recognized that both $\boldsymbol{L}_o$ and $\boldsymbol{L}_f$ are norm bounded, i.e.

$$\|\boldsymbol{L}_o\| \leq k_o, \quad k_o > 0, \tag{A.7}$$

$$\|\boldsymbol{L}_f\| \leq k_n, \quad k_n > 0. \tag{A.8}$$

A.2 System Equilibrium

System (3.22) under the control law (3.21) can be described by the closed-loop dynamics

$$\boldsymbol{M}\ddot{\boldsymbol{x}} + \boldsymbol{C}\dot{\boldsymbol{x}} = \boldsymbol{K}_P\,\Delta\boldsymbol{x} - \boldsymbol{K}_D\,\dot{\boldsymbol{x}} + \Delta\boldsymbol{f}_n + k_F\,\Delta\boldsymbol{f}_n + k_I\int_0^t \Delta\boldsymbol{f}_n d\zeta. \tag{A.9}$$

At the equilibrium, i.e., $\ddot{\boldsymbol{x}} = \dot{\boldsymbol{x}} = \mathbf{0}$, $\boldsymbol{x} = \boldsymbol{x}_\infty$, the following equality holds

$$\boldsymbol{K}_P(\boldsymbol{x}_d - \boldsymbol{x}_\infty) + (1 + k_F)(\boldsymbol{f}_d - \boldsymbol{f}_{n_\infty}) + k_I \int_0^{+\infty} \Delta \boldsymbol{f}_n d\zeta = \mathbf{0}. \tag{A.10}$$

Projection of (A.10) onto the tangent plane and along the normal unit vector leads to

$$\left(\boldsymbol{I}_6 - \boldsymbol{n}\boldsymbol{n}^{\mathrm{T}}\right) \boldsymbol{K}_P \left(\boldsymbol{x}_d - \boldsymbol{x}_\infty\right) = \mathbf{0}, \tag{A.11}$$

$$\boldsymbol{n}\boldsymbol{n}^{\mathrm{T}} \left(\boldsymbol{K}_P \left(\boldsymbol{x}_d - \boldsymbol{x}_\infty\right) + (1 + k_F) \left(\boldsymbol{f}_d - \boldsymbol{f}_{n_\infty}\right) + k_I \int_0^{+\infty} \Delta \boldsymbol{f}_n d\zeta \right) = \mathbf{0}. \tag{A.12}$$

By virtue of the integral action, which gives $\Delta \boldsymbol{f}_n = \boldsymbol{f}_d - \boldsymbol{f}_{n_\infty} = 0$, and of (3.28), it can be seen that $\boldsymbol{n}^{\mathrm{T}} \left(\boldsymbol{x}_d - \boldsymbol{x}_\infty\right) = 0$; Equation (A.11) ensures that the tangential part of $\boldsymbol{x}_d - \boldsymbol{x}_\infty$ is null and thus $\boldsymbol{x}_\infty = \boldsymbol{x}_d$. Moreover, from (A.12) it can be noticed that $\int_0^{\infty} \Delta \boldsymbol{f}_n d\zeta = \mathbf{0}$ as well.

A.3 Proof of inequality (A.22)

By considering the expression of s in Equation (3.30), the term s_∞ is given by

$$s_\infty = \int_0^{+\infty} \left(\Delta f_n - \frac{k}{\rho} \dot{\boldsymbol{n}}^{\mathrm{T}} \Delta \boldsymbol{x} \right) d\zeta = - \int_0^{+\infty} \frac{k}{\rho} \dot{\boldsymbol{n}}^{\mathrm{T}} \Delta \boldsymbol{x} d\zeta. \tag{A.13}$$

Therefore, I_n becomes

$$I_n = \frac{k}{\rho} \int_t^{+\infty} \Delta \boldsymbol{x}^{\mathrm{T}} \dot{\boldsymbol{n}} d\zeta, \tag{A.14}$$

where $\dot{\boldsymbol{n}} = \begin{bmatrix} \dot{\hat{\boldsymbol{n}}}^{\mathrm{T}} & \mathbf{0}^{\mathrm{T}} \end{bmatrix}^{\mathrm{T}}$. From the assumption of quasi-static manipulation, i.e., $\boldsymbol{v}_o = \mathbf{0}$, the following equality follows

$$\dot{\boldsymbol{n}} = \begin{bmatrix} \boldsymbol{L}_f \dot{\boldsymbol{p}}_f \\ \mathbf{0} \end{bmatrix}, \tag{A.15}$$

through which it can be recognized that

$$\|\dot{\boldsymbol{n}}\| = \|\dot{\hat{\boldsymbol{n}}}\| \leq k_n \|\dot{\boldsymbol{p}}_f\|. \tag{A.16}$$

Equation (A.16) allows to upper-bound I_n in the domain $\mathcal{D}$ as follows

$$\begin{aligned} I_n &= \frac{k}{\rho}\int_t^{+\infty} \Delta\boldsymbol{x}^{\mathrm{T}}\dot{\boldsymbol{n}}d\zeta = \frac{k}{\rho}\int_t^{+\infty} \boldsymbol{z}_2^{\mathrm{T}}\dot{\boldsymbol{n}}d\zeta \leq \frac{k}{\rho}\int_t^{+\infty} \|\boldsymbol{z}_2\|\,\boldsymbol{h}_6^{\mathrm{T}}\dot{\boldsymbol{n}}d\zeta \\ &\leq \frac{k}{\rho}\Phi\int_t^{+\infty} \boldsymbol{h}_3^{\mathrm{T}}\boldsymbol{L}_f\dot{\boldsymbol{p}}_f d\zeta \leq \frac{k}{\rho}\Phi\,\|\boldsymbol{L}_f\|\int_t^{+\infty} \boldsymbol{h}_3^{\mathrm{T}}\dot{\boldsymbol{p}}_f d\zeta \leq \frac{k}{\rho}k_n\Phi\|\boldsymbol{z}_2\|. \end{aligned} \tag{A.17}$$

where $\boldsymbol{h}_\alpha$ is a $(\alpha \times 1)$ vector of ones.

A.4 Proof of Theorem 1

Consider the candidate Lyapunov function

$$V = \frac{1}{2}\boldsymbol{z}^{\mathrm{T}}\boldsymbol{P}\boldsymbol{z}, \tag{A.18}$$

where $\boldsymbol{P}$ is a symmetric matrix

$$\boldsymbol{P} = \begin{bmatrix} \boldsymbol{M} & \rho\boldsymbol{M} & \boldsymbol{0} \\ \rho\boldsymbol{M} & \rho\boldsymbol{K}_D + \boldsymbol{K}_P & -k_I\boldsymbol{n} \\ \boldsymbol{0} & -k_I\boldsymbol{n}^T & \rho\dfrac{k_I}{k} \end{bmatrix}, \tag{A.19}$$

positive definite under the following condition

$$\rho\lambda_m(\boldsymbol{K}_D) + \lambda_m(\boldsymbol{K}_P) > \max\left\{\frac{2\rho^2\lambda_M(\boldsymbol{M})^2}{\lambda_m(\boldsymbol{M})}, \frac{k_I k}{\rho}\right\}. \tag{A.20}$$

Under condition (A.20), the function V can be bounded as

$$\frac{1}{2}\overline{\lambda}_m(\boldsymbol{P})\|\boldsymbol{z}\|^2 \leq V \leq \frac{1}{2}\overline{\lambda}_M(\boldsymbol{P})\|\boldsymbol{z}\|^2, \tag{A.21}$$

where, since $\boldsymbol{P}$ is time varying, $\overline{\lambda}_m = \min\limits_{t\geq 0}\{\lambda_m(\boldsymbol{P}(t))\}$ and $\overline{\lambda}_M = \max\limits_{t\geq 0}\{\lambda_M(\boldsymbol{P}(t))\}$.

Consider the state-space domain defined as $\mathcal{D} = \{\boldsymbol{z} : \|\boldsymbol{z}\| < \Phi\}$. It can be recognized that the following inequality holds in the domain $\mathcal{D}$:

$$I_n \leq \frac{k}{\rho}\Phi k_n \|\boldsymbol{z}_2\|. \tag{A.22}$$

Some details about inequality (A.22) are given in Appendix A.3.

The time derivative $\dot{V}$ is given by

$$\dot{V} = \boldsymbol{z}^{\mathrm{T}}\left(\boldsymbol{P}\boldsymbol{A} + \frac{1}{2}\dot{\boldsymbol{P}}\right)\boldsymbol{z} + \boldsymbol{z}^{\mathrm{T}}\boldsymbol{P}\boldsymbol{b}, \tag{A.23}$$

where $\dot{\boldsymbol{P}}$ can be computed, by exploiting Property 2, as

$$\dot{\boldsymbol{P}} = \begin{bmatrix} \boldsymbol{C} + \boldsymbol{C}^{\mathrm{T}} & \rho\left(\boldsymbol{C} + \boldsymbol{C}^{\mathrm{T}}\right) & \boldsymbol{0} \\ \rho\left(\boldsymbol{C} + \boldsymbol{C}^{\mathrm{T}}\right) & \boldsymbol{O} & -k_I\dot{\boldsymbol{n}} \\ \boldsymbol{0} & -k_I\dot{\boldsymbol{n}}^{\mathrm{T}} & 0 \end{bmatrix}. \tag{A.24}$$

After some algebraic steps, Equation (A.23) becomes

$$\begin{aligned} \dot{V} \;&= -\boldsymbol{z}_1^{\mathrm{T}}\left(\boldsymbol{K}_D - \rho\boldsymbol{M}\right)\boldsymbol{z}_1 - \boldsymbol{z}_2^{\mathrm{T}}\left(\rho\left(\boldsymbol{K}_P + \boldsymbol{F}\right) - k_I k\boldsymbol{n}\boldsymbol{n}^{\mathrm{T}} + \frac{k_I k}{\rho}\boldsymbol{n}\dot{\boldsymbol{n}}^{\mathrm{T}}\right)\boldsymbol{z}_2 \\ &\quad -\boldsymbol{z}_1^{\mathrm{T}}\boldsymbol{F}\boldsymbol{z}_2 + \rho\boldsymbol{z}_2^{\mathrm{T}}\boldsymbol{C}^{\mathrm{T}}\boldsymbol{z}_1 + k_I I_n(\boldsymbol{z}_1 + \rho\boldsymbol{z}_2)^{\mathrm{T}}\boldsymbol{n}. \end{aligned} \tag{A.25}$$

By exploiting Assumption 4 and Property 2, the time derivative $\dot{V}$ can be upper bounded as follows

$$\begin{aligned} \dot{V} \leq &-\left(\lambda_m(\boldsymbol{K}_D) - \rho\lambda_M(\boldsymbol{M}) - \rho k_c\Phi\right)\|\boldsymbol{z}_1\|^2 + \\ &-\left(\rho\lambda_m(\boldsymbol{K}_P) - k_I k - k_I k\Phi k_n\right)\|\boldsymbol{z}_2\|^2 + \\ &+\left(k\left(1 + k_f\right) + 2\frac{k_I k}{\rho}k_n\Phi\right)\|\boldsymbol{z}_1\|\|\boldsymbol{z}_2\|, \end{aligned} \tag{A.26}$$

and rearranged in a suitable quadratic form

$$\dot{V} \leq -\begin{bmatrix} \|\boldsymbol{z}_1\| & \|\boldsymbol{z}_2\| \end{bmatrix}\boldsymbol{Q}\begin{bmatrix} \|\boldsymbol{z}_1\| \\ \|\boldsymbol{z}_2\| \end{bmatrix}, \tag{A.27}$$

where $\boldsymbol{Q}$ is the (2×2) matrix

$$\mathbf{Q} = \begin{bmatrix} \lambda_m(\boldsymbol{K}_d) - \rho\lambda_M(\boldsymbol{M}) - \rho k_c \Phi\,, & -\frac{1}{2}\left(k\,(1+k_f) + 2\frac{k_I k}{\rho} k_n \Phi\right) \\ -\frac{1}{2}\left(k\,(1+k_f) + 2\frac{k_I k}{\rho} k_n \Phi\right), & \rho\lambda_m(\boldsymbol{K}_p) - k_I k(1+\Phi k_n) \end{bmatrix}. \tag{A.28}$$

On the basis of (A.27) and (A.28), $\dot{V}$ is negative semi-definite in the domain $\mathcal{D}$ provided that $\boldsymbol{Q}$ is positive definite, i.e., if the following inequality holds

$$\lambda_m(\boldsymbol{K}_d) \geq \rho\lambda_M(\boldsymbol{M}) + \rho k_c \Phi + \max\left\{0, \frac{\varphi}{4}\right\}, \tag{A.29}$$

where

$$\varphi = \left(k\,(1+k_f) + 2\frac{k_I k}{\rho} k_n \Phi\right)^2 \left(\rho\lambda_m(\boldsymbol{K}_P) - k_I k\,(1+\Phi k_n)\right)^{-1}. \tag{A.30}$$

Moreover, since V is a non-increasing function along the system trajectories, the inequality (A.21) guarantees that all the trajectories $\boldsymbol{z}(t)$ starting in the domain

$$\mathcal{D}_0 = \left\{\boldsymbol{z} : \|\boldsymbol{z}(0)\| < \Phi\sqrt{\frac{\overline{\lambda}_m(\boldsymbol{P})}{\overline{\lambda}_m(\boldsymbol{P})}}\right\}, \tag{A.31}$$

remain in the domain $\mathcal{D}$, $\forall t > 0$.

Finally, since $\dot{V} = 0$ only if $\boldsymbol{z}_1 = \mathbf{0}$ and $\boldsymbol{z}_2 = \mathbf{0}$, by invoking the La Salle's theorem [29], it can be recognized that, if $\boldsymbol{z}(0) \in \mathcal{D}_0$, $\boldsymbol{z}_1$ and $\boldsymbol{z}_2$ asymptotically converge to $\mathbf{0}$ while z_3 is only bounded.

Appendix B

B.1 Expression of $\nabla_r U(\boldsymbol{r})$

Let $\boldsymbol{r}_i$ be at least of class $\mathcal{C}^1$, in view of the chosen surface parametrization $\boldsymbol{r}_i = \boldsymbol{r}_i(u_i, v_i)$, the gradient of the scalar function U can be expressed as

$$\nabla_r U(\boldsymbol{r}) = \begin{bmatrix} f_{u_1}\hat{\boldsymbol{u}}_1 + f_{v_1}\hat{\boldsymbol{v}}_1 \\ f_{u_1}\hat{\boldsymbol{u}}_2 + f_{v_1}\hat{\boldsymbol{v}}_2 \\ \cdots \\ f_{u_N}\hat{\boldsymbol{u}}_N + f_{v_N}\hat{\boldsymbol{v}}_N \end{bmatrix}, \tag{B.1}$$

where f_{u_i} and f_{v_i} are the so-called scale factors.
From the total differential theorem it could be recognized that

$$\mathrm{d}U = \nabla_r U(\boldsymbol{r})^{\mathrm{T}} \mathrm{d}\boldsymbol{r}, \tag{B.2}$$

where the expression of $\mathrm{d}\boldsymbol{r}$ can be computed according to the following equation

$$\begin{aligned} \mathrm{d}\boldsymbol{r} \;=\; & \frac{\partial \boldsymbol{r}}{\partial \boldsymbol{r}_1}\left(\frac{\partial \boldsymbol{r}_1}{\partial u_1}\mathrm{d}u_1 + \frac{\partial \boldsymbol{r}_1}{\partial v_1}\mathrm{d}v_1\right) + \frac{\partial \boldsymbol{r}}{\partial \boldsymbol{r}_2}\left(\frac{\partial \boldsymbol{r}_2}{\partial u_2}\mathrm{d}u_2 + \frac{\partial \boldsymbol{r}_2}{\partial v_2}\mathrm{d}v_2\right) + \ldots + \\ & + \frac{\partial \boldsymbol{r}}{\partial \boldsymbol{r}_N}\left(\frac{\partial \boldsymbol{r}_N}{\partial u_N}\mathrm{d}u_N + \frac{\partial \boldsymbol{r}_N}{\partial v_N}\mathrm{d}v_N\right). \end{aligned} \tag{B.3}$$

By noting that

$$\frac{\partial \boldsymbol{r}_h}{\partial \boldsymbol{r}_k} = \begin{cases} \boldsymbol{O}_3, \text{ if } h \neq k \\ \boldsymbol{I}_3, \text{ if } h = k \end{cases}.$$

(B.3) simplifies in

$$\mathrm{d}\boldsymbol{r} = \begin{bmatrix} \dfrac{\partial \boldsymbol{r}_1}{\partial u_1}\mathrm{d}u_1 + \dfrac{\partial \boldsymbol{r}_1}{\partial v_1}\mathrm{d}v_1 \\ \dfrac{\partial \boldsymbol{r}_2}{\partial u_2}\mathrm{d}u_2 + \dfrac{\partial \boldsymbol{r}_2}{\partial v_2}\mathrm{d}v_2 \\ \cdots \\ \dfrac{\partial \boldsymbol{r}_N}{\partial u_N}\mathrm{d}u_N + \dfrac{\partial \boldsymbol{r}_N}{\partial v_N}\mathrm{d}v_N \end{bmatrix}. \tag{B.4}$$

By defining $h_{u_i} = \left\| \dfrac{\partial \boldsymbol{r}_i}{\partial u_i} \right\|$, $h_{v_i} = \left\| \dfrac{\partial \boldsymbol{r}_i}{\partial v_i} \right\|$, $\hat{\boldsymbol{u}}_i = \dfrac{\partial \boldsymbol{r}_i / \partial u_i}{\|\partial \boldsymbol{r}_i / \partial u_i\|}$ and $\hat{\boldsymbol{v}}_i = \dfrac{\partial \boldsymbol{r}_i / \partial v_i}{\|\partial \boldsymbol{r}_i / \partial v_i\|}$ the differential $\mathrm{d}\boldsymbol{r}$ can be further rewritten

$$\mathrm{d}\boldsymbol{r} = \begin{bmatrix} h_{u_1}\hat{\boldsymbol{u}}_1 du_1 + h_{v_1}\hat{\boldsymbol{v}}_1 dv_1 \\ h_{u_2}\hat{\boldsymbol{u}}_2 du_2 + h_{v_2}\hat{\boldsymbol{v}}_2 dv_2 \\ \cdots \\ h_{u_N}\hat{\boldsymbol{u}}_N du_1 + h_{v_N}\hat{\boldsymbol{v}}_N dv_N \end{bmatrix}. \tag{B.5}$$

On the basis of equation (B.1), (B.2) and (B.5) the total differential of U becomes

$$\begin{aligned} \mathrm{d}U &= \sum_{i=1}^{N} \left(f_{u_i}\hat{\boldsymbol{u}}_i + f_{v_i}\hat{\boldsymbol{v}}_i\right)^{\mathrm{T}} \left(h_{u_i}\hat{\boldsymbol{u}}_i du_i + h_{v_i}\hat{\boldsymbol{v}}_i \mathrm{d}v_i\right) = \\ &= \sum_{i=1}^{N} \left(f_{u_i} h_{u_i} \mathrm{d}u_i + f_{v_i} h_{v_i} \mathrm{d}v_i\right), \end{aligned} \tag{B.6}$$

where the last equality comes from the following properties

$$\begin{aligned} \hat{\boldsymbol{u}}_i^{\mathrm{T}}\hat{\boldsymbol{u}}_i = \hat{\boldsymbol{v}}_i^{\mathrm{T}}\hat{\boldsymbol{v}}_i = 1 \\ \hat{\boldsymbol{u}}_i^{\mathrm{T}}\hat{\boldsymbol{v}}_i = 0 \end{aligned}.$$

The total differential of U can be alternatively computed as

$$\mathrm{d}U = \sum_{i=1}^{N} \left(\frac{\partial U}{\partial u_i}\mathrm{d}u_i + \frac{\partial U}{\partial v_i}\mathrm{d}v_i \right), \tag{B.7}$$

hence, by comparing equations (B.6) and (B.7) it is possible to write the scale factors as $f_{u_i} = \dfrac{1}{h_{u_i}}\dfrac{\partial U}{\partial u_i}$ and $f_{v_i} = \dfrac{1}{h_{v_i}}\dfrac{\partial U}{\partial v_i}$.

B.2 Proof of Theorem 2

Consider the manipulation system described by (2.39) under the control law (4.5), the closed loop system dynamics, obtained by folding (4.5) in (2.39), is given by

$$\boldsymbol{M}_d\ddot{\boldsymbol{p}} + \boldsymbol{K}_d\dot{\boldsymbol{p}} = \boldsymbol{K}_{p_f}(\boldsymbol{p}_{fc} + \boldsymbol{p}_{f\nabla}). \tag{B.8}$$

The position of the ith fingertip can be written as $\boldsymbol{p}_i = \boldsymbol{p}_o + \boldsymbol{r}_i$ and, by differentiation, the finger velocity can be expressed as $\dot{\boldsymbol{p}}_i = \dot{\boldsymbol{p}}_o + \dot{\boldsymbol{r}}_i$. Suppose quasi-static manipulation during fingers sliding, the vector stacking all finger velocities becomes $\dot{\boldsymbol{p}} = \dot{\boldsymbol{r}}$. By choosing the state $\boldsymbol{z}$ as

$$\boldsymbol{z} = \begin{bmatrix} \boldsymbol{z}_1 \\ \boldsymbol{z}_2 \end{bmatrix} = \begin{bmatrix} \boldsymbol{r} - \boldsymbol{r}_k^* \\ \dot{\boldsymbol{r}} \end{bmatrix},$$

the closed loop system dynamics in state space form can written as

$$\begin{aligned} \dot{\boldsymbol{z}}_1 &= \boldsymbol{z}_2 \\ \dot{\boldsymbol{z}}_2 &= \boldsymbol{M}_d^{-1}\left(-\boldsymbol{K}_d\boldsymbol{z}_2 + \boldsymbol{K}_{p_f}\boldsymbol{p}_{fc} - \right. \\ &\qquad \left. -\boldsymbol{K}_{p_f}k_{f\nabla}\nabla U(\boldsymbol{z}_1 + \boldsymbol{r}_k^*)\right). \end{aligned} \tag{B.9}$$

Consider the following Lyapunov function

$$V = \frac{1}{2}\boldsymbol{z}_2^{\mathrm{T}}\boldsymbol{K}_{p_f}^{-1}\boldsymbol{M}_d\boldsymbol{z}_2 + k_{f\nabla}U(\boldsymbol{z}_1 + \boldsymbol{r}_k^*), \tag{B.10}$$

the time derivative is given by

$$\begin{aligned} \dot{V} = &-\boldsymbol{z}_2^{\mathrm{T}}\boldsymbol{K}_{p_f}^{-1}\boldsymbol{K}_d\boldsymbol{z}_2 + \boldsymbol{z}_2^{\mathrm{T}}\boldsymbol{p}_{fc} - k_{f\nabla}\boldsymbol{z}_2^{\mathrm{T}}\nabla U(\boldsymbol{z}_1 + \boldsymbol{r}_k^*) + \\ &+k_{f\nabla}\boldsymbol{z}_2^{\mathrm{T}}\nabla U(\boldsymbol{z}_1 + \boldsymbol{r}_k^*) = -\boldsymbol{z}_2^{\mathrm{T}}\boldsymbol{K}_d\boldsymbol{z}_2, \end{aligned} \tag{B.11}$$

in which $\boldsymbol{z}_2^{\mathrm{T}}\boldsymbol{p}_{fc} = 0$, since the finger sliding velocities, $\boldsymbol{z}_2$, are orthogonal to the vector of normal force errors, $\boldsymbol{p}_{fc}$. From (B.11) it can be seen that $\dot{V}$ is negative semi-definite and $\dot{V} = 0$ for $\boldsymbol{z}_2 = \boldsymbol{0}_{3N}$.

By invoking the Barbashin-Krasovskii-LaSalle theorem (see, e.g., Corollary 4.1 in [29]) the asymptotic stability of the origin $\boldsymbol{z} = \mathbf{0}_{6N}$ is guaranteed if no solution can stay identically in $\mathcal{I} = \{\boldsymbol{z} \in \Re^{6N} : \dot{V} = 0\}$, other than the trivial solution $\boldsymbol{z}(t) = \mathbf{0}_{6N}$.

Let $\boldsymbol{z}(t)$ be a solution belonging identically to $\mathcal{I}$, it can be recognized from (B.11) that $\boldsymbol{z}_2(t) = \mathbf{0}_{3N}$, that implies $\dot{\boldsymbol{z}}_2 = \mathbf{0}_{3N}$ and, from (B.9), $\boldsymbol{p}_{fc} - k_{f\nabla}\nabla U(\boldsymbol{z}_1 + \boldsymbol{r}_k^*) = \mathbf{0}_{3N}$. Since $\boldsymbol{p}_{fc}$ and $\nabla U(\boldsymbol{z}_1 + \boldsymbol{r}_k^*)$ are orthogonal vectors, both of them must be null. Moreover, by the convexity of $U(\boldsymbol{r})$, $\nabla U(\boldsymbol{z}_1 + \boldsymbol{r}_k^*) = \mathbf{0}_{3N}$ implies that $U(\boldsymbol{r})$ reaches a minimum for $\boldsymbol{z}_1 = \mathbf{0}_{3N}$. Hence the only solution $\boldsymbol{z}(t)$ identically in $\mathcal{I}$ is the trivial solution and it can be recognized that $\boldsymbol{z}$ asymptotically converge to $\mathbf{0}_{6N}$. In conclusion, the contact configuration $\boldsymbol{r}$ converge to $\boldsymbol{r}_k^* \in \mathcal{S}$ and this proves the theorem.

Appendix C

C.1 Stability of internal motion

The law (5.7) could be analyzed in two different orthogonal domains, in the cartesian space and in the null space of $\bar{\boldsymbol{J}}$. In Cartesian space, the asymptotic convergence of $\boldsymbol{e}_p$, $\boldsymbol{e}_v$ has been already proven [63]. In internal motion joint space, according to [28], consider the following Lyapunov candidate function

$$V_o = \frac{1}{2}\dot{\boldsymbol{q}}_0^{\mathrm{T}}\dot{\boldsymbol{q}}_0, \tag{C.1}$$

where $\dot{\boldsymbol{q}}_0$ is the vector of joint velocities, which, in turn, can be computed as $\dot{\boldsymbol{q}}_0 = \boldsymbol{N}(\bar{\boldsymbol{J}})\dot{\boldsymbol{q}}$; by taking the time derivative of $\dot{\boldsymbol{q}}_o$ it yields $\ddot{\boldsymbol{q}}_0 = \dot{\boldsymbol{N}}(\bar{\boldsymbol{J}})\dot{\boldsymbol{q}} + \boldsymbol{N}(\bar{\boldsymbol{J}})\ddot{\boldsymbol{q}}$. It is worth noticing that, since $\ddot{\boldsymbol{q}}_0$ belong to the null space of $\bar{\boldsymbol{J}}$, then $\boldsymbol{N}(\bar{\boldsymbol{J}})\ddot{\boldsymbol{q}}_0 = \ddot{\boldsymbol{q}}_0 = \boldsymbol{N}\dot{\boldsymbol{N}}(\bar{\boldsymbol{J}})\dot{\boldsymbol{q}} + \boldsymbol{N}(\bar{\boldsymbol{J}})\ddot{\boldsymbol{q}}$. The time derivative of V_0 is given by the following

$$\dot{V}_0 = \dot{\boldsymbol{q}}_0^{\mathrm{T}}\ddot{\boldsymbol{q}}_0 = \dot{\boldsymbol{q}}_0^{\mathrm{T}}\boldsymbol{N}(\bar{\boldsymbol{J}})\ddot{\boldsymbol{q}} + \dot{\boldsymbol{q}}_0^{\mathrm{T}}\boldsymbol{N}\dot{\boldsymbol{N}}(\bar{\boldsymbol{J}})\dot{\boldsymbol{q}}, \tag{C.2}$$

by recalling (5.7) and after some computation, (C.2) becomes

$$\dot{V}_0 = -k_s||\dot{\boldsymbol{q}}_0||^2,\ k_s > 0, \tag{C.3}$$

which is negative definite. Since

$$\begin{array}{l} V_0 = \dfrac{1}{2}||\dot{\boldsymbol{q}}_0||^2 \leftrightarrow \dfrac{1}{2}||\dot{\boldsymbol{q}}_0||^2 \leq V_0 \leq \dfrac{1}{2}||\dot{\boldsymbol{q}}_0||^2 \\ \dot{V}_0 = -k_s||\dot{\boldsymbol{q}}_0||^2 \end{array}, \tag{C.4}$$

the equilibrium $\dot{\boldsymbol{q}}_0 = \mathbf{0}$ is exponentially stable. By being V_0 radially unbounded the result holds globally.

Bibliography

[1] A. Albu-Schaffer, S. Haddadin, C. Ott, A. Stemmer, T. Wimbock, and G. Hirzinger, The DLR lightweight robot: design and control concepts for robots in human environments. *Industrial Robot: An International Journal,* pp. 376–385, 2007.

[2] G. Antonelli, "Stability analysis for prioritized closed-loop inverse kinematic algorithms for redundant robotic systems", *IEEE Transaction on Robotics*, vol. 25, pp. 985–994, 2009.

[3] A. Bicchi, D. Prattichizzo, "Manipulability of cooperative robots with unactuated joints and closed-chain mechanisms", *IEEE Transactions on Robotics and Automation*, vol. 16, pp. 336–345, 2000.

[4] Robert G. Bonitz, T.C. Hsia, "Force decomposition in cooperative manipulators using the theory of metric spaces and generalized inverses," *In Proc. of the IEEE Int. Conf. on Robotics and Automation*, pp. 1521–1527, 1994.

[5] Robert G. Bonitz, T.C. Hsia, "Internal force-based impedance control for cooperating manipulators," *IEEE Transanction on Robotics and Automation*, vol. 12, no. 1, pp. 78–89, 1996.

[6] C. Borst , T. Wimbock, F. Schmidt, M. Fuchs, B. Brunner, F. Zacharias, P.R. Giordano, R. Konietschke, W. Sepp, S. Fuchs, C. Rink, A. Albu-

Schaffer, G. Hirzinger, "Rollin' Justin - Mobile platform with variable base," *Robotics and Automation, 2009. ICRA '09. IEEE International Conference on* , vol., no., pp. 1597–1598, 2009.

[7] J. Butterfass, M. Grebenstein, H. Liu, G. Hirzinger, "DLR-Hand II: next generation of a dextrous robot hand," *Robotics and Automation, 2001. Proceedings 2001 ICRA. IEEE International Conference on* , vol.1, no., pp.109–114 vol.1, 2001

[8] F. Caccavale, C. Natale, B. Siciliano, L. Villani, "Six-DOF impedance control based on angle/axis representations", *IEEE Transactions on Robotics and Automation*, vol. 15, pp. 289–300, 1999.

[9] F. Caccavale and L. Villani, "Impedance control of cooperative manipulators," *Mach. Intell. Robot. Control,* vol. 2, pp. 51–57, 1999.

[10] F. Caccavale, M. Uchiyama, "Cooperative manipulators", *Handbook of Robotics, B. Siciliano and O. Khatib, Eds. Berlin: Springer*, pp.701–718, 2008.

[11] F. Caccavale, P. Chiacchio, A. Marino, L.Villani, "Six-DOF Impedance Control of Dual Arm Cooperative Manipulators", *IEEE Transactions On Mechatronics* , vol. 13, pp. 576–587, 2008.

[12] F. Caccavale, V. Lippiello, G. Muscio, F. Pierri, F. Ruggiero, L. Villani, "Kinematic control with force feedback for a redundant bimanual manipulation system", *Proceedings of 2011 IEEE/RSJ International Conference on Intelligent Robots and Systems*, pp. 4194–4200, 2011.

[13] F. Caccavale, V. Lippiello, G. Muscio, F. Pierri, F. RUGGIERO, L. Villani, "Grasp planning and parallel control of a redundant dual-arm/hand manipulation system", Robotica, Cambridge Univesity Press in press.

[14] S. Chiaverini, B. Siciliano, "On the stability of a force/position control scheme for robot manipulators", *Proceedings of 3rd IFAC Symposium on Robot Control*, pp. 183–188, 1991.

[15] S. Chiaverini, L. Sciavicco, "The parallel approach to force/position control of robotic manipulators", *IEEE Transactions on Robotics and Automation*, vol. 4, pp. 361–373, 1993.

[16] S. Chiaverini, B. Siciliano, L. Villani, "Force/position regulation of compliant robot manipulators", *IEEE Transactions on Automatic Control*, vol. 39, pp. 647–652, 1994.

[17] S. Chiaverini, B. Siciliano, "Systems analysis, modelling and simulation", *IEEE Transactions on Robotics and Automation*, vol. 35, pp. 45–60, 1999.

[18] J. Coelho, R. Grupen, "A control basis for learning multifingered grasps", *Journal of Robotic Systems*, vol. 14, pp. 545–557, 1997.

[19] E. Coleshill, L. Oshinowo, R. Rembala, B. Bina, D. Rey and S. Sindelar, "Dextre: Improving Maintenance Operations on the International Space Station," Acta Astronautica, vol.64, pp. 869–874, 2009.

[20] A. DasGupta, H. Hatwal, "Dynamics and nonlinear coordination control of multi-fingered mechanical hands", *ASME Journal of Dynamic Systems, Measurement and Control*, vol. 120, pp. 275–281, 1998.

[21] M. Diftler, J. Mehling, M. Abdallah, N. Radford, L. Bridgwater, A. Sanders, S. Askew, D. Linn, J. Yamokoski, F. Permenter, B. Hargrave, R. Platt, R. Savely, and R. Ambrose, "Robonaut 2: The first humanoid robot in space," *Proc. IEEE International Conf. on Robotics and Automation (ICRA), 2011.*

[22] Z. Doulgeri, J. Fasoulas, S. Arimoto, “Feedback control for object manipulation by a pair of soft tip fingers”, *Robotica*, vol. 20, pp. 1–11, 2002.

[23] J. Gudio-Lau, M. A. Arteaga, L. A. Muoz, and V. Parra-Vega, "On the Control of Cooperative Robots Without Velocity Measurements," IEEE Transactions on control Systems Technology, vol. 12, pp. 600–608, 2004.

[24] W. Gueaieb, F. Karray, and S. Al-Sharhan, "A Robust Adaptive Fuzzy Position/Force Control Scheme for Cooperative Manipulators," *IEEE Transactions on Control Systems Technology,* vol. 11, pp. 516–528, 2003.

[25] L. Han, J. C. Trinkle, “The instantaneous kinematics of manipulation”, *Proceedings of 1998 IEEE International Conference on Robotics and Automation*, pp. 1944–1949, 1998.

[26] N. Hogan "Impedance control: An approach to manipulation: PartsI–III", *ASME Journal of Dynamic Systems, Measurement, and Control*, vol. 7, pp. 1–24.

[27] N. Hogan "On the stability of manipulator performing contact tasks", *IEEE Journal of Robotics and Automation*, vol. 4, pp. 677–686.

[28] P. Hsu, J. Hauser, S. Sastry, “Dynamic Control of Redundant Manipulators", *IEEE International Conference on Robotics and Automation*, vol. 1, pp. 183-187, 1988.

[29] H.K. Khalil, *Nonlinear Systems* (2nd ed.), Prentice Hall, Upper Saddle River, NJ, 1996.

[30] O. Khatib, “A unified approach for motion and force control of robot manipulators”, *IEEE Journal of Robotics and Automation*, vol. 3, pp. 43–53, 1987.

[31] I. Kao, K. Lynch, J.W. Burdick "Contact modeling and manipulation", *Handbook of Robotics, B. Siciliano and O. Khatib, Eds. Berlin: Springer*, pp. 647–670, 2008.

[32] T. Kasai, M. Oda, T. Suzuki, Results of the ETS-7 Mission - Rendezvous Docking and Space Robotics Experiments *Artificial Intelligence, Robotics and Automation in Space, Proceedings of the Fifth International Symposium, ISAIRAS '99,* European Space Agency, 1999.

[33] K.-Y. Lian, C.-S. Chiu, and P. Liu, "Semi-Decentralized Adaptive Fuzzy Control for Cooperative Multirobot Systems With H-inf Motion/Internal Force Tracking Performance," *IEEE Transactions on systems, Man, and Cybernetics, Part B: Cybernetics,* vol. 32, pp. 269–280, 2002.

[34] N. Mansard, F. Chaumette, "Task sequencing for high-level sensor-based control", *IEEE Transactions on Robotics and Automation*, vol. 23, pp. 60–72, 2007.

[35] M. T. Mason and J. K. Salisbury, "Robot Hands and the Mechanics of Manipulation", *MIT Press, Cambridge, MA*, 1985.

[36] C. Melchiorri, M. Kaneco, "Robot hands", *Handbook of Robotics, B. Siciliano and O. Khatib, Eds. Berlin: Springer*, pp. 345–360, 2008.

[37] A.T. Miller, P.K. Allen, "GraspIt! – A Versatile Simulator for Robotic Grasping", *IEEE Robotics and Automation Magazine*, vol.11, pp. 110–122, 2004.

[38] "B. Mirtich and J. Canny, Easily computable optimum grasps in 2-d and 3-d," *Proc. of the IEEE Int. Conf. on Robotics and Automation*, vol.1, pp. 739–747, 1994.

[39] D. Montana, "The kinematics of contact and grasp", *International Journal of Robotics Research*, vol. 7, no. 3, pp. 17–32, 1988.

[40] D. Montana, "The kinematics of multi-fingered manipulation", *IEEE Transactions on Robotics and Automation*, vol. 11, pp. 491–503, 1995.

[41] S. A. A. Moosavian and R. Rastegari, "Multiple-arm Space Free-flying Robots for Manipulating Objects with Force Tracking Restrictions," *Robotics and Autonomous Systems,* vol.54, no.10, pp. 779–788, 2006.

[42] R.M. Murray, Z.X. Li, S.S. Sastry, *A mathematical introduction to robotic manipulation*, CRC press, Boca Raton, 1993.

[43] K. Nagai, T. Yoshikawa, "Dynamic manipulation/grasping control of multi-fingered robot hands", *Proceedings of 1993 IEEE International Conference on Robotics and Automation*, pp. 1027–1033, 1993.

[44] K. Nagai, T. Yoshikawa, "Grasping and manipulation by arm/multifingered-hand mechanism", *Proceedings of 1995 IEEE International Conference on Robotics and Automation*, pp. 1040–1047, 1995.

[45] Y. Nakamura, K. Nagai, T. Yoshikawa, "Dynamics and stability in coordination of multiple robotic mechanisms", *The Int. Journal of Robotics Research* , vol. 8, pp. 44–61, 1989.

[46] M. P. Naylor, N. A. Scott, E. Atkins, and S. Roderick "Towards autonomous sampling and servicing with the ranger dexterous manipulator" *Proceedings of the AIAA Infotech@Aerospace Conference, AIAA,* 2005.

[47] M. Oda, "Experiences and lessons learned from the ETS-VII robot satellite," *Proceedings of 2000 IEEE International Conference on Robotics and Automation*, pp.914–919 vol.1, 2000

[48] A. M. Okamura, N. Smaby, M.R. Cutkosky, "An overview of dexterous manipulation", *Proceedings of 2000 IEEE International Conference on Robotics and Automation*, pp. 255–262, 2000.

[49] E. Papadopoulos and S. A. A. Moosavian, "Dynamics and "Control of Multi-arm Space Robots During Chase and Capture Operations," *Proceeding of IEEE International Conference on Intelligent Robots and Systems,* Munich, pp. 1554-1561, 1994.

[50] R. Platt, A.H. Fagg, R. Grupen, "Null-space grasp control: Theory and experiments", *IEEE Transactions on Robotics*, vol. 26, pp. 282–295, 2010.

[51] J. Ponce, S. Sullivan, A. Sudsang, J. Boissonnat, J. Merlet, "On computing four-finger equilibrium and force-closure grasps of polyhedral objects", *International Journal of Robotic Research*, vol. 16, pp. 11–35, 1996.

[52] D. Prattichizzo, J.C. Trinkle, "Grasping", *Handbook of Robotics, B. Siciliano and O. Khatib, Eds. Berlin: Springer*, pp. 671–700, 2008.

[53] M. Quigley, K. Conley, B. P. Gerkey, J. Faust, T. Foote, J. Leibs, R. Wheeler, A.Y. Ng, "ROS: an open-source Robot Operating System", *ICRA Workshop on Open Source Software,* 2009.

[54] M.H. Raibert, J.J. Craig, "Hybrid force/position control of manipulator *ASME Journal of Dynamic Systems, Measurement, and Control*, vol. 103, pp. 126–133, 1981.

[55] C. Remond, V. Perderau, M. Drouin, "A hierarchical multi-fingered hand control structure with rolling contact compensation", *Proceedings of 2002 IEEE International Conference on Robotics and Automation*, pp. 3731–3736, 2002.

[56] A. Rodriguez-Angeles and H.Nijmeijer, "Mutual Synchronization of Robots via Estimated State Feedback: A Cooperative Approach," *IEEE Transactions on Control Systems Technology,* vol. 12, pp. 542–554, 2004.

[57] B. Rubinger, P. Fulford, L. Gregoris, C. Gosselin, T. Laliberté, "Self-Adapting Robotic Auxiliary Hand (SARAH) for SPDM Operations on the International Space Station," *6th International Symposium on Artificial Intelligence, Robotics and Automation in Space, Programme and Abstracts, Canadian Space Agency*, 2002.

[58] E. Sabelli, D. L. Akin and C. R. Carignan, "Selecting Impedance Parameters for the Ranger 8-DOF Dexterous Space Manipulator," *Proceeding of AIAA Aerospace Conference and Exhibit, Rohnert Park, California,* pp.1-15, 2007.

[59] K.S. Sang, R. Holmberg, and O. Khatib, "The Augmented Object Model: Cooperative Manipulation and ParallelMechanisms Dynmaics," *Proceedings of the 2000 IEEE International Conference on Robot- ics and Automation, San Francisco,* pp.470-475, 1995.

[60] T. Schlegl, M. Buss, T. Omata, G. Schmidt, "Fast dexterous regrasping with optimal contract forces and contact sensor-based impedance control", *Proceedings of 2001 IEEE International Conference on Robotics and Automation*, pp. 103–108, 2001.

[61] S. A. Schneider and R. H. Cannon Jr., "Object impedance control for cooperative manipulation: Theory and experimental results," *IEEE Transaction on Robotics and Automation,* vol. 8, no. 3, pp. 383–394, 1992.

[62] B. Siciliano, L. Villani, "An adaptive force/position regulator for robot manipulators", *International Journal of Adaptive Control and Signal Processing*, vol. 7, pp. 389–403, 1993.

[63] B. Siciliano, L. Sciavicco, L. Villani, G. Oriolo, "Robotics. Modelling, Planning and Control", *Springer*, 2009.

[64] P. Soueres, S. Tarbouriech, B. Gao, "A robust vision-based controller for mobile robots navigation: application to the task sequencing problem", *Proceedings of 2005 IEEE/RSJ International Conference on Intelligent Robots and Systems*, pp. 2191–2196, 2005.

[65] S. Stramigioli, C. Melchiorri, S. Andreotti, "A passivity based control scheme for robotic grasping and manipulation", *Proceedings of the 38th Conference on Decision and Control*, pp. 2951–2956, 1999.

[66] S. Stramigioli, "Modeling and IPC control of interactive mechanical systems", *Springer-Verlag*, 2001.

[67] D. Sun, and J.K. Mills, "Adaptive Synchronized Control for Coordination of Multirobot Assembly Tasks," *IEEE Transactions on Robotics and Au- tomation* vol. 18, pp.498–510, 2002.

[68] M. Uchiyama and P. Dauchez, "A Symmetric Hybrid Position/Force Control Scheme for the Coordination of Two Robots," *Proceeding of 1988 IEEE International Conference on Robotics and Automation, Philadelphia,* USA, April 1988, pp.350–356.

[69] M. Uchiyama and P. Dauchez, "Symmetric Kinematic Formulation and Non-Master/Slave Coordinated Control of Two-Arm Robots," *Advanced Robotics: The International Journal of the Robotics Society of Japan,* vol. 7, no. 4, pp. 361–383, 1993.

[70] I. D. Walker, R. A. Freeman, and S. I. Marcus, "Analysis of Motion and Internal Force Loading of Objects Grasped by Multiple Cooperating Manipulators," *International Journal of Robotics Research,* vol. 10, no. 4, pp. 396–409, 1991.

[71] D. Williams and O. Khatib, "The Virtual Linkage: A Model for Internal Forces in Multi-Grasp Manipulation," *Proceeding of 1993 IEEE International Conference on Robotics and Automation, Atlanta,* pp. 1025–1030, 1993.

[72] T. Wimboeck, C. Ott, G. Hirzinger, "Passivity-based object-level impedance control for a multifingered hand", *Proceedings of 2006 IEEE/RSJ International Conference on Intelligent Robots and Systems*, pp. 4621–4627, 2006.

[73] T. Wimboeck, C. Ott, G. Hirzinger, "Analysis and experimental evaluation of the intrinsically passive controller (IPC) for multi-fingered hands", *Proceedings of 2008 IEEE International Conference on Robotics and Automation*, pp. 278–284, 2008.